FLUVIAL SEDIMENT TRANSPORT AT A LARGE BED SHEAR STRESS

A Thesis
Presented for the Degree
of
Doctor of Philosophy
in
Engineering

in the
University of Canterbury,
Christchurch, New Zealand.

by
Ian Kennedy Hill
1967

ACKNOWLEDGMENTS

I acknowledge with thanks the help received from Professor H. J. Hopkins, Head of the Department of Civil Engineering, and other members of the Civil Engineering staff.

Equipment and material was generously supplied by all other Departments of the School of Engineering and by the Southland County Council.

Construction and operation of the apparatus were carried out in conjunction with the technical staff of the Department of Civil Engineering, particularly Messrs F. Archer, J. Byers, P. Dawson and N. Prebble.

In writing this thesis I have received much helpful criticism from my supervisor, Professor F. M. Henderson, and I acknowledge with sincere thanks the considerable assistance I have received from both Professor Henderson and Dr H. R. Thorpe during the course of this project.

Thanks are also extended to my wife who helped in the preparation of and typed the manuscript.

Financial assistance was received from the University Grants Committee and the University of Canterbury.

I.K.H.

ABSTRACT

The mechanics of a layer, many particle diameters thick, of a particle fluid system where the particles are large and exist at high concentrations is examined.

Two distinct matters are examined, the first being the development of equations describing the overall characteristics of the system if the "local" equations governing the system at a point are known, and the second being the development of these local equations for large particles.

It is shown that, if the local equations describing the dispersive stress - shear stress relationship and the stress - rate of strain relationship are single valued functions of the concentration, then the concentration profile in the bed of an open channel can be obtained by integrating a first order differential equation and the velocity profile obtained by carrying out a further integration.

A method of obtaining the local equations is developed using previous results from a theory of a gas of rigid elastic spheres. Using these results and an equation derived from the calculated energy dissipation, local equations are developed.

Results obtained theoretically are compared with previous experimental results and also with the results obtained using an open channel with a bed of gravel particles. A significant discrepancy between the results predicted by the theory developed and the results found by experiment was observed at high concentrations.

TABLE OF CONTENTS

TABLE OF CONTENTS (CONTD):

TABLE OF CONTENTS (CONTD):

TABLE OF CONTENTS (CONTD):

TABLE OF CONTENTS (CONTD):

TABLE OF CONTENTS (CONTD):

TABLE OF CONTENTS (CONTD):

LIST OF FIGURES

LIST OF FIGURES (CONTD.):

LIST OF FIGURES (CONTD.):

LIST OF FIGURES (CONTD):

LIST OF TABLES

LIST OF SYMBOLS

(Note: Symbols or uses of a symbol occurring in one section only are generally not listed.)

A	Constant defined by $ds/dt = -As^2$
A	Constant defined by $\lambda = A\,10^{-BC}$
A_2, A_1	Constants used in theory developed in Chapter 3
a	$4/\pi \bar{s}^2$
a	$4/\pi \bar{l}^2$
B	Constant defined by $\lambda = A\ 10^{-BC}$
B_i	Constants used in Chapter 2 to define particular flow and channel
C	Solids concentration, volume of solids per unit total volume
C_D	Drag coefficient of particle
C_s	Suspended solids concentration
C_b	C at bottom of the moving bed
C	Maximum static concentration
D	Diameter of particles
De	Function of θ, S, C defined in equation (2-50)
d	Depth
E_b	Bulk modulus of fluid
E_d	Energy dissipated per unit volume
E_l	Energy lost per collision
E_y	Elastic modulus of solids
E_i	Constants used in interpreting local equations, see Chapter 2.

LIST OF SYMBOLS (CONTD):

e	2.71828
F_1	Ratio of dispersive stress to total shear stress
F_2	Dimensionless particle shear stress
F_3	Dimensionless total shear stress
F_5	Dimensionless dispersive stress
F_7	Ratio of dispersive stress to particle shear stress
F_8	Dimensionless fluid shear stress
F_{1b}	F_1 in the bed
F_{1c}	F_1 in the bed at incipient shear failure
f	Frequency of collisions
f(x)	Function (of x)
f_r	Ratio of frequency of collisions with fluid present and without fluid present
g	Gravitational constant
H_1, H_2	Parameters defining given flow and channel, see equations (2-56) and (2-57)
K	Attenuation factor for gamma radiation
K	Unity minus the coefficient of restitution
K_f	Attenuation in flume walls
K_2, K_5	Constants related to proportion of energy lost per collision.
k	Velocity gradient transverse to the flow
k	Gas equation constant occurring in $k = (\pi m \bar{s})^2/8$ Te
L_e	Dissipation length
l	Length of path travelled by a particle
$\bar{l}$	Mean free path of particles

LIST OF SYMBOLS (CONTD):

l_g	Ten folding length in gravel
l_w	Ten folding length in water
M	Momentum of particle
M_a	Correction to F_2 allowing for the effect of the interparticle fluid
M_c	$M_r m/m_e$
M_r	Ratio of momentum transport rate with fluid to that without fluid
m	Mass of particle
m_e	Effective mass of particle
n	Number of particles per unit volume
n	Number of counts from source
n_b	Total background counts
n_t	Total number of counts
P	Dispersive stress, interparticle normal stress in y direction
P_f	Average stress in y direction caused by fluid pressure
P_t	Total normal stress in y direction
P_x	Total normal stress in x direction
p(x)	Probability density (of x)
Re	Reynolds number
S	Submerged specific gravity of solids ($\rho_s/\rho_f - 1$)
s	Magnitude of particle velocity
s_r	Magnitude of relative velocity of one particle with respect to another.

LIST OF SYMBOLS (CONTD):

T	Average particle shear stress in the plane perpendicular to y
T_b	Shear stress in bed at incipient failure
T_f	Average fluid shear stress in the plane perpendicular to y
T_t	Average total shear stress in the plane perpendicular to y
T_t	Time taken to measure total count
T_b	Time taken to measure background count
Tr	Ratio of time required for a given accuracy with and without background
Te	Gas temperature
T_*	Dimensionless bed shear
tr	Ratio of time between collisions for a given particle with and without fluid present
u	Mean velocity in x direction
v	Velocity component perpendicular to u
x	Co-ordinate distance along direction of mean velocity
Y	Function of C defined in Chapter 3 by Y = (P/n k Te) - 1
y	Co-ordinate distance perpendicular to the shear bed measured from the bottom of the moving bed
z	Source strength in curies
α	$\cos^{-1}$ 5/6
η	Detector efficiency
η'	Photons emitted per curie
θ	Angle between horizontal plane and the velocity vector

LIST OF SYMBOLS (CONTD):

λ	Counts from source detected per minute
λ	Parameter related to concentration
λ_b	Background counts detected per minute
λ_t	Total counts detected per minute
μ	Dynamic viscosity
μ_e	Effective viscosity
π	Stability parameter
ρ_a	Mean density of system
ρ_f	Fluid density
ρ_s	Solids density
$\phi(x)$	Function (of x)

CHAPTER 1

I N T R O D U C T I O N

SCOPE OF THESIS

In this thesis, a mathematical model of a system of discrete particles dispersed in a fluid is developed. The model applies to large particles at high concentrations in a steady shear flow.

HISTORICAL NOTE

General Trends in Sediment Transport Studies

This thesis is particularly directed to the problem of a fluid flowing over a non-cohesive bed of particles; prediction of the behaviour of such a system has occupied many previous workers and proved very difficult. The system of a flow over a non-cohesive bed occurs in many forms and situations, appearing, for example, as river and canal flow in non-cohesive material, local scour around obstacles in a flowing stream, and (more recently) in the transport of solids in particle form along a pipeline.

At present there is no general solution to the basic fluid-particle system problem and consequently no general criteria could be used in the analysis of more particular

problems. As a result, particular situations have been studied in greater or lesser degrees of isolation, and a large number of techniques for analysis have been developed. The most common procedure has been to use dimensional analysis combined with experimental correlation of selected dimensionless groups of parameters. One difficulty associated with this practice is the selection of the appropriate parameters so that there are sufficient to define the system without rendering the experimental programme unwieldy.

The mathematical solutions sought can be divided into two categories.

Firstly, there are the equations describing the behaviour of a system at a given point as a function of the system properties at that point. This type of equation, which is frequently of differential form, will be called a local equation, and an example is an equation whereby the strain rate at a given point in a viscous fluid is related to the shear stress and coefficient of viscosity at the same point. In this thesis, the term "local equation" will include equations applying to the average behaviour, at a point, of the system over a finite period of time.

Secondly, there are the equations relating the overall behaviour of the system to its properties. This type of equation will be called a bulk equation and an example is the

equation whereby the discharge in an open channel is related to the channel properties. Frequently, it is in principle possible to obtain bulk equations for different systems by integrating the local equations and fitting appropriate boundary conditions.

Development of Different Approaches to the Problem

One important approach in open channel flow problems of this type has been to determine the bulk equations for the channel without considering details of the particle fluid interaction. This approach has led to the regime theories of open channels carrying sediment, these theories being particularly designed to predict the shape of stable channel that will exist for a given flow. One weakness of this approach is that, because of the very empirical nature of the equations, they cannot be readily applied to situations differing from those used in the experimental derivation of the regime equations. Details of the application of these methods to actual river and canal problems are given by Blench (1).

Laboratory examination of simple systems of particle or sediment transport is an important technique in determining the relative importance of various parameters. It has also been utilised in an attempt to discover local equations which could be used in a systematic method of finding bulk equations

for particular boundary conditions.

One of the early workers using a laboratory open channel was Shields (2) who in particular examined the conditions prevailing at the "threshhold of motion", that is, when the first particles begin to move. Shields found that the shear stress acting on the bed, divided by the submerged specific weight of the particles multiplied by the particle diameter, was a function of a Reynolds number with the particle diameter as a length dimension.

This was one of the first approaches in determining local equations as it applied at a point in the system and could be used at any similar point in any other system, with the proviso that a "similar point" implies similarity with respect to upstream and downstream conditions. Therefore, as the solution depends on the situation existing some distance away from the point in the bed, as well as at the point itself, it is not a true local equation.

Another important aspect of Shields' work was its examination of the behaviour of points lying in a clearly defined plane, that between the fluid and the fixed bed. From Shields results it was clear that the average shear stress on the bed required to initiate particle movement was very much less than the local value of shear calculated to be necessary, and it became apparent that the motion was strongly influenced by the

turbulent eddies in the flow. This dependence on the flow turbulence is one of the major difficulties in developing a theory of sediment movement based on equations applying generally to a wide variety of flows. After the particle movement has started, this turbulence is an important factor in determining the interaction of the fluid and the bed. The bed profile is dependent on the sediment particle movement which, in turn, depends strongly on the turbulent eddies set up by the profile shape. In particular, Raudkivi (3) has observed particles kept in a state of agitation in the lee of ripples, even when the average bed shear stress at the point is zero. It is apparent that Shields' equation is not sufficient to describe the threshhold of motion under these conditions.

As the shear stress on the bed is increased, more material is set in motion. This material may be moved in different ways and separate parts of it are classified according to the method of transport. It has been observed that some particles move by rapid jumps from the bed to a height of a few diameters and from here they are carried along by the current, gradually sinking back into the bed. Such motion is called "saltation". Other particles may move by rolling and bouncing along the bed. The total material moved by both types of action is frequently termed the "bed load".

Alternatively, the particles may be lifted from the bed into the main turbulent eddies of the flow and be supported by the mixing action of the turbulence acting upon a concentration gradient of particles. The total of these particles is termed the "suspended load".

There are two measures of the load. One is the weight of particulate material transported across a cross-section of a channel per unit time. The other is the weight of particulate material above a unit area of the bed at a given time.

Although very fine particles may be supported by Brownian motion, in almost all flows of interest in civil engineering, the effect of turbulence will completely over-shadow this effect.

The solids transport rate across any section is dependent not only upon the conditions at the section, but also upon the transport rate upstream of the section. In the laboratory, however, it is possible to examine a steady uniform flow situation in which the transport rate of solids is constant along the length of a channel. The development of theoretical models is much simplified by restriction to the steady uniform 2-dimensional case.

There are two distinct approaches in developing equations relating to the behaviour of the bed material. The first of these, which is the more common and was until recently the only

approach, is to consider in the system a definite dividing surface which divides the system into a fixed bed below the surface and the moving fluid and particles above the surface. By a consideration of the behaviour of particles in this dividing surface (denoted hereafter as a "single surface"), the behaviour of the bed material is predicted. Two important single surface treatments are those of Einstein and Kalinske. Einstein (4) assumed a saltation mechanism acting on the surface particles in a plane. Kalinske (5), on the other hand, considered the critical shear required to roll a particle over its neighbour and once again assumed the fluid shear acted upon a fixed particle in the bed.

The second, or "deep bed", approach is to consider the behaviour of the moving bed in depth, not just at a single surface, and to examine the interaction of the upper bed particles with those in the layer below, and so on to the fixed bed.

Development of the Deep Bed Approach

The first, or single surface, approach appears to be physically reasonable for small particle flow rates, that is, when the particles have little mutual interference. As the shear stress is increased, however, and more material is set into motion, the second or deep bed approach should give more reliable results as the physical situation used in deriving

any equations represents more closely that naturally occurring.

The deep bed approach was considered by Bagnold (6, 7). Bagnold considered a layer many particle diameters thick and composed of a mixture of solid particles and fluid. He then examined the behaviour of such a system under a steady rate of shear strain. A misture of spheres and fluid was sheared between two concentric cylinders and Bagnold measured the shear stress and rate of strain of the mixture. He also measured the dispersive stress or the direct stress required at the boundaries to stop the particles dispersing throughout the fluid. This dispersive stress is the effective pressure of the particles acting upon each other and is similar in concept to pressure in a fluid where the pressure is the result of all the molecules acting upon each other. In Bagnold's experiments, the fluid and particle densities were equal and the particle size was not changed throughout the experiments. Two values of viscosity were used and the volumetric concentration C of solids varied over the range 0.13 to 0.63. The results of the measurement of shear stress as a function of strain rate were consistent. However, the relation between shear stress and dispersive stress was not so well defined because the dispersive stress was measured for $C > 0.31$ only and the experimental results showed a wide scatter. Graphs showing Bagnold's experimental results reduced to a dimensionless form are given in Fig. (2-5) and Fig. (2-6). As the ratio of apparatus size

to particle size was constant, it was not possible to deduce from the results whether the overall Reynolds number of the system was a significant parameter. Nor was it possible to deduce whether wall effects were significant. The presence of the wall may have altered the flow close to it, or the roughness of the wall may have affected the flow, both types of wall effect being possible.

Bagnold, in second and third papers (7, 8), extended the above concepts and applied them to a wide range of examples, including open channel flow situations ranging from the threshhold of motion to the flow of a deep, concentrated bed of saturated gravel with little or no water above it. In these papers, both suspended load and bed load were considered and bulk equations for the solids flow rate were developed. These equations were dependent on some arbitrary assumptions about the energy relations in the flow and, if they were to be used numerically, also relied upon the use of empirical constants.

Miller (9) examined Bagnold's first paper containing the results of his experiments with the concentric cylinders, and carried out further experiments using a larger apparatus to particle size ratio. His experimental results differed considerably from Bagnold's, particularly at low concentrations. However, Miller observed that the particles he was using were

stratified in the apparatus because of small variations in density. There was, therefore, a region between the cylinders with little or no solids at all, this stratification being accentuated at low concentrations. Bagnold made no mention of this phenomena occurring with his apparatus, but, even if this were the case, the effect would have been different as such stratification would depend upon the dimensions of the apparatus and the particles.

Miller (9) also developed a model for the particle behaviour. The model, based on some results from the molecular theory of gases, gives an effective viscosity and dispersive pressure related to the gas temperature. The particle property equivalent to the gas temperature is the r.m.s. random velocity of the particles. Miller assumed that the r.m.s. velocity was proportional to the velocity gradient and was left with one arbitrary constant. This arbitrary constant was determined by matching the theoretical and experimental curves at some point. There was a wide discrepancy between the curves of Miller and Bagnold, but this was largely caused by an error in converting terms containing the effective volume of a molecule to terms containing the concentration of particles. If Miller's equation is corrected in this way, the agreement with Bagnold's experimental curve is improved.

CONTENTS OF THIS THESIS

At present there are two sets of experimental results (those of Bagnold and those of Miller) for the dispersive stress and shear stress variation at large Reynolds numbers. Neither set is conclusive and all the results apply to solid particles of the same density as the fluid. In order to obtain local equations from Miller's theory, an arbitrary constant must be used, the value of this constant varying from one system to another. Bagnold's bulk equations depend on evaluating certain arbitrary constants which are difficult to estimate for any given situation. Also, they give no indication of the particle concentration to be expected near the bed. In most theories that have been developed, this concentration is, in fact, assumed to be high.

In this thesis, there are two distinct theoretical developments:

Firstly, Chapter 2 uses dimensional arguments to find local equations for the shear stress - rate of strain relation, and for the shear stress - dispersive stress relation. These equations contain functions of the particle Reynolds number, concentration, density ratio, etc. In general, each new equation introduces a new function denoted by F_i where i depends upon the particular relation being considered. Postponing any attempt at evaluating the F_i until later in

the thesis, Chapter 2 develops the equations for the concentration and velocity profiles in the bed flow region of an open channel. It is shown that the numerical values for this solution depend on the maximum ratio of dispersive stress to shear stress at which the stationary bed particles will shear. This ratio will be called the critical stress ratio F_{1c}. To some extent, the shape of the concentration profile depends upon the concentration immediately above the bed, but it is shown that this concentration has a restricted range of possible values, limited by the form of one of the F_i. Therefore, Chapter 2 ultimately propounds a method of obtaining the velocity and concentration as functions of y if the critical stress ration and C at the top of the stationary bed are known and if the F_i are known as functions of C. Chapter 2 also contains a brief discussion on the limitations of this approach and particularly the inadequacy of the analysis when large scale turbulence sets in.

Secondly, Chapter 3 re-examines and proposes a method of calculating the F_i, commencing with the equations used by Miller (9). Miller's dimensional arguments for the r.m.s. velocity are discarded, the flow is restricted to high particle Reynolds numbers and a new approach is followed. The energy supplied to the particle system per unit volume at a given level is equated to the energy dissipated in interparticle collision. From this assumption is obtained an equation which,

together with a viscosity equation derived from the molecular theory of dense gases, can be used to eliminate the r.m.s. velocity. The resulting equation for the stress - strain rate relation includes no arbitrary constants, although certain terms contain approximations in their evaluations. A dispersive stress - shear stress relation can be found from this equation and, by extension, the effect of the surrounding fluid on the local equations has been estimated. No previous work has considered this latter effect. The final equations apply to the case of a dense solid in a lighter fluid as well as to cases of equal density. Chapter 3 concludes with a table of numerical values for the important F_i. These values may be substituted into the equations developed in Chapter 2 in order to determine the concentration and velocity profiles.

An experimental facility was set up to examine open channel flow over a deep moving bed and this is described in Chapter 4. This chapter includes a discussion of the apparatus used to measure the concentration and velocity profiles.

In Chapter 5, there is a description of the experimental programme. This was designed with two objects. The first object was to observe the form in which a deep bed movement occurred and the second object was to compare the predicted and the actual velocity and concentration profiles.

Listed in Chapter 6 are the experimental results and well

calculated values of F_i. This chapter also includes results of tests carried out on the measuring equipment used.

Chapter 7 contains the conclusions based on the theoretical development and experimental measurements. The theory developed, although not accurate numerically, is considered useful in predicting the behaviour of a deep moving bed. Velocity and concentration profiles were of the general form predicted, particularly at concentrations less than 0.30. The model used is believed to be an inadequate representation of the system at high concentrations.

Conclusions reached as to the suitability of the apparatus are contained in Chapter 8. Particular attention was paid to the concentration profile measuring equipment. It was concluded that, although the methods used were very satisfactory and far superior to any other technique known to the writer, they could be improved. The time taken for a single concentration measurement was in some cases a matter of minutes and, when the bed profile is unsteady, this is too long.

Chapter 9 concludes the thesis with a brief resume of results and conclusions, together with suggestions for further experimental and theoretical work. Although the methods developed form a skeleton structure, it is considered that much work is needed to give this approach a more reliable experimental evaluation. In addition, the mechanism of particle

interaction requires further development, and there is a need for closer study of certain theoretical points. For example, numerical simulation techniques could be utilised in an examination of interparticle behaviour.

CHAPTER 2

APPLICATION OF DISPERSIVE STRESS APPROACH TO OPEN CHANNEL FLOW

SYNOPSIS

In this chapter a model is developed for a fluid-particle shear flow in a gravitational field. The concept of a dispersive or interparticle stress or pressure described by Bagnold is used. Although the interparticle pressure concept is the same as Bagnold's, its application to solving the shear flow problem in a gravitational field is not that used by Bagnold in (7). This study is restricted to a two dimensional uniform steady state flow and initially the behaviour of a small element of the system is examined. From this examination a system of differential equations is set up. The differential equations are then applied to the bed region of an open channel and equations giving the velocity and concentration profiles for this region are developed. These bed region equations are generally also of differential form and so finally the fitting of appropriate boundary conditions must be examined if a solution is required. The end results of the chapter are the velocity and concentration profiles for the bed region of any given steady uniform open channel flow. The methods could also have been applied to pipe flow to obtain

similar types of equation.

This analysis does not include any study of the stability of the bed-fluid interaction. Nor does it consider the system when such instability has occurred.

PRELIMINARY ANALYSIS

In this section, the particular flow pattern being analysed is discussed and this discussion is followed by a dimensional analysis of the problem. This concludes with a discussion of the relative importance of the dimensionless numbers.

Flow Pattern

The system considered here is a uniform flow of fluid over a bed of non-cohesive particles. The bed may be of sufficient depth to be stationary for the lower part of its depth, as in a deep layer of gravel under a river. Alternatively, the bed may all be in motion, sliding along a rigid boundary as in a pipe at high flow rates or for a shallow gravel river bed overlying a rock bed. A co-ordinate system in which y is perpendicular to the bed and is +ve upwards, and in which x lies in the direction of the velocity vector, is used, and a gravitational field (in the x-y plane) of magnitude g acting at an angle θ to the y direction, isincluded as in Fig. 2-1.

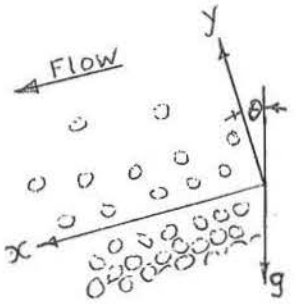

Fig. 2-1

The volumetric concentration, C, of particles is defined as volume of solid divided by volume of solid plus liquid.

Stress System

Because only uniform flow is considered, $u_y = 0$ and $\frac{du_x}{dx} = 0$, where u_y is the component of mean velocity in the y direction. The total stress at a point is defined if we know the direct stresses in the three co-ordinate directions and the shear stress in the x-z plane, the shear stress in the x-y plane being equal to zero. It is not necessary in using this model to postulate a single pressure defining the magnitude of direct stress in any direction. For the stress components, the following symbols will be used:

(a) The direct stress in the y-direction = P_t

(b) The direct stress in the x-direction = P_x

(c) The shear stress on the x-z plane = T_t

It is convenient to consider the total fluid particle system to be made up of two parts: the particles exerting forces on each other either by hydrodynamic repulsion or

collision effects, and the fluid with its own pressure and shear stresses. For the particle system alone, the direct stress in the y-direction and the shear on the x-z plane will be called P and T respectively. The corresponding fluid properties will be P_f and T_f where P_f is the fluid pressure and T_f the fluid shear resistance, measured as the shear force in the fluid per unit area of the x-z plane in the fluid-particle system. Therefore we can write,

$$P_t = P_f + P, \qquad (2\text{-}1)$$

$$T_t = T_f + T. \qquad (2\text{-}2)$$

Dimensional Analysis of System

At any point in the flow, the stress must be a function of the strain rate, the particle properties and the fluid properties. These properties are listed below with the symbols used in this thesis.

Fluid Properties		Particle Properties	
Dynamic Viscosity	μ	Size of Particles	$D_1, D_2 \ldots$
Density	ρ_f	Density	ρ_s
Bulk Modulus	E_b	Elastic Modulus	E_y

Volumetric Concentration C

Concentration Gradient dC/dy, $d^2C/dy^2 \ldots$

The particle size will be represented by sufficient characteristic lengths to define the mixture of sizes. If the

grading is uniquely dependent on one diameter, say the D_{70}, then only that one length is required.

The particle distribution is defined by the concentration and values of d^iC/dy^i. Initially we will include the first order gradient only, dC/dy.

All the above parameters and the strain rate are organized into a set of dimensionless parameters. Combining these with the dependent variables P_i and T_i gives,

$$P_i = T_j F_k\left(\frac{\rho_s D^2 T_j}{\mu^2}, \frac{\rho_s}{\rho_f}, C, D\frac{dC}{dy}, \frac{E_b}{E_y}, \rho_s D^2 E_b/\mu^2\right) \qquad (2\text{-}3)$$

$$T_i = \rho_s\left(\frac{du}{dy}\right)^2 D^2 F_l\left[\rho_s \frac{du}{dy} D^2/\mu, \frac{\rho_s}{\rho_f}, C, D\frac{dC}{dy}, \frac{E_b}{E_y}, \frac{\rho_s D^2 E_b}{\mu^2}\right] \qquad (2\text{-}4)$$

In these equations i, j, represent either t, f or nothing and k and l represent numerical indices depending on the values given to i and j as follows:

$$P = T\, F_7 \qquad (2\text{-}5)$$

$$P = T_t\, F_1 \qquad (2\text{-}6)$$

$$T = \rho_s\left(\frac{du}{dy}\right)^2 D^2\, F_2 \qquad (2\text{-}7)$$

$$T_t = \rho_s\left(\frac{du}{dy}\right)^2 D^2\, F_3 \qquad (2\text{-}8)$$

$$T_f = \rho_s\left(\frac{du}{dy}\right)^2 D^2\, F_2\, F_8 \qquad (2\text{-}9)$$

Examining the parameters in (2-3) and (2-4), the first term is a form of Reynolds number (or ratio of inertial to

viscous forces) and generally the larger this number the less important it becomes. The two forms of Reynolds number used in (2-3) and (2-4) are interchangeable. The next two terms could be expected to be significant, although as ρ_s/ρ_f becomes large it should become less important, the fluid having little effect on the particles. The term $D\frac{dc}{dy}$ is a measure of the concentration gradient and would be expected to become less important as its value decreases.

The remaining terms containing E_b will be important when the elastic properties of the system are important. This will not be so for situations where interparticle collisions are small but will be important where the energy recovery on collision of two particles is significant. These last two terms can therefore only be important where inertial collisions are important. Experiments carried out with stone bouncing on concrete in water have shown that the energy recovery is very small. For this case, the influence of E_b/E_y and $\rho_s D^2 E_b/\mu^2$ will be very small and if $D\frac{dc}{dy}$ is small we can reduce (2-3) and (2-4) to,

$$P_i = T_j F_k(\rho_s D^2 T_j/\mu^2, \frac{\rho_s}{\rho_f}, C) \qquad (2\text{-}10)$$

$$T_i = \rho_s D^2 (\frac{du}{dy})^2 F_1(\rho_s D^2 \frac{du}{dy}/\mu, \frac{\rho_s}{\rho_f}, C) \qquad (2\text{-}11)$$

For high values of the first term (Reynolds number), the value of F would tend to depend on ρ_s/ρ_f and C alone.

The arrangement in (2-11) is advantageous for high Reynolds number flows as the dependent dimensionless number contains the inertial term $\rho_s D^2 (\frac{du}{dy})^2$ and, in consequence, for cases where inertial effects predominate over viscous effects, the Reynolds number is not important. If the viscous forces predominate over the inertial ones, however, it is better to arrange the dependent number as $T_i / \mu \frac{du}{dy}$ so as to include the viscous effects in this term.

This gives the grouping for T_t,

$$T_t = \mu \frac{du}{dy} F_9 (\rho_s D^2 \frac{du}{dy} / \mu, \frac{\rho_s}{\rho_f}, C). \qquad (2\text{-}12)$$

In this case, if the inertial effects are small compared with the viscous ones, the Reynolds number and also ρ_s / ρ_f will have a small influence on F_9.

Comparison of Dimensional Arguments with Bagnold's Results

Bagnold (6) defined a parameter λ by the equation,

$$\lambda = 1 / \left[(\frac{C_*}{C})^{\frac{1}{3}} - 1 \right] \qquad (2\text{-}13)$$

where C_* is the maximum static concentration, and plotted his results in terms of λ. All of his experiments were carried out by shearing a mixture of spheres and fluid of the same density between two coaxial cylinders. One size of particle only was used, but the shear rate varied over a range of values.

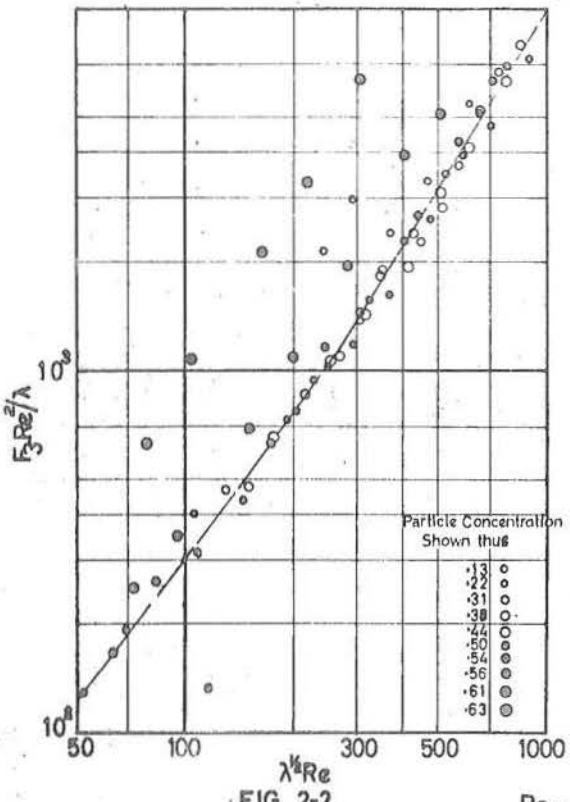

FIG 2-2

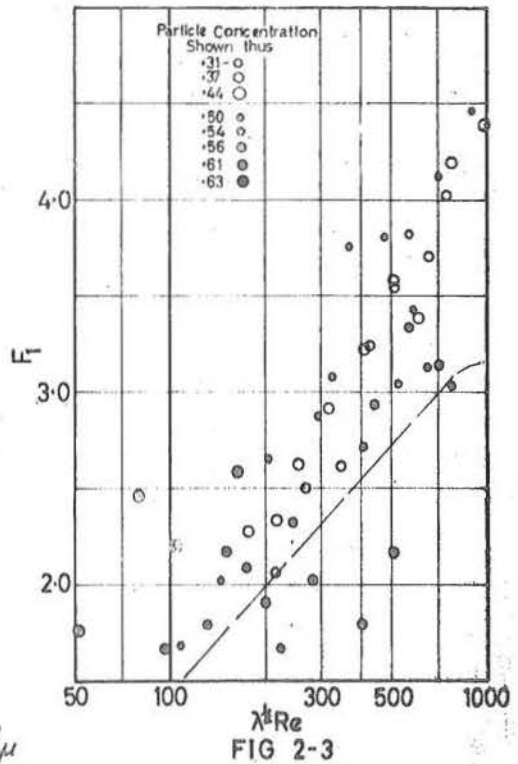

FIG 2-3

$$Re = \rho D^2 \left|\frac{du}{dy}\right| / \mu$$

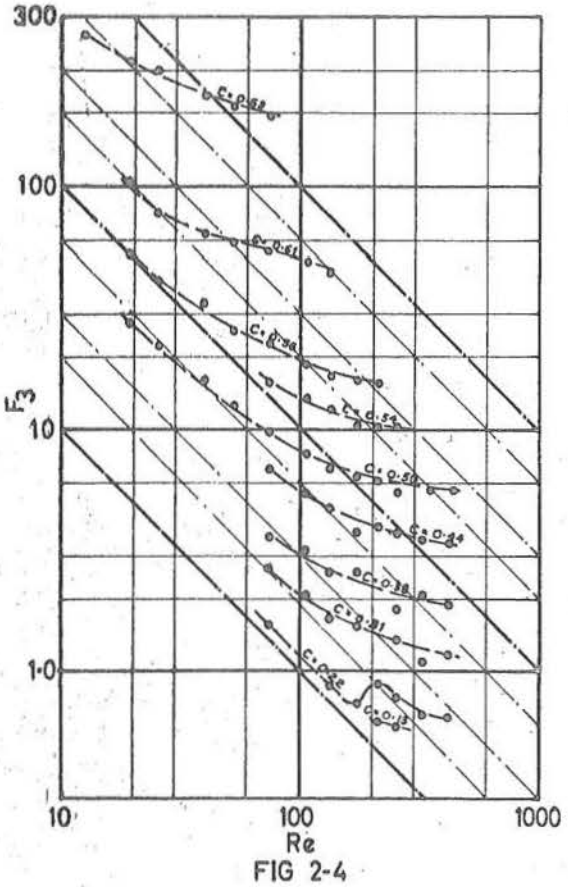

FIG 2-4

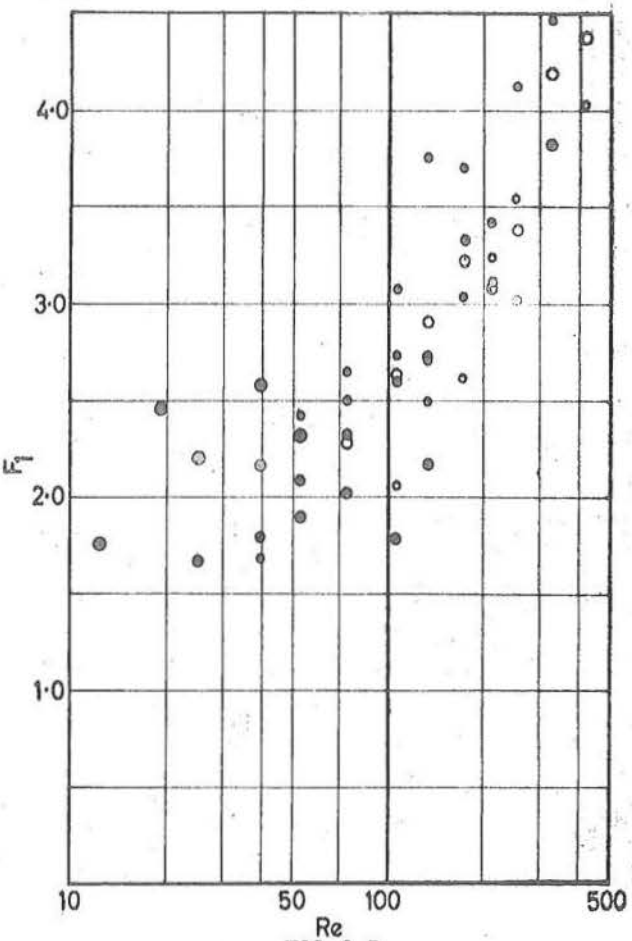

FIG 2-5

Bagnolds Experimental Results

Two different viscosities were used. The shear stress T_t and particle dispersive pressure P were both measured. From T_t, T was estimated, the correction required being small for all concentrations of interest. Bagnold arranged all of his results as graphs of $\rho D^2 T/\mu^2\lambda$ and $\rho D^2 P/\mu^2\lambda$ against $\lambda^{\frac{1}{2}}\rho D^2 \frac{du}{dy}/\mu$, forming for each of the dependent parameters $\rho D^2 T/\mu^2\lambda$ and $\rho D^2 P/\mu^2\lambda$ a single curve.

This single function relationship obtained by Bagnold can be written in terms of F_2, λ and Re_2 as follows. Noting that $\rho_s = \rho_f$ for all experiments,

$$F_2 = \frac{\lambda}{Re_2^2}\phi(\lambda^{\frac{1}{2}}Re) \text{ where } Re = \rho(\frac{du}{dy})D^2/\mu. \qquad (2\text{-}14)$$

Bagnold found that a similar relationship held for F_5 defined by $P = \rho_s(\frac{du}{dy})^2 D^2 F_5$ and it therefore follows that his results imply that F_7 is a unique function of $(\lambda^{\frac{1}{2}}Re)$, that is,

$$\frac{P}{T} = F_7 = F_7(\lambda^{\frac{1}{2}}Re). \qquad (2\text{-}15)$$

Bagnold measured T_t in his apparatus and then applied a somewhat arbitrary correction allowing for T_f to obtain T. This correction was very small at high concentrations and we will therefore examine Bagnold's results in terms of $F_3(Re)^2/\lambda$ and F_1 plotted against $\lambda^{\frac{1}{2}}Re$. To obtain F_3 and F_1, the measured values of T_t obtained from the results given in (6) are used.

Graphs of Bagnold's results plotted as $F_3(Re)^2/\lambda$ and F_1 against $\lambda^{\frac{1}{2}}Re$ are given in Figs. (2-2) and (2-3). Included in these Figs. are the curves fitted to these points by Bagnold.

In Fig. (2-4), Bagnold's experimental points are plotted on the F_3 - Re plane. These results show a definite trend towards Re independence for large Re. Also shown in Figs. (2-5) of this chapter and (3-12) of Chapter 3 are Bagnold's experimental values on the F_1 - Re and F_1 - C planes.

From (2-7),

$$F_2 = \frac{T}{\mu(\frac{du}{dy})} \left(\frac{\mu}{\rho_s D^2 (\frac{du}{dy})}\right)$$

$$= F_9/Re. \qquad (2\text{-}16)$$

And from (2-12) et.seq. F_9 tends to be a function of C alone for low values of Re_2, so that,

$$F_2 \rightarrow F_9(C)/Re. \qquad (2\text{-}17)$$

On the F_2 - Re plane, the curves for constant C should tend to approach, for low values of Re , the asymptotes,

$$F_2 = \text{Constant}/Re \ . \qquad (2\text{-}18)$$

Summary of Dimensional Analysis and Bagnold's Results

The results of the dimensional analysis can be summarised for the extreme values of Reynolds' number as,

$$F_3 = F_3(C, \frac{\rho_s}{\rho_f}),\ F_1 = F_1(C, \frac{\rho_s}{\rho_f}),\ Re_2 \text{ large} \qquad (2\text{-}19)$$

$$F_3 = F_9(C)/Re_2,\ F_1 = F_1\ (C, \frac{\rho_s}{\rho_f}),\ Re_2 \text{ small} \qquad (2\text{-}20)$$

Bagnold's numerical conclusions were that for $\rho_s/\rho_f = 1.0$,

$$\begin{aligned} F_2 &= 2.2\lambda^{3/2},\ F_7 = 1.33 \qquad (\text{for } \lambda^{\frac{1}{2}}R_e < 60) \\ F_2 &= 0.013\lambda^2,\ F_7 = 3.1 \qquad (\text{for } \lambda^{\frac{1}{2}}R_e > 300) \end{aligned} \qquad (2\text{-}21)$$

Other Methods of Obtaining F

The functions F_7 and F_1 are important in finding the concentration distribution and, as can be seen from Bagnold's experimental points on Fig. (2-3), the empirical curve shown is not very reliable. In Chapter 3 of this thesis, a theoretical approach to the problem is developed giving equations for F_1, F_2, F_3, F_7 and F_8 in terms of the concentration, for the particular case of a high Reynolds number Re .

In principle, F_3 and F_1 can be measured experimentally for any values of Re_2 and ρ_s/ρ_f. However, this is difficult in practice for values of ρ_s/ρ_f other than unity. This experimental approach for ρ_s/ρ_f = unity has been carried out by Miller (9) as well as Bagnold, and Miller also developed a theoretical approach. At present, however, experimentally reliable values for F_1 over the range $.05<C<0.63$ have not been obtained for $\rho_s/\rho_f = 1.0$ and there are no experimental values at all for $\rho_s/\rho_f \neq 1.0$.

DEVELOPMENT OF FLOW SYSTEM EQUATIONS FROM EQUATIONS FOR F

Initial Development

In 1956 Bagnold (7) extended the concept of a dispersive pressure to the analysis of steady state open channel flow problems. This analysis was based upon energy principles and included both suspended load and bed load. In this thesis, a different approach is used and only the behaviour of the bed is considered.

The situation of Fig. (2-1) with a steady two dimensional flow in the x direction is considered. The forces acting on an element of the system shown in Fig. 2-7 are equated to zero.

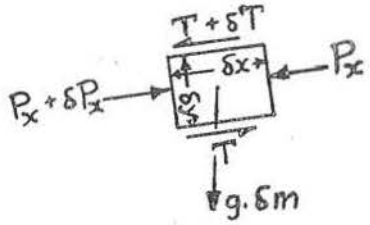

Fig. 2-7

In the x-direction, putting the average density of the element = $\rho_f + C(\rho_s - \rho_f)$,

$$\frac{dT_t}{dy} - \frac{dP_x}{dx} + \left[\rho_f + C(\rho_s - \rho_f)\right] g \sin\theta = 0, \qquad (2\text{-}22)$$

and in the y-direction,

$$\frac{dP_t}{dy} + \left[\rho_f + C(\rho_s - \rho_f)\right] g \cos\theta = 0. \qquad (2\text{-}23)$$

P_t includes the hydrostatic pressure as well as the interparticle action, the relative importance of the interparticle action increasing with concentration. If large scale turbulence sets in, the mixing action combined with a concentration gradient will induce an excess fluid pressure gradient in the -y direction above $\rho_f g \cos\theta$. This excess pressure gradient will be supporting the suspended load. As the concentration increases, the interparticle stress will increase. Also, as the bed is approached, the turbulence will decrease until for a sufficiently high concentration the large scale turbulence will be fully damped and $\frac{dP_f}{dy} + \rho_f g \cos\theta \rightarrow 0$. This region will be called the bed region in this thesis and in it we have,

$$\frac{dP}{dy} = -C(\rho_s - \rho_f) g \cos\theta . \qquad (2\text{-}24)$$

In the lowest part of the bed (2-24) will apply and in the region above this (2-23) is valid with $dP_f/dy + \rho_f g \cos\theta$ a function of the turbulent intensity as well as the concentration gradient dC/dy.

Equations for Bed Region

Substituting the constants,

$$B_1 = dP_x/dx - \rho_f g \sin\theta \qquad (2\text{-}25)$$

$$B_2 = (\rho_s - \rho_f) g \sin\theta \tag{2-26}$$

$$B_3 = (\rho_s - \rho_f) g \cos\theta \tag{2-27}$$

in equations (2-22) and (2-24) gives,

$$\frac{dT_t}{dy} = B_1 - B_2 C \tag{2-28}$$

$$\frac{dP}{dy} = - B_3 C \tag{2-29}$$

Integration of (2-28) and (2-29) gives the equations,

$$T_t = B_1 y - B_2 \int C \, dy + E_1 B_1, \tag{2-30}$$

$$P = - B_3 \int C \, dy + E_2 B_1, \tag{2-31}$$

where E_1 and E_2 are constants of integration. These constants will be considered later in the development of this argument.

From (2-6) we have $P/T_t = F_1$ and, by combining (2-30) and (2-31), we obtain,

$$\int C \, dy = B_1 \left[F_1 (y + E_1) - E_2 \right] / (F_1 B_2 - B_3). \tag{2-32}$$

Differentiating equation (2-32) with respect to y, and noting that C and F_1 will both be functions of y,

$$\frac{C}{B_1} = \left[\frac{F_1 + \frac{dF}{dy} 1 (y + E_1)}{F_1 B_2 - B_3} \right] - B_2 \frac{dF}{dy} 1 \left[\frac{F_1 (y + E_1) - E_2}{(F_1 B_2 - B_3)^2} \right] \tag{2-33}$$

If F_1 is a function of C, which can in principle be found either theoretically or experimentally, equation (2-33) can

be rearranged. We note that,

$$\frac{dF_1}{dy} = \frac{dF_1}{dC}\,\frac{dC}{dy} \quad . \tag{2-34}$$

Substitution of (2-34) in (2-33) and rearranging gives,

$$\frac{dC}{dy} = \frac{\left[(F_1B_2 - B_3)C - F_1B_1\right](F_1B_2 - B_3)}{B_1\left[B_2E_2 - B_3(y + E_1)\right](dF_1/dC)} \tag{2-35}$$

The terms F_1 and dF_1/dC in equation (2-35) can both be obtained as functions of C from experiments or from a theory such as in Chapter 3. Also, B_1, B_2 and B_3 are known for a particular flow situation and, if E_1 and E_2 can be evaluated, equation (2-35) can be integrated. The relatively simple form of (2-35) depends on F_1 being dependent on C alone.

Evaluation of E_1 and E_2 for an Open Channel

In the suspended load region, F_1 is not a function of C alone. This means that the use of (2-35) depends upon evaluation of E_1 and E_2 in the bed region. Physically, we have an equation for the concentration gradient but, to apply it, we need two further equations. For any particular non-cohesive material, the shear stress required for general shearing action to take place is proportional to the normal stress acting on the material. Shearing will be assumed to take place if

$$P/T_t \leq F_{1c}, \tag{2-36}$$

where F_{1c} is the critical value of F below which a shear failure of the packed bed will occur.

The shear stress at the bed will depend upon the conditions in the flow above the bed, particularly the slope and depth. The depth is dependent upon the discharge, which would normally be known. At this point in the argument, we will assume that the shear stress at the top surface of the fixed bed is known. This particular assumption has the advantage of simplicity in application. From the complete analysis of the flow, including the suspended flow region, it would be possible to obtain from a given slope and assumed shear stress at the top of the fixed bed the discharge of fluid Q. As Q is normally known, the bed analysis would proceed by trial and error. First, a shear stress for the top of the fixed bed would be assumed and Q calculated. As Q is more sensitive to changes in depth than the bed shear, this method of solution will always converge. The shear stress at the level of shear failure in the bed will be called T_b.

If y is taken as zero at this failure plane, the integral $\int C dy$ will also be zero. Therefore, from equation (2-30) we obtain,

$$T_b = E_1 B_1 \qquad (2\text{-}37)$$

and also from equation (2-32), if F_{1b} is the value of F_1 at the

failure zone,

$$F_{1b}E_1 - E_2 = 0. \tag{2-38}$$

Final Solution for Open Channel Flow

By substitution of (2-37) and (2-38) into (2-35), the constants E_1 and E_2 are eliminated, leaving the equation,

$$\frac{dC}{dy} = \frac{\left[C(F_1B_2 - B_3) - F_1B_1\right](F_1B_2 - B_3)}{\left[T_bB_2F_{1b} - B_3(yB_1 + T_b)\right] dF_1/dC} \tag{2-39}$$

By dividing by B_3 the numerator and denominator of the right hand member, we obtain

$$\frac{dC}{dy} = \frac{B_3\left[C(F_1(\frac{B_1}{B_3}) - 1) - F_1(\frac{B_1}{B_3})\right](F_1(\frac{B_2}{B_3}) - 1)}{\left[T_bF_{1b}(\frac{B_2}{B_3}) - (yB_1 + T_b)\right]\frac{dF_1}{dC}} . \tag{2-40}$$

From equations (2-25), (2-26) and (2-27),

$$B_2/B_3 = \tan\theta \tag{2-41}$$

and

$$B_1/B_3 = \frac{dh}{dx} - \frac{\tan\theta}{S} \tag{2-42}$$

where $h = P_x/(\rho_s - \rho_f)\, g \cos\theta$, and $S = \rho_s/\rho_f - 1$.

Substitution of (2-41) and (2-42) into (2-40) gives for $\frac{dh}{dx} = 0$, the open channel case,

$$\frac{dC}{dy} = (\rho_s - \rho_f) g \cos\theta \frac{\left[C(1-F_1 \tan\theta) - \frac{F_1 \tan\theta}{S}\right]\left[1-F_1 \tan\theta\right]}{\left[T_b(F_{1b}\tan\theta - 1) + \rho_f gy \sin\theta\right]\left(\frac{dF_1}{dC}\right)} \qquad (2\text{-}43)$$

Discussion of Solution

The term dF_1/dC is the first to be examined. If $dF_1/dC = 0$, that is, F_1 is a constant as assumed by Bagnold in his first paper, then, if $\rho_s \neq \rho_f$, from (2-43) one or more of the following three equations must be valid,

$$(i) \quad \frac{dC}{dy} \to \infty$$

$$(ii) \quad 1 - F_1 \tan\theta = 0 \qquad (2\text{-}44)$$

$$(iii) \quad (1 - F_1 \tan\theta)\, C = + F_1 \tan\theta / S \qquad (2\text{-}45)$$

The physical system described by equation (2-44) and (2-45) is now examined. Noting that $\tan\theta$ is a constant for any given channel, equation 2-44 implies F_1 is constant and equal to $\cot\theta$. Therefore, as F_1 is assumed constant, the situation is a channel of slope $= \tan^{-1} 1/F_1$. Such a channel will be sufficiently steep to transport the solids in a thick layer the full depth of the channel, that is, a saturated gravel slide.

In equation (2-45), F_1, and S are constant, so that (2-45) gives an equation for C,

$$C = \frac{F_1 \tan\theta}{S(1 - F_1 \tan\theta)}$$

and the physical situation is a uniform concentration throughout the flow.

If dC/dy is finite and F_1 is a constant, one of the two situations considered above must exist. Observation shows that, for many channels, $\tan\theta$ is small and C is not a constant given by equation (2-45). From now on we will consider F_1 is some unknown function of C as from the above $F_1 \neq$ constant.

To integrate (2-43), the concentration at a given level in the region of integration must be known. The value of C at y = 0 will be used for this purpose and denoted by C_b.

One particular solution is given when

$$\tan\theta = 1/F_{1b} \left(1 + \frac{1}{C_b S}\right) \qquad (2\text{-}46)$$

In this case, dC/dy = 0 and therefore C is constant and equal to C_b for all y below the free surface. If $\tan\theta$ is less than the value given in (2-46) - and this will be the usual case for a river - the following argument will apply. First the value of C_b will be examined.

Maximum Value of C in Moving Bed

When $F_1(C)$ has a maximum value, the behaviour of the concentration will be governed by which side of the maximum is considered. If C_b is taken such that $dF_1/dC < 0$ is considered, the only solution of equation (2-43) possible is for dC/dy to be positive and therefore for C to increase rapidly. This

solution cannot be fitted to any realistic boundaries (finite shear and finite total load at the bed) or to a small value of C for large y.

If, however, $dF_1/dC>0$ for $C = C_b$, then dC/dy is negative and a real solution is possible for the open channel flow case with $\tan\theta$ small. It follows from the above that an upper limit to C_b will be the value of C giving the maximum value of F_1.

Examination of Bagnold's results, Fig. 3-12, shows a definite tendency for a sharp drop in F_1 to occur for concentrations just above 0.50. At about the same concentration, numerical studies of elastic spheres have shown a similar discontinuity. This maximum in $F_1(C)$ is discussed in more detail in Chapter 3 of this thesis. The concentration of particles at the bottom of the moving bed layer will therefore be less than or equal to 0.50.

From equations (2-43) to (2-45) it can be seen that the concentration immediately above the bed will be reduced until dF_1/dC is greater than 0 or until equation (2-45) is satisfied. The theory developed in Chapter 3 predicts $dF_1/dC = 0$ from about $C = 0.40$ to $C = 0.50$. An assumption of a high value of C will not lead to error in the calculations as the integrated form of (2-43) will show a step change in concentration from 0.50 to 0.40, or if (2-45) holds for some value of C in the range

$0.50 > C > 0.40$, from 0.50 to this value of C.

At a concentration of 50 per cent, the particles are capable of supporting a greater load through interparticle stresses than could exist at the time of initial shear failure. The surface between the fixed and moving bed is expected to have an F_1 similar to that in the moving part of the bed.

If a flow was slowly increasing, the initial parameter would be F_{1c} and immediately above the bed there would exist a concentration such that F_1 for the moving material was equal to F_{1c}. If the theory in Chapter 3 applied, it follows that there would be a concentration of probably less than 10 per cent immediately above the bed. If the flow was decreasing, however, the material would continue to move until the concentration immediately above the bed exceeded 0.50. In this second case, the total mass of material moving over a unit area of the bed will be greater as this is governed by F_1 at the base of the moving layer, that is, F_{1b}.

If the flow is steady, local fluctuations may cause spasmodic erosion and deposition of particles. The existence of a stable band of values of F_1 where neither erosion or deposition will occur will tend to reduce the rate of return to equilibrium flow.

The equilibrium value of F_1 in this case will lie between the two extreme values of F_{1c} and the maximum value of F_1.

The exact position in this region is difficult to determine. However, as both erosion and deposition will be occurring, F_1 will be close to the mid-point of the stable band.

Velocity Profile

The previous section discusses the concentration profile. The shear stress and F_3 profiles follow directly from this concentration profile. Hence, the velocity gradient can be obtained from equation (2-8) rearranged as follows:

$$\frac{du}{dy} = \frac{(T_t/F_3)^{\frac{1}{2}}}{\rho_s^{-\frac{1}{2}} D} \quad . \qquad (2\text{-}47)$$

Numerical integration of (2-47) from u = 0.0 at y = 0.0 gives the velocity profile in the bed region of the flow. The upper limit beyond which large scale turbulence will occur is discussed in Chapter 3. No attempt is made in this thesis to extend the analysis into this region of large scale turbulence.

Specific Solutions

Equation (2-43) can be written in the form:

$$\frac{dC}{dy} = \frac{\phi(C)}{f(C) - ky}$$

or:

$$\left(\frac{dy}{dC} + ky\right)/\phi(C) = f(C)/\phi(C) \quad . \qquad (2\text{-}48)$$

This is a linear equation and y can be solved in general using an integrating factor approach.

$$y(C) = e^{-h}\left[\int e^{h}\ (f/\phi)\ dC + C\right] \text{ where } h = k\int\frac{dC}{\phi} \quad . \quad (2\text{-}49)$$

As ϕ and therefore h are not simple functions, the integrals can, in general, only be solved numerically. However, it is possible to solve (2-42) directly by a finite difference method.

If a new function De of C and θ is introduced such that

$$De = \frac{dF_1}{dC}\Big/\left[C(1-F_1\ \tan\theta) - F_1\ \tan\theta/S\right](1-F_1\ \tan\theta), \quad (2\text{-}50)$$

then from equation (2-42)

$$\frac{dC}{dy} = (\rho_s-\rho_f)\ g\ \cos\theta\Big/De\left[T_b(F_{1b}\tan\theta - 1)+\rho_f\ g\ y\ \sin\theta\right] \quad (2\text{-}51)$$

and, taking the reciprocal of each side,

$$\frac{dy}{dC} = De\left[\frac{T_b(F_{1b}\ \tan\theta - 1)}{(\rho_s-\rho_f)\ g\ \cos\theta} + \frac{y\ \tan\theta}{S}\right], \quad (2\text{-}52)$$

$$= De\ (H_1 + y\ H_2). \quad (2\text{-}53)$$

Both H_1 and H_2 are constants for a given system and De is a function of C, S and θ. The simplest form of (2-53) to use is

$$\Delta y_i = \left[De\ H_1 + y\ H_2\right]\Delta C_i, \quad (2\text{-}54)$$

where H_1 and H_2 are evaluated for $C = \frac{1}{2}(C_i + C_{i+1})$. A higher order of approximation can be used after the first values

of y have been calculated or, if y is replaced by $y + \frac{1}{2}\Delta y_i$, we obtain

$$y_i = \frac{De(H_1 + yH_2)\ C}{1 - \frac{1}{2}De\ C\ H_2} \qquad (2\text{-}55)$$

Equation (2-55) also gives an indication of when (2-54) is liable to be inaccurate. This is when $\frac{1}{2}De\ C\ H_2$ is not small compared with unity.

For the particular case of particles of specific gravity 2.65, De has been calculated and a table containing F_1 and dF_1/dC as used in the calculation and the resulting values of De at four different values of $\tan\theta$ is given below in Table (2-1). In this table, the values of F_1 used are those obtained from Fig. (7-1) based on experimental work described in subsequent chapters. dF_1/dC was obtained by numerical differentiation of the table of F_1 as a function of C. Consequently, the accuracy with which De was obtained decreases at the extreme ends of the range of concentrations. As the curve of F_1 is not reliably known, the results for De are illustrative of the method and will not be any more reliable than F_1.

Table 2-1

C	F_1	$\frac{dF_1}{dC}$	De		
			$\tan\theta = 0.00$	$\tan\theta = 0.01$	$\tan\theta = 0.10$
0.05	0.24	5.0	100	103	149
0.10	0.50	6.2	62	64	96
0.15	0.86	7.2	48	50	84
0.20	1.23	8.3	41	44	81
0.25	1.75	12.7	51	54	121
0.30	2.46	14.4	48	52	160
0.35	3.05	9.6	27	30	117
0.40	3.42	6.3	15.7	17.4	72
0.45	3.67	3.3	7.3	8.1	33

Values of De are calculated for S = 1.65 and three separate values of $\tan\theta$. Calculations are based on F_1 estimated from experimental results.

The values of De obtained from Table (2-1) have been plotted against concentrations in Fig. (2-8).

SUMMARY

A method of calculating the concentration profile in a channel has been developed. This problem has been reduced to the integration of

$$\frac{dC}{dy} = \frac{1}{De\ (H_1 + y\ H_2)} \qquad (2\text{-}53)$$

in the positive y direction from the surface separating the moving bed material and the fixed bed. De has been defined in equation (2-50), tabulated in Table (2-1) and plotted in Fig. (2-8). The constants H_1 and H_2 are given by

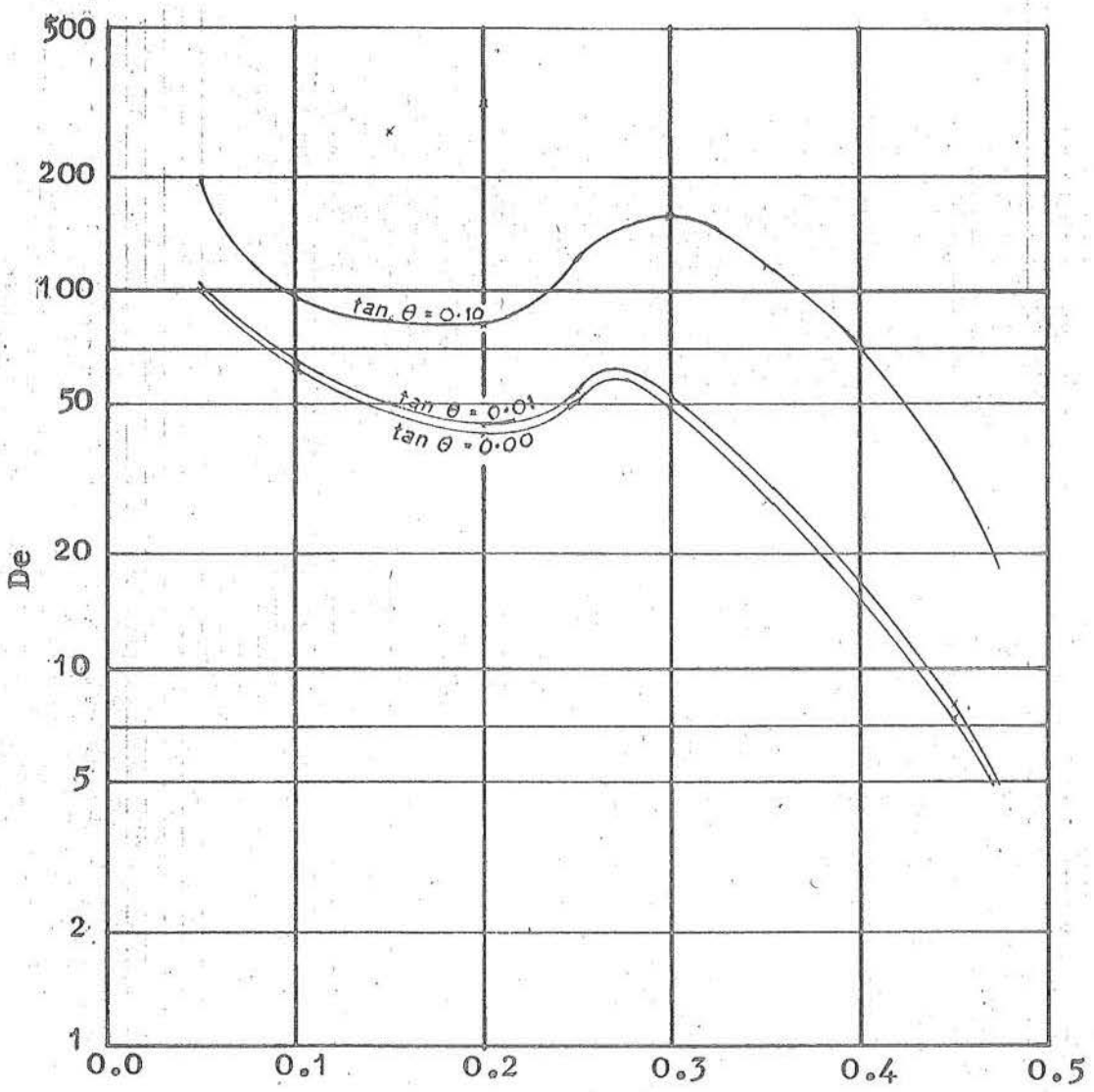

FIG 2-8

De as a function of concentration for $\rho_s = 2.65\rho_f$ and three values of tan θ

$$H_1 = T_b (F_{1b} \tan\theta - 1)/(\rho_s - \rho_f) g \cos\theta \qquad (2\text{-}56)$$

$$H_2 = \tan\theta / S \text{ where } S = \frac{\rho_s}{\rho_f} - 1 \qquad (2\text{-}57)$$

and are constant for a given flow, H_1 varying for different bed conditions.

The results of the calculation depend on the value of F_{1b} used at the separating surface, this value being determined to some extent by the previous history of the flow. If this value of F_{1b} is in error, then the total material in the moving bed region per unit area of bed will be in error by the same proportion. For most flows, $\tan\theta$ is small and, as dF_1/dC is small for high values of concentration, the region of high concentration of solids will also be small.

The concentration profile depends on the bed shear stress which in turn depends on the depth and hence the total flow. But the depth for a given flow is a function of the concentration profile.

The process of solution for a known total fluid flow rate is therefore to estimate $T_b (1 - F_{1b} \tan\theta)$ and carry out the integration of (2-53). The solution of the concentration and velocity profiles should then be carried through the suspended load region, although methods for carrying out this particular calculation have not been included in this thesis. The result of the complete calculation would be a given total

fluid and solid flow rate. The calculated fluid flow would be compared with the true value and then, using equation (2-58) below, a new estimate of T_b could be obtained by calculating the correction to the depth. This process would have to be repeated until the calculated Q converged on the required value.

An estimate of the bed shear stress can be obtained from an estimate of the depth d by writing the equation for shear at the bed,

$$T_b = (F_{1b}\, T_b + (\rho_s - \rho_f)\, g \int_0^\infty C_s\, dy + g\, \rho_f d)\, \tan\theta\,,$$

where C_s is the volumetric concentration of suspended load. Rearranging, we obtain

$$T_b\,(1 - F_{1b}\, \tan\theta) = g\, \rho_f d\, \tan\theta + (\rho_s - \rho_f)\, g \int_0^\infty C_s\, dy. \quad (2\text{-}58)$$

From this, it can be seen that a complete solution of the bed region requires a knowledge of the behaviour of the suspended load region, both to evaluate the integral in (2-58) and to calculate the velocity of flow above the bed region.

CHAPTER 3

THEORETICAL DEVELOPMENT OF F_i

SYNOPSIS

In this section, a model of particle behaviour, exhibiting similar properties to those determined by Bagnold (6), is examined. The viscosity equation for a gas of elastic spheres is used, as has been done by J. B. Miller (9).

In the theory of a perfectly elastic set of spheres, the properties of the colliding spheres are related to the r.m.s. velocity of the spheres, usually in a gas described by the temperature. Using dimensional reasoning, Miller (9) assumed that the r.m.s. velocity was proportional to the velocity gradient. In this thesis, we use instead an equation relating the energy supplied to a region, to the energy absorbed in various mechanisms, the predominant one being interparticle collisions.

Using the energy and viscosity equations, the relations between the shear stress, rate of strain and interparticle stress can be calculated without resort to any arbitrary constants. Throughout this section, we have assumed a force function between the particles in the form of an impulse. One requirement for a sudden impulsive force is that the inertial forces are large compared with the viscous forces, that is, the particle Reynolds number is large.

In the first section, we will develop the equations ignoring the effect of the surrounding fluid. In the next sections, we will consider the effect of the surrounding fluid and the limitations of the results. The final result of the chapter is in the form of equations relating the shear stress and dispersive stress in a fluid particle system to the geometric and kinematic properties of the system.

INITIAL ASSUMPTIONS

We consider a model of rigid elastic spheres and use the results of workers in the statistical mechanics of molecules. Various proposed force functions between molecules have been used and for our purposes we will assume that the only inter-particle force is an impact at collision. This is the simplest possible model available and extensive work has been carried out on it. For molecular theory, a basic assumption is the conservation of energy at collision. However, in the present case, a considerable loss of energy occurs during collisions. It has been found that the results of the simplified theory of no loss at collision can be applied to the case where there is energy transfer to the internal vibration of the molecules (10). It is therefore assumed that the results can be applied to non-elastic particles to give the correct velocity distribution of the particles and hence

the correct viscosity and pressure distribution. This assumption has, in effect, been made by Miller (9) who also gives a discussion of the errors likely to arise because of it.

The loss of energy per unit volume in our first simple model is assumed to be proportional to the square of the particles' relative velocity and a function of the distribution of possible collisions. This is equated to the energy supply per unit volume $\mathbb{T} \frac{du}{dy}$, the shear stress times the velocity gradient, which is, in effect, an assumption of no dispersion of energy between different levels. This will be true in the case of small changes in properties over a distance equal to the mean free path of the particles.

CALCULATIONS IGNORING THE SURROUNDING FLUID

Velocity Distribution

The mean velocity distribution will have superimposed on it a fluctuating velocity which we will assume has the probability distribution,

$$p\ (u,v,w) = \left(\frac{a}{\pi}\right)^{3/2} e^{-a(u^2+v^2+w^2)}, \qquad (3\text{-}1)$$

where u, v and w are the velocity components in three mutually perpendicular directions, and a is a constant. This distribution is normal along any radius from the origin and symmetrical

about the origin.

If (3-1) is transformed into a co-ordinate system s, θ, ϕ, where s, θ, ϕ are the magnitude, longitude and latitutde of the velocity vector, we have from Fry (11),

$$p\ (s,\theta,\phi) = \frac{\partial(u,v,w)}{\partial(s,\theta,\phi)}\ p\ (u,v,w) \qquad (3\text{-}2)$$

If we put $u = s\cos\theta\cos\phi$, $v = s\cos\phi\sin\theta$, $w = s\sin\phi$, then the Jacobian becomes

$$\frac{\partial(u,v,w)}{\partial(s,\theta,\phi)} = s^2\cos\phi$$

and we have, therefore,

$$p\ (s,\theta,\phi) = \left(\frac{a}{\pi}\right)^{3/2} s^2\cos\phi\ e^{-as^2}. \qquad (3\text{-}3)$$

To obtain the probability distribution of s, we now integrate (3-3) with respect to θ and ϕ from 0 to 2π and obtain

$$p(s) = 4\sqrt{\frac{a^3}{\pi}}\ s^2\ e^{-as^2} \qquad (3\text{-}4)$$

where s is the magnitude of the fluctuating velocity vector.

Similarly, integrating (3-1) with respect to v and w for all v and w we obtain

$$p(u) = \sqrt{\frac{a}{\pi}}\ e^{-au^2}. \qquad (3\text{-}5)$$

Now the mean value of s can be calculated from (3-4) as follows:

$$\bar{s} = \int_0^\infty 4\sqrt{\frac{a^3}{\pi}}\, s^3 \cdot e^{-as^2}\, ds$$

$$= \sqrt{\frac{2}{\pi a}} \qquad (3\text{-}6)$$

Similarly,

$$\overline{s^2} = \frac{3}{2a}$$

In the kinetic theory of gases, $a = \frac{m}{2k\ Te}$ where Te is the gas temperature, m the mass of the molecule and k a constant. The relation between $\bar{s}$ and Te is from (3-6) of the form,

$$\bar{s} = 2\sqrt{\frac{2k\ Te}{m\ \pi}} \qquad (3\text{-}7)$$

Viscosity

The viscosity of a dilute gas is normally given in terms of (k, Te), but all quoted equations will be transformed to give the viscosity in terms of the mean velocity magnitude $\bar{s}$ using (3-7).

The general form of the equation for viscosity is,

$$\mu = A_1 \frac{m\bar{s}}{D^2} \qquad (3\text{-}8)$$

where m and D are the mass and diameter of the particles and A_1 is a constant calculated in Hirschfelder (10) to be $\frac{5}{32\sqrt{2}}$. From Miller (9), substituting in terms of $\bar{s}$, we obtain

$A_1 = \frac{5\sqrt{3}}{32\sqrt{2}}$. By a simple approximate method given by Hirschfelder (10), it is found that $A_1 = \frac{.286}{\pi}$. Both the approximate value and exact value calculated in (10) are similar and we shall use $\frac{5}{32\sqrt{2}}$ as the value of A_1 for all our calculations.

In dealing with a dense gas, a function, Y, of the concentration, is defined such that the pressure is given by the equation

$$P = n\,k\,Te\,(1 + Y) \qquad (3\text{-}9)$$

which, by substituting from (3-7), gives

$$P = nm\bar{s}^2\,\frac{\pi}{8}\,(1 + Y). \qquad (3\text{-}10)$$

The function Y can be obtained as a polynomial in C called a virial expansion. The Enskog theory of dense gases gives rise to an equation for viscosity (10, p.645) in terms of the proportion of space occupied by the molecules. After substituting for the molecular volume in terms of C (the volume of space occupied by the particles), this viscosity equation becomes

$$T/\frac{du}{dy} = A_1\,\frac{m\bar{s}}{D^2}\,4C\,\left(\frac{1}{Y} + 0.8 + 0.761\,Y\right) \qquad (3\text{-}11)$$

Calculation of Y

To obtain Y as a function of the concentration, the

results of gas dynamics are used. Much work has been done in gas dynamics to find Y as a function of C for various laws of attraction (or repulsion) between molecules. The simplest form of molecule is the rigid elastic sphere. This is a good approximation if the repulsive force is a short range type, as would be the case for the particles considered. A more refined form of the repulsion force could, in fact, be used, as is frequently the case with molecular dynamics calculations (10).

The most serious approximation made, however, is in assuming that the elastic collisions are equivalent in their effect on the molecules to inelastic collisions with a continuous supply of energy keeping $\bar{s}$ constant. The equations of conservation of mass and momentum will not be affected by this non-elastic behaviour and the situation could be considered similar to molecules capable of storing some energy of collision as internal vibration. We will asume, therefore, that the elastic sphere gas model is suitable for calculating Y.

Even then, however, we have different models giving different relations between Y and C. One of the most widely used methods of calculating Y is to use a virial expansion, i.e., a series expansion in powers of C. A discussion of the derivation of the coefficients of the series is given in Hirschfelder (10, p.131-157) for rigid spheres and continuing

to other shapes and potential functions. Numerical experiments carried out by Alder and Wainwright (12) have shown very close agreement with the fourth order virial expansion up to concentrations greater than 30 per cent and this was improved empirically by fitting a fifth order virial term, this final expansion being used by J. B. Miller (9). Miller's results are in error because of an algebraic error in changing the independent variable to C.

A method using the radial distribution function (13) has been developed to give a relation between C and Y which can be used to obtain Y for densities up to the liquid state. All these relations are plotted in Fig. (3-7). The behaviour of the particles is assumed to be similar to that of the molecules of a gas and to have a minimum of order. This could possibly be modified in certain regions by the effect of gravity tending to give an ordered form to the particles. This would not be expected to be very stable, however, and so the gas model will be used and the virial expansion with the empirical fifth coefficient will be used to obtain Y.

This expansion is given by

$$Y = 4C + 0.6250(4C)^2 + 0.2869(4C)^3 + 0.115(4C)^4 + 0.079(4C)^5. \quad (3\text{-}12)$$

Table (3-1) gives Y as a function of C and a graphical plot of Y obtained by various methods is given in Fig. (3-7).

Energy Equation

The energy dispersion will be small wherever $\frac{D+\bar{l}}{D}\frac{dC}{dy}$ and $\frac{(D+\bar{l})}{\bar{s}}\frac{d\bar{s}}{dy}$ are small where $\bar{l}$ is the mean free path of the particles. This will be true for movement of a layer many stone diameters thick except in a possible region of rapid concentration change near the top of the bed layer. It is therefore assumed that all the energy supplied in a given region is dissipated in that region.

If the collision rate is f collisions per unit volume per second, then we have the energy production $T\frac{du}{dy}$ equal to the dissipation

$$T\frac{du}{dy} = K_2 f m\bar{s}^2 \qquad (3\text{-}13)$$

where K_2 is a constant to be determined. The collision rate can be predicted from the Enskog theory and this prediction has been verified up to very high concentrations by numerical experiments of Alder and Wainwright (12). The results of this calculation are

$$f = A_2 n^2 D^2 \bar{s}\frac{Y}{4C}, \qquad (3\text{-}14)$$

where n is the number of particles per unit volume.

In this equation, Alder and Wainwright put $A_2 = 2\sqrt{\frac{\pi}{3}}$ whereas Hirschfelder (10) uses $A_2 = \sqrt{\frac{\pi}{2}}$ which is approximately 7½ per cent higher.

Substituting (3-14) into (3-13) gives for the energy

equation

$$T \frac{du}{dy} = K_2 A_2 n^2 D^2 \bar{s}^3 m Y/4C \quad . \qquad (3\text{-}15)$$

Elimination of $\bar{s}$

Multiplication of (3-11) and (3-15) gives

$$T^2 = K_2 A_1 A_2 m^2 \bar{s}^4 n^2 Y \left(\frac{1}{Y} + 0.8 + 0.761 Y\right). \qquad (3\text{-}16)$$

Substituting (3-16) in (3-11), we obtain

$$T = \left(\frac{du}{dy}\right)^2 \frac{m}{nD^4} A_1^{3/2} 16C^2 \left(\frac{1}{Y} + 0.8 + 0.761Y\right)^{3/2} (K_2 A_2 Y)^{-1/2}$$

and, putting $m = D^3 \rho_s/6$ and $n = \frac{\rho_s C}{m}$, where ρ_s is the density of particles, gives

$$T = \rho_s D^2 \left(\frac{du}{dy}\right)^2 \frac{\pi^2}{9} \frac{A_1^{3/2}}{\sqrt{A_2}} \frac{4C}{\sqrt{K_2}} \left(\frac{1}{Y} + 0.8 + 0.761 Y\right)^{3/2} Y^{-1/2} \qquad (3\text{-}17)$$

Similarly, by substituting (3-16) into (3-10), we obtain for the pressure P,

$$P = T \frac{\pi}{8} (1 + Y) \left[Y \left(\frac{1}{Y} + 0.8 + 0.761 Y\right) K_2 A_1 A_2\right]^{-1/2}, \qquad (3\text{-}18)$$

where P and T are the normal and shear stresses caused by interparticle collisions.

Calculation of K_2

To obtain numerical values of $T/\rho_s D^2 \left(\frac{du}{dy}\right)^2$ and P/T from equations (3-17) and (3-18), it is necessary to know the

value of K_2. It is assumed that the fluctuating velocity is independent of position of the particles and that the probability of two particles colliding is proportional to their relative velocity of approach.

Consider an arbitrary rectangular co-ordinate system. Then the probability density for a velocity component u in any given direction is given by (3-5),

$$p(u) = \sqrt{\frac{a}{\pi}}\, e^{-au^2} \quad .$$

We consider another particle with the same probability distribution of velocity. Then the difference of the u components of velocity, which we will denote by x, has a probability density given by

$$p(x) = \int_{-\infty}^{+\infty} p(u)\, p(u + x)\, du$$

which, by substitution from (3-5), gives

$$p(x) = \frac{a}{\pi} \int_{-\infty}^{+\infty} e^{-au^2}\, e^{-a\,(u + x)^2}\, du \quad .$$

Rearranging and substituting $z = u + \frac{x}{2}$, we obtain

$$p(x) = \frac{a}{\pi}\, e^{-ax^2/2}\, 2 \int_{0}^{+\infty} e^{-2az^2}\, dz$$

and, carrying out the integration, gives

$$p(x) = \frac{1}{2} \frac{a}{\pi}\, e^{-ax^2/2} \qquad (3\text{-}19)$$

which is the same form as (3-5) with a/2 where a occurs in (3-5), and so we have from (3-4) for the probability density of the magnitude of the relative velocity s_r

$$p(s_r) = \sqrt{\frac{2a^3}{\pi}}\, s_r^2\, e^{-as_r^2/2} \qquad (3\text{-}20)$$

If the collision rate is proportional to s_r, then the r.m.s. relative velocity magnitude at collision is given by

$$\overline{s_r^2} = \int_0^\infty s_r^3\, p(s_r)\, ds_r \Big/ \int_0^\infty s_r\, p(s_r)\, ds_r \,.$$

Substituting $z = as_r^2/2$, we obtain

$$\overline{s_r^2} = \frac{4}{a^3} \int_0^\infty z^2 e^{-z} dz \Big/ \frac{2}{a^2} \int_0^\infty z e^{-z} dz$$

which becomes, on carrying out the integration and putting $\bar{s} = 2/\sqrt{\pi a}$,

$$\overline{s_r^2} = \frac{4}{a} = \pi \bar{s}^2 \qquad (3\text{-}21)$$

Consider now a co-ordinate system embedded in one particle and another particle touching the first with a velocity $\underline{s_r}$ at an angle θ to the line joining the particle centres, as shown in Fig. 3-1.

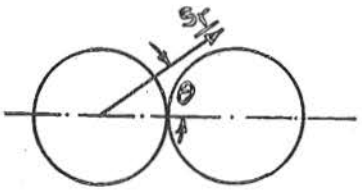

Fig. 3-1

Now, the loss of energy at impact will be taken to be $Kms_r^2 \cos^2\theta$. This is K times the kinetic energy of the approaching particle along the line of centres relative to a velocity equal to the mean of the approach velocities.

The loss of energy caused by tangential forces is ignored. K is thus just unity, less the coefficient of restitution of the particles measured under water.

The mean value of $\cos^2\theta$ at impact is now required and we shall set up the simple model of a single particle surrounded by 12 others, all equally spaced at a centre to centre distance 1, as in Fig. 3-2.

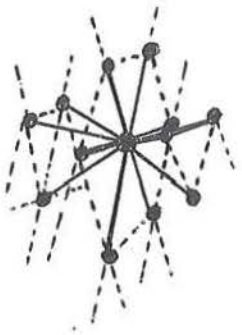

Fig. 3-2

The concentration C is given by

$$C = \frac{\sqrt{2}\,\pi}{6} \left(\frac{D}{1}\right)^3 \qquad (3\text{-}22)$$

A sphere of radius 1 passes through all the surrounding particles and it will be considered necessary for a collision between the central particle and a particular one of the

surrounding particles for the pathline of the centre particle to pass inside a cone of semi-angle α such that the area of sphere included is 1/12 of the total sphere. From geometric considerations,

$$\cos\alpha = 5/6 \ . \qquad (3\text{-}23)$$

Consider the plane containing the centres of the central and the colliding surrounding particle as well as the pathline. This is shown in Fig. (3-3):

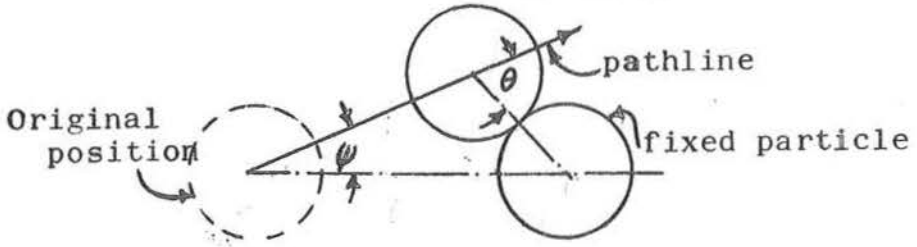

Fig. (3-3)

To find $\overline{\cos^2\theta}$ from Fig. (3-3), we first obtain from the geometry

$$\cos^2\theta = 1 - \frac{l^2}{D^2}\sin^2\psi \ . \qquad (3\text{-}24)$$

As the area of sphere covered by changing from ψ to $\psi + \delta\psi$ is $2\pi l^2 \sin\psi$,

$$\overline{\cos^2\theta} = \int_0^{\alpha} \cos^2\theta \; 2\pi l^2 \sin\psi \, d\psi \Big/ \int_0^{\alpha} 2\pi l^2 \sin\psi \, d\psi \qquad (3\text{-}25)$$

and, substituting (3-24) in (3-25),

$$\overline{\cos^2\theta} = \int_0^{\alpha} \left(\sin\psi - \frac{l^2}{D^2}\sin^3\psi\right) d\psi \Big/ \int_0^{\alpha} \sin\psi \, d\psi \ .$$

Integrating and putting $\cos\alpha = 5/6$ gives

$$\overline{\cos^2\theta} = 1 - \frac{17}{108}\frac{l^2}{D^2} \quad \text{for } D<l<2D \qquad (3\text{-}26)$$

If $l>2D$, then the problem is reduced to finding the mean of $\overline{\cos^2\theta}$ given that a collision does occur. On any plane drawn perpendicular to the pathline, there will be a uniform probability of the pathline crossing a given area of the plane.

This gives the equation

$$\overline{\cos^2\theta} = \int_0^D \cos^2\theta \; 2\pi r \, dr \,/\pi D^2 \;, \qquad (3\text{-}27)$$

where r is the radius in the plane from the centre of the stationary particle.

Integrating (3-27), we obtain

$$\overline{\cos^2\theta} = \tfrac{1}{2}, \quad 2D < l \;. \qquad (3\text{-}28)$$

It can be seen that at $l = 2D$ (3-28) and (3-26) give different values of $\overline{\cos^2\theta}$ and, to avoid this discontinuity, the constant 1.0 in (3-26) will be modified to 1.082. Making this modification and using (3-22) to transform from l to C gives

$$\left.\begin{aligned} \overline{\cos^2\theta} &= 1.082 - 0.1287/C^{\frac{2}{3}} && 0.74 > C > 0.092 \\ &= 0.500 && 0.092 > C \end{aligned}\right\} \qquad (3\text{-}29)$$

The mean energy loss $\bar{E}_1$ in each collision will be given by

$$\bar{E}_1 = \frac{K}{4} m \overline{s_r^2 \cos^2\theta} \qquad (3\text{-}30)$$

and, if s_r^2 and $\cos^2\theta$ are statistically independent, then,

$$\bar{E}_1 = \frac{K}{4} m \overline{s_r^2}\ \overline{\cos^2\theta} \ .$$

Substituting from (3-21) and putting $\overline{s^2} = \frac{3}{2a}$, we obtain

$$\overline{E_1} = \tfrac{1}{4} m \ \bar{s}^2\ \overline{\cos^2\theta} \ .$$

From (3-13) we have

$$K_2 = (\pi K/4)\ \overline{\cos^2\theta} \qquad (3\text{-}31)$$

where $\overline{\cos^2\theta}$ is defined in (3-29).

Summary

Substituting (3-29) for K_2 in (3-17) and (3-18) and putting $A_2 = \frac{\pi}{\sqrt{2}}$ and $A_1 = \frac{5}{32\sqrt{2}}$ we have evaluated the functions

$$F_2 = T/\rho_s D^2 \left(\frac{du}{dy}\right)^2 \qquad (3\text{-}32)$$

$$F_7 = \frac{P}{T} \qquad (3\text{-}33)$$

for the case of particles unaffected by the fluid except in the alteration of the coefficient of restitution.

Tabulated values of F_2 and F_7 calculated by (3-17) and (3-18) are given in Table (3-1) and plotted in Fig. (3-3) for the case of K = 1.0.

In this case, the equation becomes

$$F_2 = 0.1081C\ (\tfrac{1}{Y} + 0.8 + 0.761Y)^{3/2}/(K_2Y)^{\frac{1}{2}} \qquad (3\text{-}34)$$

$$F_7 = \frac{.901}{\cos^2\theta}\ \frac{(1 + Y)}{\left[KY(\frac{1}{Y} + 0.8 + 0.761Y)\right]^{\frac{1}{2}}} \qquad (3\text{-}35)$$

CONSIDERATION OF FLUID ACTION ON THE PARTICLE

Vertical Momentum Transfer

In the previous section, the particles were considered to move with a constant velocity between collisions. In so doing, there was a transport of momentum between the particles, both by physical transport and by stresses within the particles. When the particle moves through a fluid, the effective mass is increased and also the particle is slowed down by fluid drag. The effective mass of the particle will be taken as

$$m_e = m\ (1 + \frac{\rho_f}{2\rho_s}). \qquad (3\text{-}36)$$

As the particles move away from a collision, the boundary layer will build up until separation occurs behind the particle and the full form drag is developed. This development will take place over about two particle diameters. The

simple case of a constant drag coefficient C_D is now considered. Equating the acceleration times effective mass to the drag force,

$$\frac{ds}{dt} = - As^2 \tag{3-37}$$

$$\text{where } A = \frac{C_D \rho_f \pi D^2 \; 6}{8 \pi D^3 \; (\rho_s + \tfrac{1}{2}\rho_f)} = \frac{3C_D}{4D \; (\frac{\rho_s}{\rho_f} + \tfrac{1}{2})}$$

In the case of the vertical component of s there is no change in velocity of the fluid as y changes.

Substituting $\frac{ds_y}{dt} = \frac{ds_y}{dy} \frac{dy}{dt}$ into (3-37) gives

$$\frac{ds_y}{dy} = - As_y$$

which can be integrated to give for $s_y = s_{yi}$ at $y = 0$

$$s_y = s_{yi} e^{-Ay} \tag{3-38}$$

The momentum of a particle at distance y is

$$M = m_e \; s_{yi} e^{-Ay} \tag{3-39}$$

and, differentiating with respect to y to obtain the rate of change of momentum with distance,

$$\frac{dM}{dy} = - m_e \; s_{yi} A e^{-Ay} \tag{3-40}$$

The particles are transferring momentum to the fluid before reaching the next collision. The total movement of

momentum will therefore be reduced. We first calculate the total momentum transport for the momentum moved from the particle to the fluids.

This will be

$$\int_0^{l_y} \frac{dM}{dy}\, dy \qquad (3\text{-}41)$$

where l_y is the y component of the total path.

Substituting from (3-40) and carrying out the integration (3-41) is equal to

$$m_e\, s_{yi}\, A^{-1}\, (e^{-Al_y}\, (Al_y + 1.0) - 1.0)\ . \qquad (3\text{-}42).$$

When the two particles collide, the remaining momentum will be considered transported a distance equal to $l_y + \frac{2D}{\pi}$. The $\frac{2D}{\pi}$ term is to allow for the transfer from the centre of one particle to the centre of the other for collision at a random angle. For this particle-particle effect, the total momentum transported is therefore given by

$$m_e\, s_{yi}\, (l_y + \tfrac{2D}{\pi}) e^{-Al_y}\ . \qquad (3\text{-}43)$$

The total momentum transport will be the sum of (3-42) and (3-43) and, if these two terms are added and divided by the momentum transport for no fluid, $m\, s_{yi}(l_y + \frac{2D}{\pi})$, we obtain the ratio M_r where

$$M_r = \left[e^{-Al_y} + \{e^{-Al_y}\, (Al_y + 1) - 1\} \Big/ (A\, l_y + \tfrac{2}{} D.A.)\right] \frac{m_e}{m}. \qquad (3\text{-}44)$$

For $C_D = 0.5$ and $l_y = 2D$, we have from (3-37) $Al_y = 0.25$ and $D.A = 0.125$, and, substituting in (3-44), we obtain $M_r = 0.70$. As this is a significant change and, in the region up to $l_y = 2D$, the drag coefficient will be a variable, the above calculation can be considered approximate only.

Horizontal Momentum Transfer

The horizontal momentum transport is complicated by the velocity distribution of the fluid. If we assumed this is linear with $ds_x/dy = k$ and that the particle has velocities s_y and s_x in the y and x directions, then the x component of acceleration will be given by

$$\left.\begin{aligned} \frac{ds_x}{dt} &= -A\,(s_x - ky)^2 && s_x > ky \\ \frac{ds_x}{dt} &= +A\,(s_x - ky)^2 && s_x < ky \end{aligned}\right\} \qquad (3\text{-}45)$$

Substituting $\frac{ds_x}{dt} = \frac{ds_x}{dy}\frac{dy}{dt}$ into 3-45 and putting $s_x - ky = w$, we obtain

$$\frac{dw}{dy} = \mp\left[\frac{Aw^2}{s_y} - k\right]. \qquad (3\text{-}46)$$

Substituting for s_y from 3-38,

$$\frac{dw}{dy} = \mp\left[\frac{A}{s_{yi}}\, w^2 e^{Ay} - k\right] \qquad (3\text{-}47)$$

An exact solution of (3-47) could be found in only two cases, one of which was when k = 0, the solution in this case being

$$\frac{1}{s_x} = \frac{1}{s_{xi}} + (e^{Ay} - 1)/s_{yi} \quad . \tag{3-48}$$

The other case is when s_y = constant. In this second case, if $z = \frac{A}{s_y k}$, the equations for w are given by

$$\begin{aligned} &\tanh^{-1} w_z - \tanh^{-1} w_i z = yz\,k && s_x > ky \\ &\tan^{-1} w\,z - \tan^{-1} w_i z = yzk && s_x < ky \end{aligned} \tag{3-49}$$

In this second solution, the assumption is made that the y and x velocities are independent.

A closer representation of the physical situation is obtained if we let s_y = aw where a is a constant. It was found, however, that this substitution gave a very lengthy expression for the momentum ratio in terms of the concentration, random velocity and mean velocity gradient.

The solution (3-48) for k = 0 is therefore used and, if also for random velocity fluctuations s_{yi} and s_{xi} are interchangeable, we have

$$s_x = s_i e^{-Ay} \quad . \tag{3-50}$$

This equation is of exactly the same form as (3-39), so that the value of M_r for vertical transport of horizontal

momentum is the same as for vertical momentum.

Energy Transferred to the Fluid by Moving Particles

The energy absorbed by the system of particles will include a term covering the energy lost to the fluid during progress from one collision to another. If the loss in energy along each path is related to the energy immediately after the initial collision $\frac{1}{2}m_e s_i^2$, then there will be negligible change if the coefficient of restitution is low. This is because almost all the energy will be lost along the path or in the final collision.

However, if the mean velocity $\bar{s}$ is the reference velocity, then the energy transferred to the fluid can be described by E_f, where E_f is the energy loss of the particles along these paths per unit volume, per unit time. If the drag coefficient is constant, then we have

$$E_f = \frac{1}{2}\rho_f C_D n D^2 \overline{s^3}/4 \quad . \tag{3-51}$$

Using (3-4), we obtain

$$\overline{s^3} = 4\sqrt{\frac{a^3}{\pi}} \int_0^\infty s^5 e^{-as^2} ds$$

$$= \frac{\pi}{2} \bar{s}^3 \quad . \tag{3-52}$$

Substituting (3-52) into (3-51) and putting n in terms of C, the energy loss E_f is obtained in the form

$$E_f = 3\,C\,\rho_f C_D \bar{s}^3 / 8D \quad . \tag{3-53}$$

Frequency of Collisions

For a given initial velocity s_i and mean path $\bar{l}$, the frequency of collisions will be reduced by the fluid. From (3-37) we have by integration

$$\frac{1}{s_i} - \frac{1}{s} = -At,$$

or,

$$s = \frac{1}{1/s_i + At} \quad . \tag{3-54}$$

The path length l is given by $\int s\,dt$, that is,

$$l = \int_0^t \frac{dt}{1/s_i + At}$$

$$l = \frac{1}{A} \log_e (A\,t\,s_i + 1) \quad . \tag{3-55}$$

Rearranging (3-55) to obtain t as the dependent variable,

$$t = \frac{1}{A\,s_i} (e^{Al} - 1). \tag{3-56}$$

The time in the non-fluid case was simply l/s_i, so that t_r, the ratio of time required with fluid to time required without fluid, is, from (3-56),

$$t_r = (e^{Al} - 1)/A\,l \quad , \tag{3-57}$$

and the frequency of collision ratio f_r is the reciprocal of t_r,

$$f_r = Al/(e^{Al} - 1). \qquad (3\text{-}58)$$

If the distribution of the path vectors is assumed random about a fixed origin, then the distribution can be considered to have a similar form to that of the velocity vector. Taking the magnitude of the path vector as l and defining $a = 4/\pi \bar{l}^2$, we have from (3-4) a probability distribution for l given by

$$p(l) = 4\sqrt{\frac{a^3}{\pi}}\, l^2 e^{-al^2} \qquad (3\text{-}59)$$

The mean value of t_r calculated according to (3-57) is therefore given by

$$\bar{t}_r = \int_0^\infty \left[4\sqrt{\frac{a^3}{\pi}}\, l^2\, e^{-al^2}\, (e^{Al} - 1)/Al\right] dl \,. \qquad (3\text{-}60)$$

If we put $N = 32/\pi^2 \bar{l}^3$, equation (3-60) becomes

$$\bar{t}_r = \frac{N}{A}\left[\int_0^\infty l\, e^{Al - al^2}\, dl - \int_0^\infty l\, e^{-al^2}\, dl\right] . \qquad (3\text{-}61)$$

If the first integral in (3-61) is evaluated first by putting $z = \sqrt{a}\, l - A/2\sqrt{a}$ and completing the square of the exponent of e, we obtain for the first integral I_1

$$I_1 = \frac{1}{\sqrt{a}}\, e^{\frac{A^2}{4a}} \int_{-A/2\sqrt{a}}^\infty (z/\sqrt{a} + A/2a)\, e^{-z^2}\, dz \,. \qquad (3\text{-}62)$$

Evaluating (3-62) we have

$$\int_{-A/2\sqrt{a}}^\infty \frac{z}{\sqrt{a}} e^{-z^2}\, dz = \frac{1}{\sqrt{a}} \left[-\tfrac{1}{2} e^{-z^2}\right]_{-A/2\sqrt{a}}$$

$$= \frac{e^{-A^2/4a}}{2\sqrt{a}} \quad , \tag{3-63}$$

and also putting

$$z = x/\sqrt{2}$$

$$\frac{A}{2a}\int_{-A/2\sqrt{a}}^{\infty} e^{-z^2}\,dz = \frac{A\sqrt{\pi}}{2a}\int_{-A/\sqrt{2a}}^{\infty} \frac{1}{\sqrt{2\pi}}\; e^{-x^2/2}\,dx$$

$$= \frac{A\sqrt{\pi}}{2a}\left[\tfrac{1}{2} + \rho\left(\frac{A}{2a}\right)\right] \tag{3-64}$$

where $\rho\left(\frac{A}{2a}\right)$ is the area from 0 to $\frac{A}{2a}$ under the normal error curve $y = \left(\frac{1}{\sqrt{2\pi}}\right)\; e^{-x^2/2}$.

Adding (3-63) and (3-64), we obtain

$$I_1 = \frac{1}{2a} + \frac{A\sqrt{\pi}}{2a\sqrt{a}}\left[\tfrac{1}{2} + \rho\left(\frac{A}{2a}\right)\right]\; e^{A^2/4a} \quad .$$

For the second integral in 3-61, I_2, we put $1 = z/\sqrt{a}$ to obtain

$$I_2 = \frac{1}{a}\int z e^{-z^2}\,dz$$

$$= \tfrac{1}{2}a \quad . \tag{3-65}$$

Subtracting I_2 from I_1, we obtain for 3-61

$$\bar{t}_r = N\,\frac{\sqrt{\pi}}{2a\sqrt{a}}\; e^{\frac{A^2}{4a}}\left[\tfrac{1}{2} + \rho\left(\frac{A}{2a}\right)\right] . \tag{3-66}$$

Substituting $\bar{I}$ for a and N,

$$\bar{t}_r = 2\, e^{A^2 \bar{l}^2}\, \pi/16 \left[0.5 + \rho\left(\frac{A\bar{l}\sqrt{\pi}}{2\sqrt{2}}\right)\right] \qquad (3\text{-}67)$$

Corrections to F_2 and F_7 using M_r and $\bar{t}_r$

From equation (3-44) by putting $ly = \bar{l}/\sqrt{2}$ as an approximation and from (3-67), we obtain M_r and t_r in terms of $A\bar{l}$. $A\bar{l}$ is a function of concentration and is plotted in Fig. (3-6). Tabulated values of $A\bar{l}$, M_r and t_r are included in Table (3-2) for D.A., a constant calculated for $C_D = 0.5$.

The corrections to the viscosity and pressure equations (3-10) and (3-11) will contain the term $\frac{me}{m} M_c = M_r$ to allow for the reduced momentum transfer per path travelled. They will also contain the term t_r^{-1} to allow for the reduction caused by the reduced number of paths travelled per unit time for a given initial velocity s_i. Putting in these corrections, we obtain from (3-11)

$$T/\frac{du}{dy} = 4A_1\, m_e\, \bar{s}_i\, C\left(\frac{1}{Y} + 0.8 + 0.761Y\right) M_c/D^2\, t_r. \qquad (3\text{-}68)$$

When the correction to f is applied, equation (3-15) becomes

$$T\,\frac{du}{dy} = K_2\, A_2\, n^2\, D^2\, \bar{s}_i^{3}\, m_e\, Y/4C\, t_r\,. \qquad (3\text{-}69)$$

Eliminating s_i, we obtain the corrected version of (3-17),

$$\frac{T}{\rho_s D^2 \left(\frac{du}{dy}\right)^2} = \frac{\pi^2}{9} \frac{A_1^{3/2}}{A_2} \frac{4C\left(\frac{1}{Y} + 0.8 + 0.761Y\right)}{K_2 Y^{1/2}} \underline{M_c^{3/2} t_r^{-1/2} \frac{m_e}{m}} \quad . \quad (3\text{-}70)$$

The term above the broken line is the correction for the fluid, (M_a) and is tabulated for spheres in water in Table (3-3) as a function of C. Similarly, equation (3-10) is altered to become

$$P = n m_e \bar{s}_i^2 \frac{\pi}{8} (1 + Y) M_c / t_r \quad . \quad (3\text{-}71)$$

Equation (3-16) after modification is given by

$$T^2 = K_2 A_1 A_2 m_e^2 s_i^4 n^2 Y\left(\frac{1}{Y} + 0.8 + 0.761Y\right) M_c / t_r^2 \quad (3\text{-}72)$$

and, eliminating s_i between 3-71 and 3-72, we get

$$P/T = \frac{\pi}{8} (1 + Y)\left(Y\left(\frac{1}{Y} + 0.8 + 0.761Y\right) K_2 A_1 A_2\right)^{-1/2} M_c^{1/2} \quad (3\text{-}73)$$

where $M_c^{1/2}$ is tabulated in Table (3-3) and plotted on Fig. (3-6).

Summary

Corrections to be made to F_2 and F_7 allowing for the inter-particle fluid have been obtained. F_7 and F_2 still, however, apply to the particle stresses alone and do not include the shear stress in the fluid. These corrections are as follows.

Corrected F_2 = (No fluid F_2) times $M_c^{3/2} t_r^{-1/2} m_e/m$ (3-74)

Corrected F_7 = (No fluid F_7) times $M_c^{1/2}$ (3-75)

and are tabulated in Table (3-3).

THE INTERPARTICLE FLUID

In this section, the behaviour of the interparticle fluid in resisting the shear strain imposed upon it will be considered.

Two distinct possibilities exist. The first is that the fluid turbulence will be restricted to small eddies in the particle interstices, such that a general resistance to distortion of the fluid body is set up. The second is that turbulence of the whole particle fluid system will be set up with eddies including a number of particles within their orbit. This turbulence will be that promoting suspension. If the conditions governing this overall turbulence were understood and their effect known, it would be possible to carry out a complete analysis of the flow pattern.

Effect of Local Interparticle Turbulence

When the particle system is sheared, the surrounding fluid also undergoes a shear strain. This will be resisted by a mean shear stress T_f, defined as shear force in fluid per unit area of fluid and solid in a given plane, which can be added to the particle shear stress T to give the total shear stress T_t. A model is developed below for the interparticle fluid which, although very much simplified, is expected to

give a guide to the magnitude of T_f.

A fluid in a state of homogeneous isotropic turbulence is assumed to fill the particle interstices and the mean velocity gradient is assumed to be acting on this fluid, such that the form of the turbulence is not affected. The energy supplied to the fluid is then equated to the energy dissipated to obtain a value of effective viscosity μ_e.

Townsend (13, p.59) showed from similarity considerations that for a wake flow

$$\mu_e = \rho_f K_5 (\overline{u_1^2})^{\frac{1}{2}} L_e \qquad (3\text{-}76)$$

where $(\overline{u_1^2})^{\frac{1}{2}}$ is the velocity scale, and in the particular case of flow behind a screen is the r.m.s. longitudinal velocity. K_5 is a constant depending on the type of flow and definition of u_1. The term L_e is a dissipation length which for homogeneous turbulence from (13 p.51) is given by

$$\frac{d\,\overline{u_1^2}}{dt} = -\frac{(\overline{u_1^2})^{3/2}}{L_e} \quad . \qquad (3\text{-}77)$$

The energy dissipated per unit volume of mixture, E_d, is

$$E_d = \tfrac{1}{2}\rho_f \frac{\overline{du^2}}{dt} (1 - C) \quad .$$

If we assume homogeneous turbulence and put $u^2 = 3u_1^2$, and substitute from (3-77) to eliminate $\overline{du^2}/dt$, we obtain

$$E_d = \frac{3}{2} \rho_f \, (\overline{u_1^2})^{3/2} \, (1 - C)/L_e \, . \qquad (3\text{-}78)$$

Substituting $\overline{u_1^2}$ from (3-78) into (3-76) gives

$$\mu_e = (\tfrac{2}{3})^{1/3} K_5 \, E_d^{1/3} \rho_f^{2/3} \, L_e^{4/3}/(1 - C)^{1/3} \, . \qquad (3\text{-}79)$$

Experimental values of K_5 have been obtained for a flow behind a grid. The results of these experiments have been tabulated by Townsend (13, p.62). The most accurate experiments gave a value of $K_5 = 0.73$. This value is higher than the values given by similar experiments carried out measuring heat diffusion also tabulated by Townsend (13) .

It is assumed that the rate of energy supplied to the fluid is $K_6 E$ where E is the total energy absorbed by the particles, and K_6 is a function of the concentration and coefficient of restitution of the particles but will in general be slightly less than unity. Then

$$E_d = (T K_6 + T_f) \frac{du}{dy} \, . \qquad (3\text{-}80)$$

For a viscous flow, an approximation for the effective coefficient of viscosity when solid particles are present is $\mu/(1-2.5C)$ as described in (14). Cubing equation (3-79), then substituting for E_d from (3-80), we find

$$\mu_e^3 = \tfrac{2}{3} K_5^3 \rho_f^2 \, L_e^4 \, (T K_6 + T_f) \frac{du}{dy}/(1 - C)$$

and, noting that $T_f / \frac{du}{dy} = \mu_e / (1-2.5C)$ for small C, we find

$$T_f^3 = \tfrac{2}{3} K_5^3 \rho_f^2 L_e^4 \left(\frac{du}{dy}\right)^4 (T K_6 + T_f) (1-2.5C)^3 (1-C). \quad (3-81)$$

Equation (3-81) is a cubic in T_f but, when $T K_6 > T_f$, which is usually true, an approximate solution is given by

$$T_f = \rho_s D^2 \left(\frac{du}{dy}\right)^2 F_2 \left[\frac{\left(\frac{\rho_f}{\rho_s}\right)^{\frac{2}{3}} \left(\frac{L_e}{D}\right)^{4/3} K_5 F_2^{-2/3} K_6^{\frac{1}{3}}}{(1 - 2.5C)(1 - C)^{\frac{1}{3}}} \right] \quad (3-82)$$

where the factor in square brackets, denoted hereafter by F_8, is defined by

$$T_f = T F_8 . \quad (3-83)$$

Evaluation of F_8 depends on evaluating K_6 and L_e/D. K_6 can be evaluated quite accurately for any given case but for all cases where $\rho_s/\rho_f < 3$ tends to be close to unity. The cube root will therefore be even closer and from now on $K_6^{\frac{1}{3}}$ is assumed equal to 1.0.

Unfortunately, the evaluation of L_e cannot be carried out accurately. When two particles collide, most of the energy transmitted to the fluid will be in the form of a ring-shaped pulsed jet, as in Fig. (3-5).

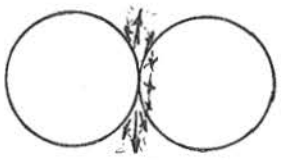

Fig. (3-5)

For a simple jet Townsend notes that values of the transverse integral scale of turbulence, which could be expected to be similar to L_e, were given by 0.02 times the jet length. For particles very close together, the maximum length of jet would be of the order of D/2 and the mean value of $L_e = 0.005D$. As the concentration is reduced, the value of jet length would tend to increase. If the mean value of jet length is assumed equal to $D/2 + \bar{l}$, that is, the sum of the particle radius and the mean free path, and, if the average value of L_e is assumed equal to half this value of jet length, we have

$$L_e = 0.01 \ (D/2 + \bar{l}) \ . \qquad (3-84)$$

It is expected that the movement of the particles will tend to develop a larger eddy structure than that postulated above and (3-84) could be considered a lower limit to L_e. As an upper limit we will take $0.2\ \bar{l}$, noting that in wake flow L_e is approximately 0.2 times the width of the wake (13) . Both limiting values of L_e have been used in the calculation of upper and lower bounds for F_8, F_1 and F_3. Tabulated values of F_8 are given in Table (3-4) and have been plotted on Fig. (3-8).

Using (3-84), F_8 has been tabulated as a function of C in Table (3-4) and plotted on Fig. (3-8).

Large Scale Turbulence

Up to now, a small section only of the fluid particle system has been considered. This is similar to considering,

for the flow of a fluid, only the transport of momentum or other properties by molecular scale processes. There is in the fluid-particle system the possibility of large scale random motion with a length scale greater than the mean particle spacing. The combined fluid and particle system is characterised by a stress-strain relationship of the form $T = K_7 \left(\frac{du}{dy}\right)^2$ where K_7 is, in fact, a function of the concentration and hence in general a function of position within the "fluid" .

While this local parameter K_7 is important when considering initial instability, it is not expected to be a significant parameter in determining the behaviour of fully developed turbulence. The overall large scale motion is continually supplying energy to a smaller scale of motion, so that the final form of damping is not significant. For fully developed turbulence, therefore, no difference in type of behaviour is expected as the concentration is reduced from that in which collisions are significant to that in which the solids have negligible effect.

That the situation is different for a fluid containing solid particles is widely reported (15, p.67) and one attempt to explain this phenomena quantitatively has been given by Hino (16, p.161).

In this thesis, we will consider only the possibility of

defining the condition under which the system will develop large-scale turbulence. The "fluid" we are considering is completely defined by the distribution of K_7 and the density $\rho_a = \rho_f + C(\rho_s - \rho_f)$, and the flow is defined by the geometry of the system and the shear stress T.

Now, if we examine the dimensions of the above parameters in terms of mass, length and time, we find that the only term with a time included in the dimension is T. We therefore conclude that T is not one of the parameters governing the stability directly. If we define the distribution of K_7 by its value and the value of the first derivative at a point, then we find the stability parameter given by

$$\Pi = \frac{\rho_a K_7}{\left(\frac{dK_7}{dy}\right)^2}$$

and, putting $K_7 = \rho_s D^2 F_3$, gives

$$\Pi = \frac{\rho_a}{\rho_s} \frac{F_3}{D^2 (dF_3/dy)^2} \qquad (3\text{-}85)$$

Therefore, it is concluded that, for values of Π less than $\Pi_{crit.}$, the flow will tend to form large eddies and suspension will be important. At present, the writer does not know of any experimental results from which $\Pi_{crit.}$ could be determined. From the experiments described in this thesis, an estimate of the stability has been made. In most open

channels, there will be regions where both types of flow exist, but it does not follow that, if $\Pi_{crit.}$ exists in a channel, both types of flow will exist. It may well be that Π has to rise well above $\Pi_{crit.}$ before a flow will initially divide into two regions, and it will only be after this division that $\Pi_{crit.}$ will define the type of flow; a similar effect to the growth of a laminar boundary layer which ultimately divides into a turbulent and laminar region. For this pure fluid case, the viscosity distribution is described by the distance to the solid boundary.

SUMMARY, LIMITATIONS AND RESULTS

Summary

In this chapter, equations have been developed for T and T_f in terms of $\frac{du}{dy}$. These have been obtained in the form of dimensionless functions F_2 and F_8 which can be evaluated by (3-70) and (3-82). The dispersive pressure has also been calculated in terms of F_7 which can be evaluated by (3-73).

$$T = \rho_s D \left(\frac{du}{dy}\right)^2 F_2 \qquad (3\text{-}86)$$

$$P/T = F_7 \qquad (3\text{-}87)$$

$$T_f = \rho_s D^2 \left(\frac{du}{dy}\right)^2 F_2 F_8 . \qquad (3\text{-}88)$$

If we define

$$F_1 = \frac{P}{T + T_f} = \frac{P}{T_t}, \qquad (3\text{-}89)$$

then

$$F_1 = \frac{F_7}{1 + F_8} \, . \qquad (3\text{-}90)$$

The tabulated values of F_2, F_7, F_8, and F_1 are included at the end of this section.

Limitations

As the concentration C is increased, this analysis breaks down. The reason is that, as the particle packing increases, the particles ultimately "condense" to a solid mass. This condensation has been observed by Alder and Wainwright (12) at concentrations of about 0.46. Concurrently, there is a sudden drop in Y. For this reason, the calculations detailed up to this point are not expected to apply above some value of C not greater than 0.50.

At the lower end of the scale, the calculations have included approximations which will reduce the accuracy for small values of C. However, at these low values of C, large scale turbulence will normally have set in increasing the solids supported, this latter effect rapidly predominating in importance.

The application of these results to particular flows is carried out in Chapter 2.

No account has been taken of various sized particles or of other shapes of particles. These problems have been examined by Hirschfelder et al. (10) and present more complex algebraic difficulties although they can usually be solved by methods similar to those presented in this chapter. The effect of a large gradient in the independent variables can also be accounted for (10) for a gas of hard spheres. Again, more complex algebra is encountered, and also more complex equations connecting T and (du/dy).

Numerical Calculation of Functions

The results as tabulated below are calculated using $A_1 = 5/32\sqrt{2}$ and $A_2 = \pi/\sqrt{2}$. All calculations have been made to slide-rule accuracy except where the column is headed (g.i.). This heading indicates that graphical methods have been used in obtaining the results. The first table includes functions which are independent of the surrounding fluid. The third table includes the effect of the fluid for the two cases, $\rho_f = \rho_s$ and $\rho_s = 2.65\rho_f$.

Below each table, the methods of calculation required for that table have been outlined.

Table (3-1)

C	Y	Y_m	(g.i.) Y_r	N_1	K_2	Neglecting Fluid F_7	F_2
.05	.2275	.207	.23	5.368	.392	1.406	.224
.10	.5221	.431	.52	3.112	.392	1.510	.131
.15	.9079	.677	.87	2.593	.483	1.409	.101
.20	1.4209	.955	1.25	2.585	.554	1.349	.1011
.25	2.1058	1.28	1.73	2.877	.594	1.298	.1176
.30	3.0306	1.66	2.31	3.436	.624	1.256	.1496
.35	4.278	2.12	3.00	4.290	.646	1.223	.2015
.40	5.957	2.69	3.70	5.503	.663	1.183	.280
.45	8.198	3.40	4.46	7.157	.677	1.161	.394
.50	11.16	4.29	5.23	9.38	.689	1.137	.560

Table (3-1) includes three values of Y, that from the virial expansion Y, the value used by Miller, Y_m, and the value obtained from the radial distribution function, Y_r. Following Y_r is a table N_1 where

$$N_1 = 1/Y + 0.8 + 0.761\ Y \qquad (3\text{-}90)$$

and Y is obtained from the virial expansion as are all functions of Y hereafter. K_2 is calculated according to equation (3-31). Finally, the values of F_7 and F_2 calculated according to (3-34) and (3-35), where the effect of the fluid has been neglected, appear.

Table (3-2)

$A\bar{l}$	M_c	t_r	$M_c^{3/2}\, t_r^{-1/2}$	$M_c^{1/2}$
.01	.993	1.005	.987	.996
.02	.986	1.010	.974	.994
.04	.969	1.020	.945	.985
.06	.953	1.031	.916	.976
.10	.921	1.051	.862	.960
.15	.878	1.080	.791	.937
.20	.835	1.109	.724	.914
.25	.792	1.139	.661	.890
.50	.606	1.308	.413	.779
.55	.570	1.347	.370	.55

The functions M_c and t_r are calculated according to equations (3-44) and (3-67) where M_c is the term in square brackets in (3-44) and l_y is estimated at $\bar{l}/\sqrt{2}$, all in terms of $A\bar{l}$ where $\bar{l}$ is the mean free path.

Table (3-3)

	$\rho_s = \rho_f$				$\rho_s = 2.65\rho_f$				
C	$A\bar{l}$	g.i. M_a	g.i. $M_c^{1/2}$	F_2	F_7	$A\bar{l}$	g.i. M_a	g.i. $M_c^{1/2}$	F_2	F_7
.05	.517	.600	.771	.134	1.083	.247	.788	.891	.176	1.252
.10	.225	1.040	.902	.136	1.362	.107	1.014	.954	.133	1.440
.15	.130	1.231	.945	.124	1.331	.0619	1.082	.974	.109	1.371
.20	.0826	1.325	.966	.134	1.302	.0395	1.124	.984	.114	1.326
.25	.0558	1.383	.979	.163	1.270	.0266	1.134	.990	.133	1.283
.30	.0388	1.419	.985	.212	1.237	.0185	1.159	.993	.173	1.247
.35	.0275	1.444	.990	.291	1.210	.0131	1.169	.995	.236	1.216
.40	.0197	1.460	.994	.409	1.176	.0094	1.172	.997	.328	1.180
.45	.0143	1.470	.996	.579	1.157	.0068	1.176	.998	.463	1.159
.50	.0105	1.480	.997	.829	1.134	.0050	1.180	.999	.661	1.136

Table (3-3) includes the parameters F_2 and F_7 calculated according to equations (3-70) and (3-73) where the effective

mass, m_e, has been taken as the mass of the particle plus half the mass of the displaced fluid. The values of $A\bar{I}$ as a function of concentration were calculated according to (3-37) taking $C_D = 0.5$. The values of $M_c^{\frac{1}{2}}$ and M_r were obtained by finding $M_c^{\frac{1}{2}}$ from a graphical plot of the results in Table (3-2). Two sets of results are shown, one for the case of a particle density equal to the fluid density and the other for the case of a particle density equal to 2.65 times the fluid density.

Table (3-4)

C	Ratio	F_8 x 100		F_1		F_3	
		Lower	Upper	Lower	Upper	Lower	Upper
		Results below for $\rho_s = \rho_f$					
.05	1.281	4.75	76.5	.614	1.035	.141	.237
.10	1.605	2.67	34.3	1.013	1.328	.140	.183
.15	1.997	2.01	20.5	1.105	1.305	.127	.150
.20	2.486	1.72	13.7	1.145	1.280	.136	.152
.25	3.115	1.62	10.0	1.153	1.252	.165	.179
.30	3.942	1.42	6.7	1.159	1.219	.215	.224
.35	5.062	1.35	4.87	1.155	1.194	.295	.305
.40	6.621	1.32	3.62	1.134	1.160	.415	.424
.45	8.861	1.35	2.73	1.125	1.140	.587	.595
.50	12.20	1.45	2.25	1.109	1.119	.842	.849
		Results below for $\rho_s = 2.65\rho_f$					
.05	1.281	2.07	33.4	.938	1.228	.180	.235
.10	1.605	1.42	18.3	1.217	1.420	.135	.157
.15	1.997	1.19	12.1	1.222	1.354	.111	.123
.20	2.486	1.01	8.0	1.226	1.311	.115	.123
.25	3.115	.96	5.9	1.211	1.272	.135	.141
.30	3.942	.85	4.0	1.198	1.237	.175	.180
.35	5.062	.76	2.74	1.183	1.206	.238	.242
.40	6.621	.80	2.08	1.155	1.172	.330	.335
.45	8.861	.82	1.65	1.141	1.150	.467	.471
.50	12.20	.88	1.37	1.120	1.126	.666	.670

Table (3-4) contains the limiting values of parameter F_8, the ratio of the effective viscosity of the water to the viscosity of the particle system. The column headed "Ratio" lists the ratio of viscosity of the liquid plus particles at low Reynolds numbers to the viscosity of the fluid, and is a function of C only. This is the term $1/(1 - 2.5C)$ given in equation (3-82). For calculation, this has been replaced by the relative viscosity calculated by the free surface model as tabulated in (14, p.453). Following F_8 we tabulate F_1 defined as $F_7/1 + F_8$ and F_3 defined as $F_2\ (1 + F_8)$. The upper half of Table (3-4) contains the results for $\rho_s = \rho_f$ and the lower half the results for $\rho_s = 2.65\rho_f$.

Graphs

The graphed results are obtained from Tables (3-1) to (3-4). All graphs of the same function have been grouped on the one graph. Also included in Figs. (3-11) and (3-12) are graphs of the experimental points for F_3 and F_1 obtained by Bagnold.

In order, details of the graphs are:-

Fig. (3-6): Values of C, $M_c^{3/2}\ t_r^{-\frac{1}{2}}$ and $M_c^{\frac{1}{2}}$ are plotted against $A\ \bar{I}$ for the density ratios 1.0 and 2.65. The values are taken from Table (3-2).

Fig. (3-7): Values of Y, Y_m, and Y_r are plotted as functions of C where Y is obtained by a virial expansion,

Y_m is the value used by Miller and Y_r is obtained from the radial distribution function (10).

Fig. (3-8): The value of viscosity ratio used instead of $1/(1 - 2.5C)$ has been plotted against C as well as the values of F_8 for density ratios of 1.0 and 2.65. F_8 is the ratio of effective fluid shear resistance to particle system shear resistance.

Fig. (3-9): The value of F_7 and the bands within which F_1 is expected to lie are plotted against C. In obtaining F_7, ρ_s has been assumed much greater than ρ_f and the two bands for F_1 are calculated for $\rho_s = \rho_f$ and $\rho_s = 2.65\rho_f$ respectively. F_7 is the ratio of particle direct stress to particle shear stress and F_1 is the ratio of the particle direct stress to the total shear stress.

Fig. (3-10): The theoretically derived value of F_2 and the bands within which F_3 is expected to lie are plotted against C. In obtaining F_2, ρ_s has been assumed to be much greater than ρ_f and the two bands for F_3 are calculated for $\rho_s = \rho_f$ and $\rho_s = 2.65\rho_f$ respectively.

Fig. (3-11): Bagnold's experimental results of F_3 are plotted against C. Included in this graph is the theoretically derived curve of F_3 obtained for a

density ratio (ρ_s/ρ_f) of 1.0.

Fig. (3-12): Bagnold's experimental results of F_1 are plotted against C. Included in this graph is the theoretically derived curve of F_1 obtained for a density ratio of 1.0.

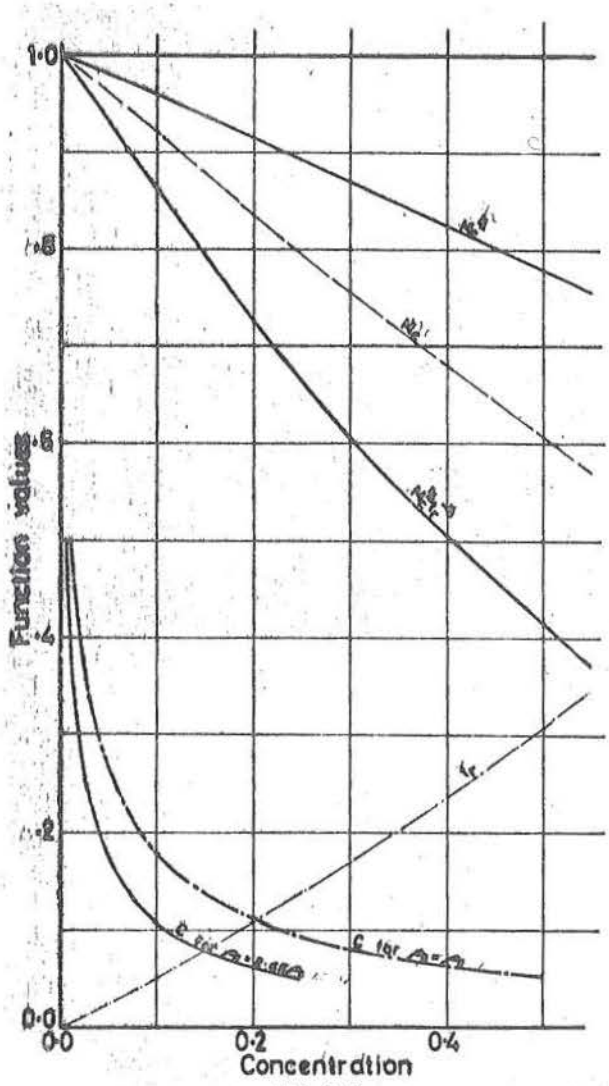

FIG 3-6

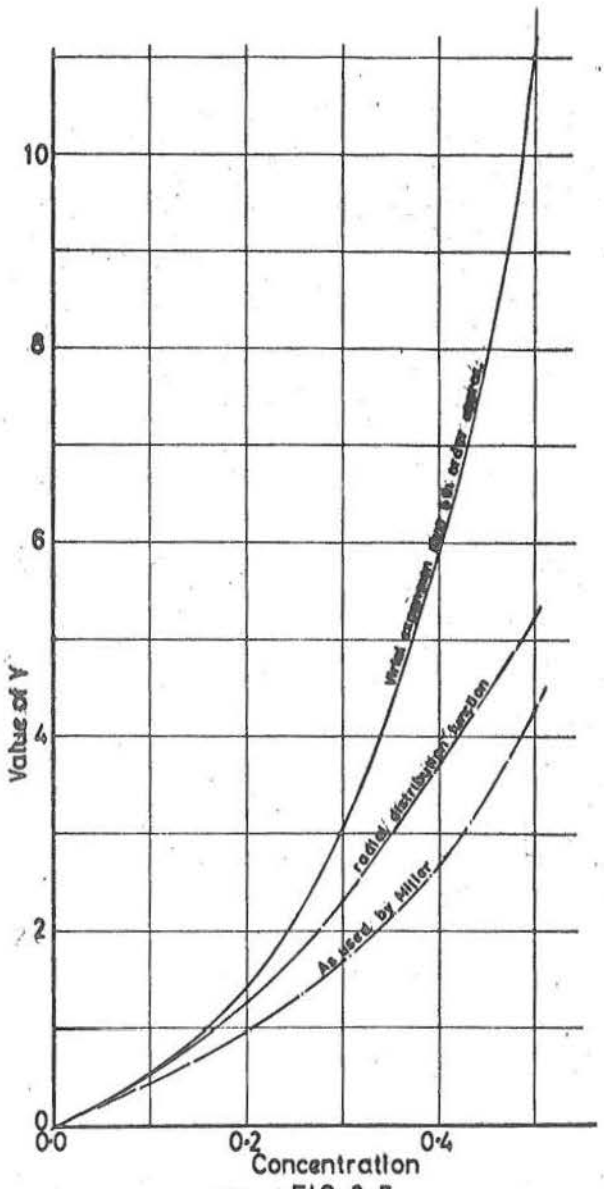

FIG 3-7

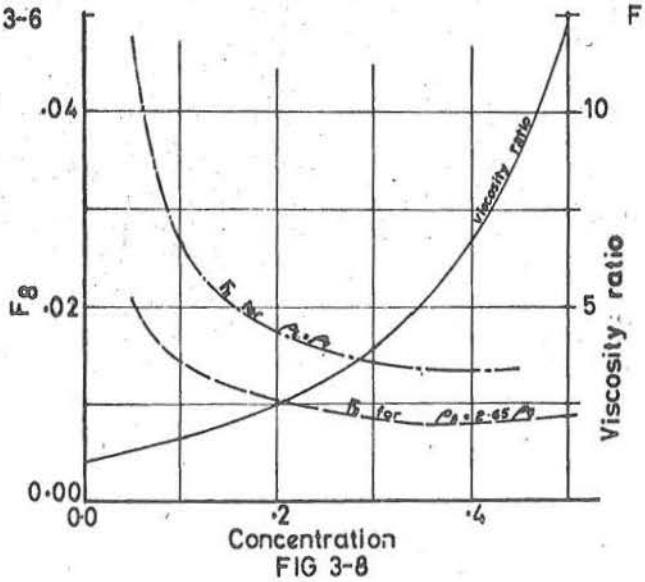

Concentration

FIG 3-8

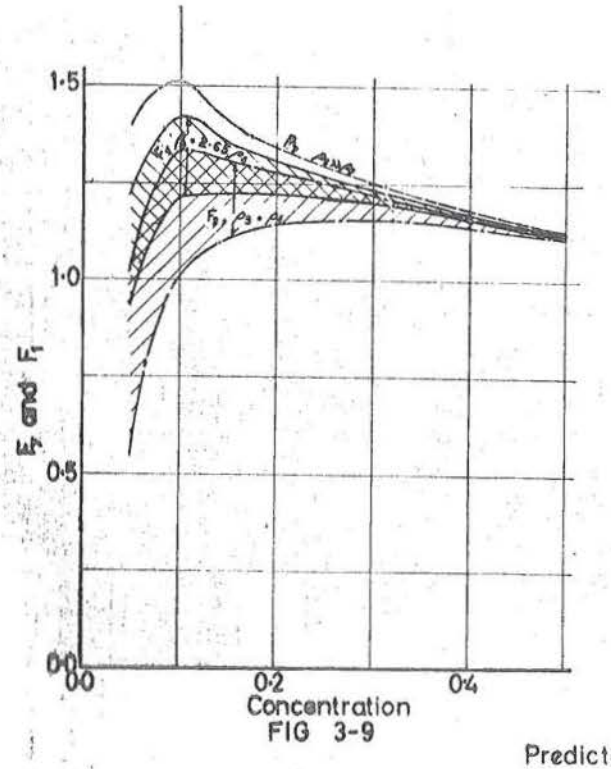

FIG 3-9

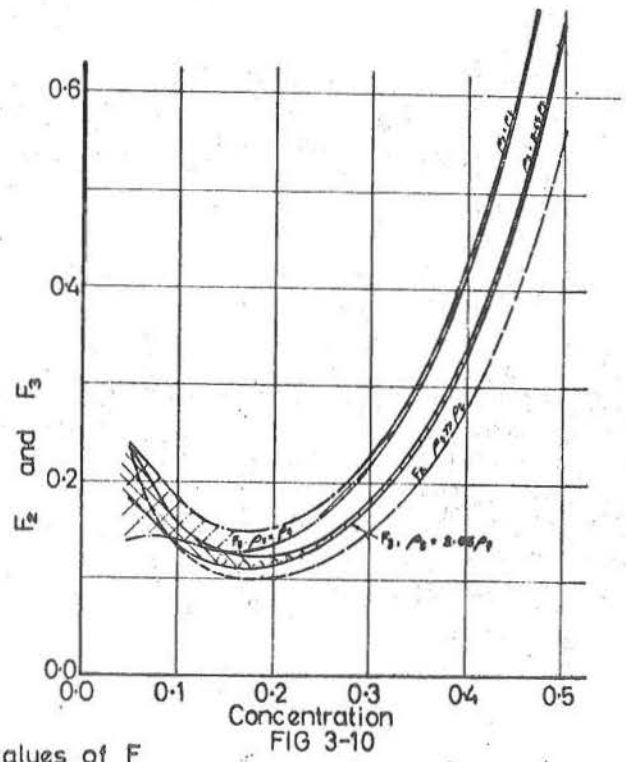

FIG 3-10

Predicted values of F

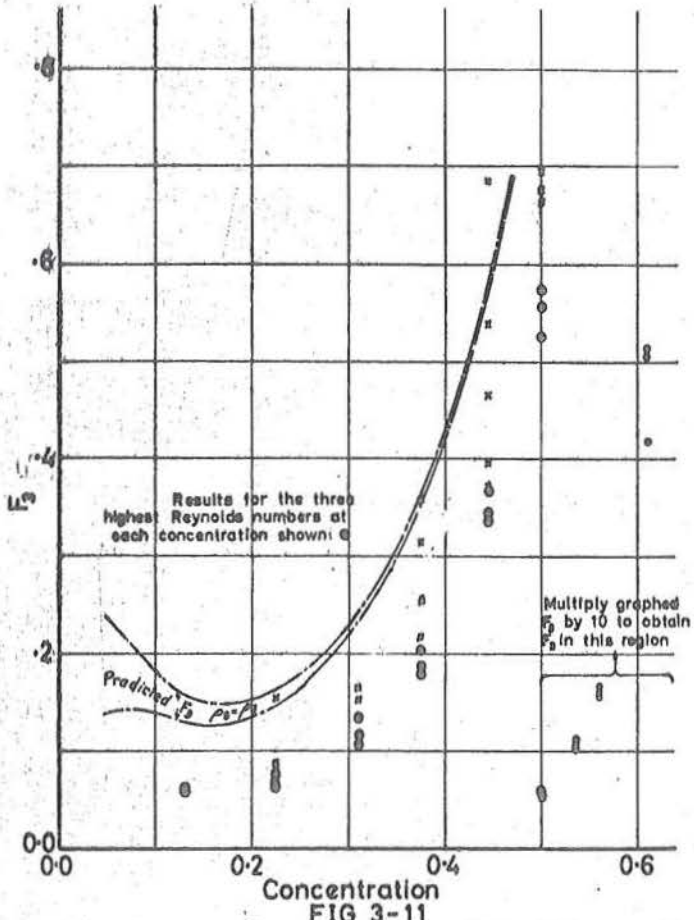

FIG 3-11

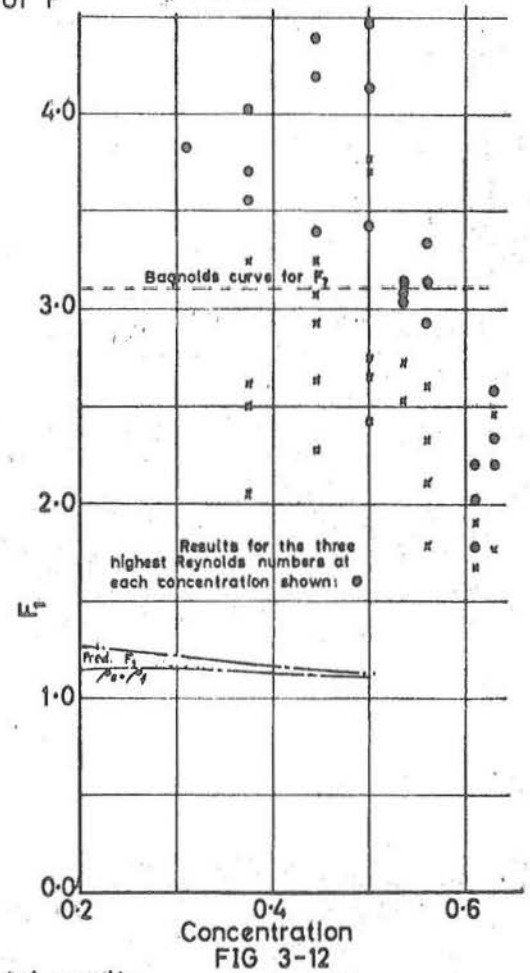

FIG 3-12

Bagnolds experimental results

CHAPTER 4

A P P A R A T U S

SYNOPSIS

The experimental programme carried out necessitated the development of the equipment detailed in this chapter. In the first part of the chapter is a discussion of the experimental measurements required and the general means of achieving them. The remainder of the chapter is devoted to a detailed explanation of each part of the apparatus. Chapter 7, in conjunction with this chapter, contains the conclusions reached about the apparatus after carrying out the experimental programme.

PRELIMINARY SPECIFICATIONS

Objects of the Experimental Programme

During the development of the theory described in the previous two chapters, it was thought desirable to set up the type of flow considered in the theoretical analysis. The primary object was to ascertain what happened to the bed under conditions of high shear stress. The secondary objects were to measure the actual values of the flow parameters and to compare them with the predicted values.

Because it was apparent that it would take some time to design and build suitable apparatus, this task could not be left until the theory had been fully worked out. The first item to be designed and built was the apparatus used to generate suitable flow conditions. As the theory became more advanced, the required experimental measurements were more easily defined and were finally reduced to:

(i) Concentration profile
(ii) Slope, depth and width of the flow
(iii) Particle grading
(iv) Particle velocity profile
(v) Fluid velocity profile
(vi) Static pressure profile

From these measurements, the experimental values of the parameters F_1 and F_3 described in Chapter 3 could be found for various distances from the bed.

With this apparatus, it was also intended to determine and examine the limit of the region within which large scale turbulence could be neglected.

Generation of Flow Conditions

From the results in Chapter 2, it would appear that, for high Reynolds numbers, the parameters F_3 and F_1 should be independent of Reynolds number. Therefore, one important

requirement for the flow apparatus was a high possible Reynolds number $R_e = \rho_f D^2 (\frac{du}{dy})/\mu$. Bagnold's experiments, Figs. (2-4) and (2-5), showed a certain dependence on Reynolds number at the maximum value reached, 500, although, in his paper, Bagnold considered this was the limit of Reynolds number dependence. It was decided to arrange the apparatus so that a Reynolds number of 1,000 was possible. All the problems to which the theory was being applied involved a bed of particles more dense than the fluid, and a deep bed was required. A minimum weight of supported particles considered suitable was $3\ (\rho_s - \rho_f)\ D\ g$ pounds per square foot of bed. If the concentration in the bed averaged 0.5, the bed thickness implied was six diameters.

To obtain dimensions for the apparatus, an estimate of F_3 and F_1 at the bed was required. From Bagnold's results, values of 1.0 for F_3 and 3.0 for F_1 were used as representing very high concentrations. From the minimum weight of moving material decided above,

$$P > 3\ (\rho_s - \rho_f)\ D\ g, \qquad (4\text{-}1)$$

and, if $P/T_t = F_1 = 3.0$,

$$T > (\rho_s - \rho_f)\ D\ g, \qquad (4\text{-}2)$$

and, from the minimum allowable Reynolds number,

$$\rho_f D^2 \left(\frac{du}{dy}\right)/\mu > 1{,}000. \qquad (4\text{-}3)$$

Now, in Chapter 2, it is shown that

$$T = \rho_s D^2 \left(\frac{du}{dy}\right)^2 F_3$$

where, putting $F_3 = 1.0$ and eliminating du/dy from 4-3,

$$D\, T^{\frac{1}{2}} > 1{,}000\, \mu \rho_s^{\frac{1}{2}}/\rho_f. \qquad (4\text{-}4)$$

Rearranging and multiplying both sides of the inequalities (4-2) and (4-4), it can be shown that

$$T > \left[1{,}000 \mu \rho_s^{\frac{1}{2}} \left(\frac{\rho_s}{\rho_f} - 1\right) g\right]^{\frac{2}{3}} \qquad (4\text{-}5)$$

and, also from (4-2) and (4-4), that

$$\frac{T}{(\rho_s - \rho_f)g} > D > 1{,}000 \mu \rho_s^{\frac{1}{2}}/\rho_f\, T^{\frac{1}{2}}. \qquad (4\text{-}6)$$

Measurements

For each flow, the measurement of total shear stress was required as a function of depth. Concentration measurements were also required at various depths. As these concentrations were the most important variables measured, being used for both shear stress and direct stress calculations, the equipment used had to be accurate and reliable. Rapid variations in concentration with vertical distance were expected and it was therefore desirable for the measuring equipment to be able to

measure the concentration in a band not wider than one particle diameter. Because the thickness of the bed was expected to be only a few particle diameters, it was necessary to disturb the flow as little as possible. Concentrations of interest are in the range $0.05 < C < 0.65$ and the meter should be accurate within as much of this range as possible.

Velocities of the particles are required for the calculation of F_3 which depends on the square of the velocity gradient. As the flow parameters will be varying rapidly, a small interval of vertical distance, of the order of one particle diameter, must be used in obtaining the velocity gradient. Therefore, an accurate mean particle velocity measurement is required. The fluid velocity profile is required if transition to large scale turbulence takes place outside the region in which the particle velocity is known.

As the concentration measurement will include both bed load and suspended load, the suspended load should be measured separately by finding the departure from hydrostatic pressure (static pressure difference) as a function of depth. The static pressure difference must be measured in a fluid with a velocity head of the order of one to two feet and will itself be of the order of 0.01 feet. Any useful method of measuring static head must therefore be almost independent of the flow velocity.

APPARATUS

Summary

The equipment used to satisfy the preliminary specifications for the flow generation was a recirculating flume using water for the fluid and rounded river gravel sieved to a narrow size range for the particles. The concentration measurements were carried out by measuring the attenuation of a beam of gamma rays. Fluid velocities were measured with pitot-static tubes. Particle velocities were either assumed to be the same as the fluid velocities or were measured from a sequence of photographs. Details of all the above apparatus and its design make up the remainder of this chapter.

Flume

General Criteria

Assuming water and gravel of specific gravity 2.65 as the media in the flume and, substituting in (4-5) and (4-6), the limits on shear stress and particle diameter become

$$T > 1.80 \text{ lbs/ft}^2 \qquad (4\text{-}7)$$

$$0.0097\ T > D > .0236/T^{\frac{1}{2}} \ . \qquad (4\text{-}8)$$

To have the channel as similar as possible to a two dimensional system, it was considered desirable to maintain

the channel width at three to four times its depth. As well as for the immediate purpose described in this thesis, the flume was to be used for a variety of future experiments. These proposed experiments could not be precisely defined at the time the flume was designed and even the requirements for this thesis were subject to change. For these reasons, versatility was predominant in the design thinking. The overall length of 100 ft was fixed by the amount of space available and the deck width of 8 ft was determined by the steel plate available as well as the possible use of the flume for meander studies. For the studies under discussion here, a very high flow per unit width is required. Therefore, the side panels were made adjustable and could be placed at any position on the deck, then clamped down. The range of slope available is from just negative up to 0.065, the upper limit fixed by the building.

Because the flume was situated in the Fluid Mechanics Laboratory where the floor area is restricted and where a 100 ft long obstruction would be very inconvenient to the other users of the laboratory, it was supported clear of the floor with a minimum head room of 6 ft 10 inches when the deck was horizontal.

The pump selection was based on a maximum flow of about 20 cusecs pumping both particles and fluid through the one system.

Because it was thought that the situation could arise where the desired flow down the deck would be insufficient to transport the solids back along the return pipe, a bypass pipe was installed. This latter pipe allowed some of the recirculated flow to bypass the deck if so desired. A secondary effect of this bypass was that in pump selection the flow range required could be reduced to lie between the maximum possible and the capacity of the bypass.

Hydraulic Design

The flume shown in elevation in Fig. (4-1) and photographically in Figs. (4-8) and (4-9) was designed and built from the above considerations. It consisted of a flat deck, 94 ft long by 8 ft wide, on which light steel or glass sided panels could be placed and tied down to form a channel. On reaching the end of the channel, the flow turned downwards into a contraction, followed by another 90 degree bend into an axial flow pump. From this pump, the flow was taken along a 15 inch pipe under the left side of the flume and up into a head tank. Plates in the head tank could, if desired, be used to bypass part of the flow, with the remaining flow continuing down the channel. Flow bypassing the channel returned through a 15 inch pipe followed by a 10 inch pipe to the contraction preceding the pump. Control of the main flow was obtained by varying the pump speed.

Filling and emptying of the flume was carried out using a flexible 6 inch hose connected to the upstream end of the bypass pipe, and an overflow was provided at the downstream end in the form of a weir. This overflow was necessary because, had a sudden stop occurred with the flume on a steep slope, there would have been insufficient storage in the tail section to contain the full contents of the flume.

After only 25 hours operation with ¾ - ½ inch gravel, the pump impeller was found to be badly worn. This wear was most noticeable at the impeller tips where the clearance increased, causing a marked reduction in head and flow for a given pump speed. Wear on such a scale was clearly unsatisfactory and the following modifications to the system were undertaken.

Close to the downstream end of the flume, the solid particles were screened out and dropped through a hole in the deck. A hopper placed under this hole collected the solids and channelled them into a jet pump from which the particles were pumped into the fifteen inch return line at a point on the delivery side of the axial flow pump. The jet pump was powered from the existing high head laboratory supply through a 6 inch pipeline, control being obtained by an hydraulically operated valve on this 6 inch line. The continual overflow from the weir was bypassed to a creek near the laboratory.

A diagram of the hydraulic layout at this final stage of development is shown in Fig. (4-2).

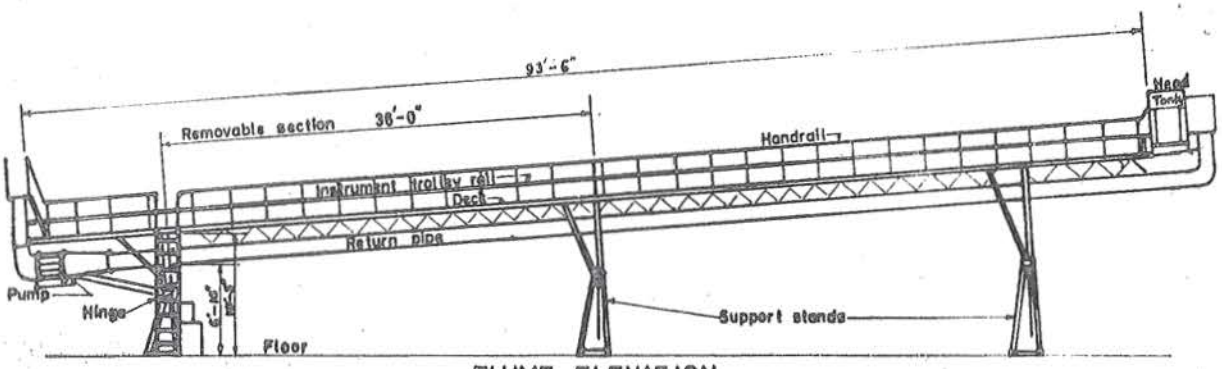

FLUME ELEVATION
FIG 4-1

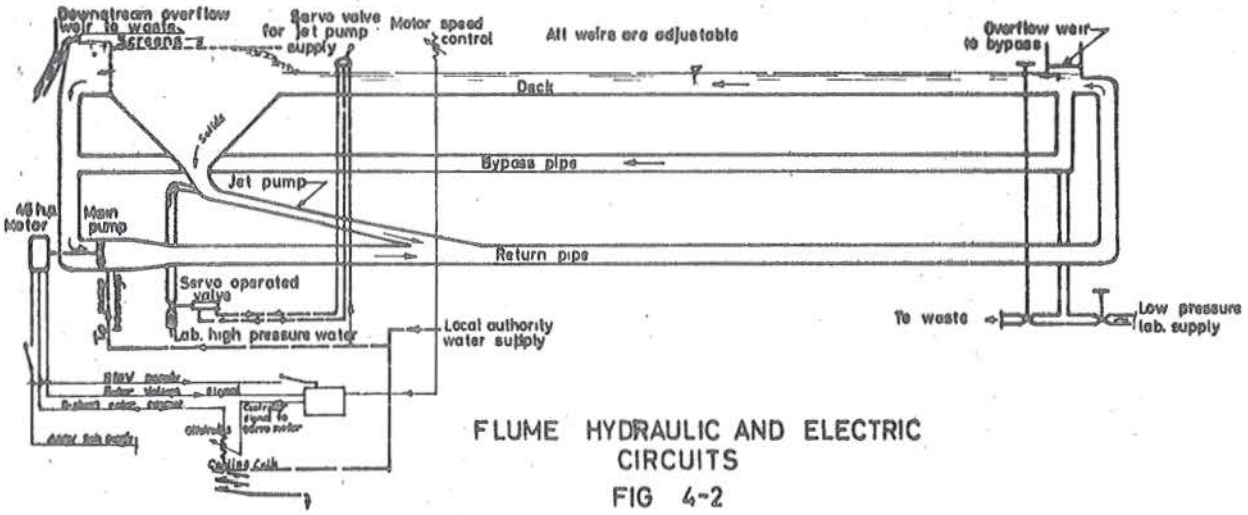

FLUME HYDRAULIC AND ELECTRIC CIRCUITS
FIG 4-2

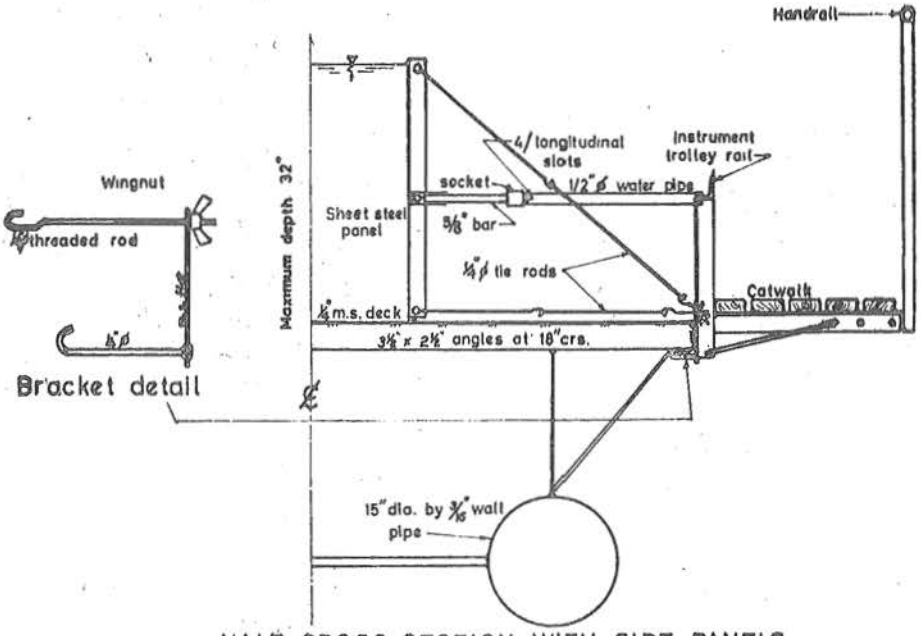

HALF CROSS-SECTION WITH SIDE PANELS IN POSITION
FIG 4-3

Structural Design

The flume was supported at three points spaced 36 ft 0 inches apart. One support acted as a hinge and at the others the flume hung on adjustable lifting screws. These screws were supported on bearings at their upper ends, the bearings resting on stands bolted to the floor. This arrangement can be seen in Fig. (4-1). The tilting flume itself was designed to act as an integral girder, the deck acting as one flange and the pipes as the other. Shear transfer was by a plate welded to the pipes and attached to the deck by a series of shear plates. Rigidity was the main criterion in deciding on this form of structure as the available depth was limited and a light structure was desirable. The tilting section of the flume was constructed as four separate sections. The first three parts were approximately 13 ft, 36 ft and 45 ft long and were followed by a short head tank section. Erection was carried out by placing the sections, then bolting them together. If desired, the flume could be unbolted and shifted, or altered in length by removing the 36 ft section.

Outside the working deck a wooden catwalk was provided. Steel angles at each side of the working deck 16 inches above the deck acted as rails for the instrument trolley and also formed part of the side panel system.

Panels forming the side of the channel were of rigid sheet

steel construction except for two steel frames glazed with ¾ inch glass. The panels all had sponge rubber strips along one end and along the bottom edge. Using a series of tie-downs on each side, each tie-down consisting of an adjustable strut and two adjustable ties, the panels could be held rigidly on any part of the deck.

Tie-down equipment used in the experiments was limited to a channel width varying continuously from nothing up to 6 ft, followed by a step up to 8 ft. In Fig. (4-3), a cross-section of the flume with the side panels set at a 2 ft channel width is shown, while Fig. (4-11) is a photograph of the panels and tie-down system. It is possible with this system to alter the angle of the panels to form a channel of trapezoidal section.

Control

No valves were included in the main flow circuit, flow control through the axial flow pump being accomplished by pump speed control only. A 45 horsepower slip-ring induction motor was used. The tappings from the motor slip rings were connected to three electrode plates immersed in sodium carbonate solution, the depth of immersion being controlled by a small motor. The rotor voltage, and therefore the motor speed, was held constant by a control system adjusting the depth of immersion of the plates. Adjustment of the voltage and consequently the

speed could be carried out with a portable controller. Flow through the jet pump was adjusted from a control valve placed on the flume catwalk and connected by hose to the hydraulic valve controlling the jet pump supply line. An adjustable section of the downstream weir allowed some control over the tail tank water. At the flow rates used, the flow in the working section was supercritical and it was therefore possible to adjust the tail tank level so as to form a hydraulic jump close to the screening position.

Filling and emptying of the flume with water were carried out from the floor of the laboratory, using hand operated valves. Filing and emptying of the solids were carried out using a perforated hopper attached to the laboratory crane.

It was possible, therefore, to control the flow from the catwalk once the flume had been filled and started.

Concentration Meter

After the decision to use gamma radiation was made, the important design problem was to obtain sufficient resolution in the vertical direction. The available counting equipment and radioactive isotopes presented definite restrictions. It was found upon reading the literature that the use of gamma radiation was common and commercial equipment was available for measuring the average density of a fluid. However, no work could be found on measuring the spatial variation in

concentration. The method finally adopted was to use a readily available one curie source of caesium 137 (Cs^{137}) behind two lead shields with small holes in them. The collimated beam passed through the flume to a detection unit shielded from as much as possible of the scattered radiation, that is, having a detector shield with a small angle of acceptance.

Initial Calculations

A general account of the calculations used to predict the behaviour of this apparatus is included at this point. The methods were developed from those described in refs. (17) and (18) and were adapted to this particular problem.

If a source of strength z curies, emitting η' photons per curie, is placed a distance d, from a detector of efficiency η counts per photon, then the count rate λ is given by

$$\lambda = z \eta \eta' \frac{A_c}{4\pi d^2} K \qquad (4\text{-}9)$$

where A_c is the effective area of the detector.

The factor K in equation (4-9) is an attenuation factor depending on the material between the source and detector. As the photons travel through material, they collide with atoms and are either destroyed, deflected, or form lower energy particles. If all the photons suffering collisions missed

the detector, the attenuation factor K would be an exponential function of the thickness of the material. Normally, however, some photons which are deflected from their course enter the detector and increase the count by a "build up factor". This factor is a function of the geometry of the system and the type of material; it may be as large as 3.0 or even higher. If the beam is very narrow and the detector window has a sufficiently small angle of acceptance, the build-up factor is close to 1.0, such a value being assumed in the rest of this thesis.

For a beam traversing the flume when the contents have a solids concentration C, there will be an initial attenuation of the beam K_f in the flume walls. Further attenuation will take place as the beam traverses w(1-C) feet of water and w C feet of solids where w is the internal width of the flume. The total attenuation is therefore given by

$$K = K_f \, 10^{-\left(\frac{C}{l_g} + \frac{1 - C}{l_w}\right) w} \qquad (4\text{-}10)$$

where l_g and l_w are the thicknesses of solids and water respectively required to reduce the photon flux by a factor of 10.

From (4-9) and (4-10), we have

$$\lambda = A \, 10^{-B C} \qquad (4\text{-}11)$$

$$\text{where } A = z\eta\eta' \frac{A_c}{A\pi d^2} K_f \, 10^{-\frac{w}{l_w}} \qquad (4\text{-}12)$$

$$B = w \left(\frac{1}{l} - \frac{1}{l_w}\right) \qquad (4\text{-}13)$$

Calculated values of A and B using equations (4-12) and (4-13) were useful in designing the apparatus, but for experimental measurements using this apparatus measured values of A and B were used. As a measure of the sensitivity of the apparatus, a suitable parameter is $d\lambda/dC$ which, from (4-11), is given by

$$\frac{d\lambda}{dC} = - A B (\log_e 10) e^{- B C(\log_e 10)} \qquad (4\text{-}14)$$

Random Nature of Photon Emission

The photons are emitted in a random fashion and it can be shown (11) that an implication of this is that the number of counts in a given period is distributed according to the Poisson distribution. When n is the number of counts measured, the confidence limits for the mean are given approximately by m_1 and m_2 defined by the equations

$$\begin{aligned} 2\,(\sqrt{n+1} - \sqrt{m_2}) &= - t_\alpha \\ 2\,(\sqrt{n} - \sqrt{m_1}) &= + t_\alpha \end{aligned} \qquad (4\text{-}15)$$

where t is defined by

$$\text{Probability } (-t_\alpha < x < t_\alpha) = 1 - \alpha$$

where x is the abscissa of the N(0,1) curve. Stated in words, when the area under a symmetrical section of the unit normal curve is $(1 - \alpha)$, then the abscissa of the positive boundary of the section is t_α.

Rearranging (4-5), the $(1 - \alpha)$ confidence limits for the true mean count about the expected mean count n, are given by

$$1 + t_\alpha\left(\sqrt{n + 1} + \frac{t_\alpha}{4}\right) - t_\alpha\left(\sqrt{n} + \frac{t_\alpha}{4}\right) \qquad (4\text{-}16)$$

Normally, the true count n is estimated by subtracting a background count n_b from the total count n_t. The total count rate λ_t is estimated as n_t/T_t where T_t is the time taken for the count. Confidence limits for λ_t can be found directly from (4-16) and these are approximated to by the relation

$$\lambda_t = \frac{n_t}{T_t} \pm t_\alpha\sqrt{\frac{n_t}{T_t^2}}\ , \qquad (4\text{-}17)$$

as an interval, within which we have a $(1 - \alpha)$ probability of including λ_t. An estimate of the variance of the measured count rate is n_t/T_t^2 and, for the background variance, n_b/T_b^2, where T_b is the time taken for the count to reach n_b. If both n_b and n_t are greater than 50, both λ_t and λ_b tend

to be normally distributed. One result of this approximation is that the difference between λ_t and λ_b will have a variance equal to the sum $\left[\text{Var.}(\lambda_t) + \text{Var.}(\lambda_b)\right]$. Using the variances given above and putting $\lambda = n/T_t$

$$\lambda = (\lambda_t - \lambda_b) \pm t_\alpha \sqrt{\frac{n_t}{T_t^2} + \frac{n_b}{T_b^2}} \,. \qquad (4\text{-}18)$$

Equation (4-18) gives limits within which there is $(1-\alpha)$ probability of including λ. The proportional accuracy ϵ will be defined by

$$\epsilon = \frac{t_\alpha \sqrt{(n_t/T_t^2) + (n_b/T_b^2)}}{\lambda_t - \lambda_b} \,. \qquad (4\text{-}19)$$

In the design of this apparatus, the time required to obtain a given accuracy is important and the effect of the background on this factor is described by T_r. Here T_r is the ratio of the time required to obtain a given accuracy with background present to the time required to obtain the same accuracy with the background removed. From (4-19), it can be shown that T_r is given by

$$T_r = \frac{1 + \lambda_{br}}{1 - \lambda_{br}/T_{br}} \qquad (4\text{-}20)$$

where $\lambda_{br} = \lambda_b/\lambda$ and $T_{br} = T_b/T_o$, T_o being the time required

for the given accuracy with the background removed. The time required for a given accuracy is therefore always increased by the presence of a background count and, as $\lambda_{br}/T_{br} \rightarrow 1.0$, the required accuracy becomes unattainable.

As it is often more convenient to time a preset count, some idea of the count necessary for a given accuracy is required. Using (4-17), the count necessary with no background to obtain λ with $(1-\alpha)$ probability that the fractional error is less than ϵ is given by n_o where

$$n_o = (\epsilon \ t_\alpha)^2 \qquad (4\text{-}21)$$

From (4-19), n_r, the ratio of counts required when a background is present to obtain a given accuracy to n_o (the counts required with no background to obtain the same accuracy), is given by

$$n_r = \frac{(1 + \lambda_{br})^2 \ n_{br}}{n_{br} - \lambda_{br}^2} \qquad (4\text{-}22)$$

where n_{br} is the ratio of counts used to determine the background to n_o.

At this point, all the equations required to estimate the behaviour of a concentration meter in the presence of a background count have been obtained where the counts n_b and n both exceed 50.

Description of Meter

With the one curie source of Cs^{137} decided upon, the terms z, η', l_g, l_w were all fixed. The Cs^{137} source emitted both gamma and beta radiation, but beta particles were all absorbed completely by the plate glass sides on the deck plates. All gamma particles (photons) were emitted with an energy of 0.663 Mev, 0.83 photons being produced for each disintegration. The term $z\eta'$ therefore had a magnitude of $3.7 \times 10^{10} \times 0.83 = 3.07 \times 10^{10}$ photons per second. Initially, a width w of 30 inches was used and, for preliminary design, the distance d from source to detector was taken as 42 inches. For 1½ inches of glass K_f was 0.4 and from (18) $l_w = 10$ inches. From (4-12) $A = 550\,\eta\,A_c$ where A_c is in square inches and B = 5.0. Initially a geiger tube was used and A_c was kept at 0.25 inches^2. Estimating the geiger tube efficiency η at 0.05, the count rate equation was given by

$$\lambda = 20 \times 10^{-5C} \text{ counts per second.}$$

The geiger tube was shielded with a minimum of 1½ inches of lead to reduce background counts. It was found, however, that the count rate at concentrations above approximately 0.4 was completely lost in the background. Accurate readings would have taken a very long time. With the window 0.25 inches deep by 1 inch long, the resolution of the apparatus was not

satisfactory and a complex correction procedure was required to obtain the true concentration profile.

Improvement by a factor of at least 10 was required and, to obtain this, the geiger tube was replaced by a scintillation detector which had an efficiency of about 0.5 counts per photon. At the same time, the shielding was modified to improve the resolution and to enable the concentration profile to be obtained directly. Fig. (4-4) shows the final design used and Fig. (4-10) includes photographs of the apparatus. The source was kept in a portable shield which could be fitted on to the source holder on the meter. The source holder and the detector were mounted on separate legs of an inverted U frame. Provision for adjustment was made, allowing the source, detector and windows to be aligned. The U frame could be raised or lowered by means of a pair of screw jacks linked together and operated from a point clear of any radiation hazard.

A Nuclear Chicago 183B scalar supplied the power and counting system for both the geiger tube and the scintillation detector. When runs of over 30 minutes were attempted, it was necessary to blow filtered air through the scalar.

Safety Considerations

Including both beta and gamma radiation, the total radiation from the unshielded source approached 1.0 roentgen/hour

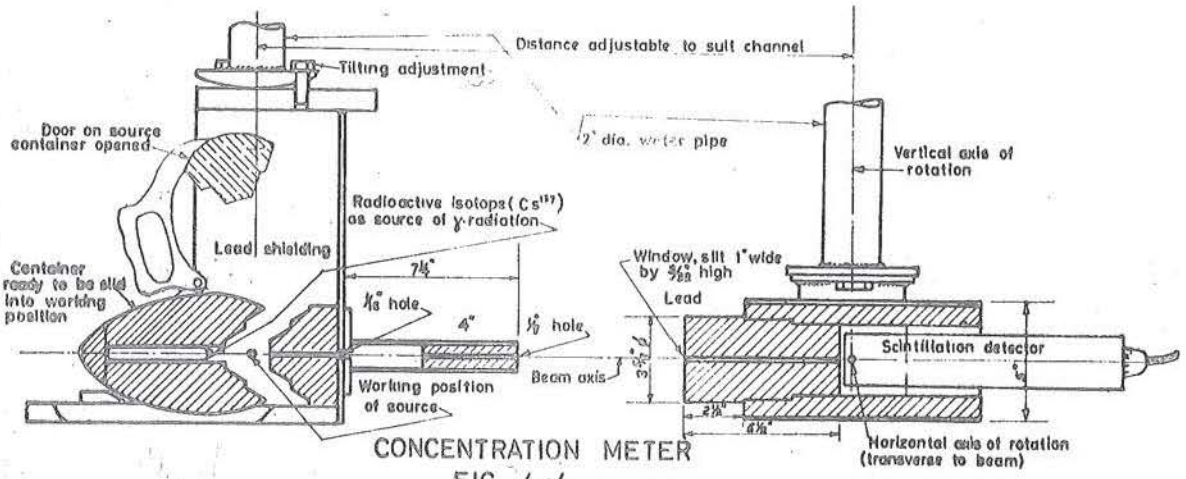

CONCENTRATION METER
FIG 4-4

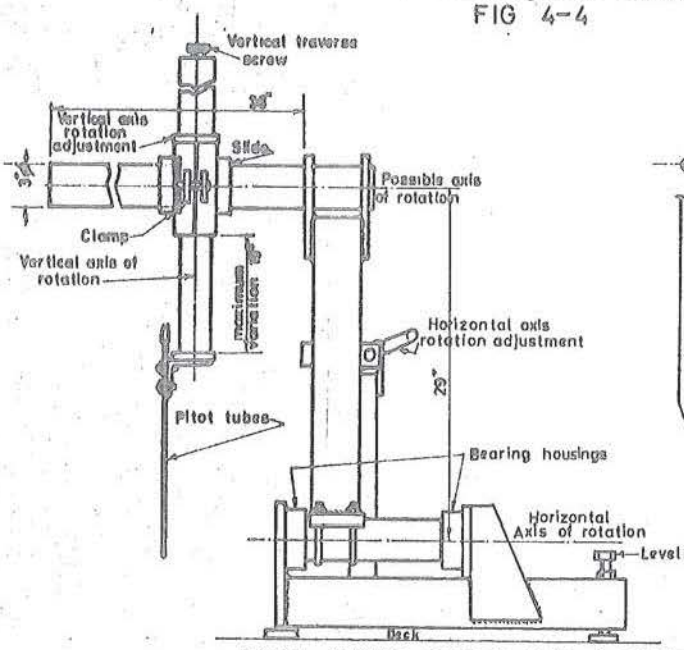

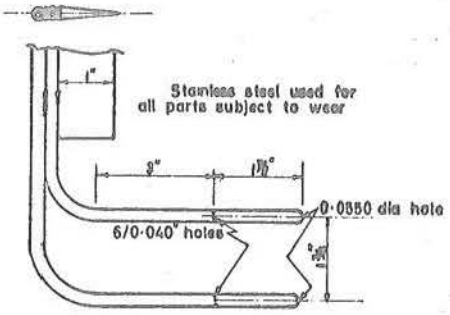

Pitot static head detail

PITOT STATIC TUBES AND MOUNT
FIG. 4-5

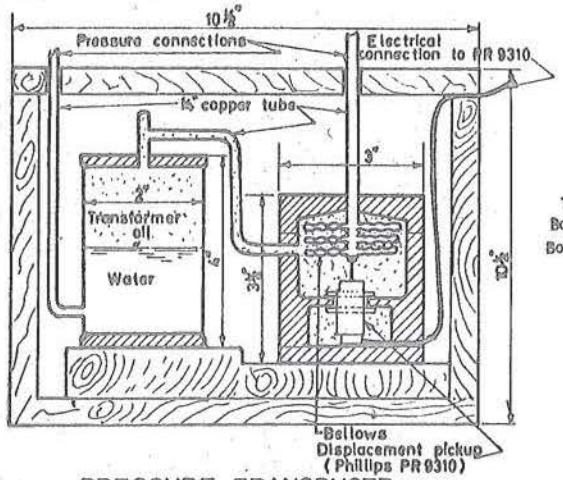

PRESSURE TRANSDUCER
FIG. 4-7

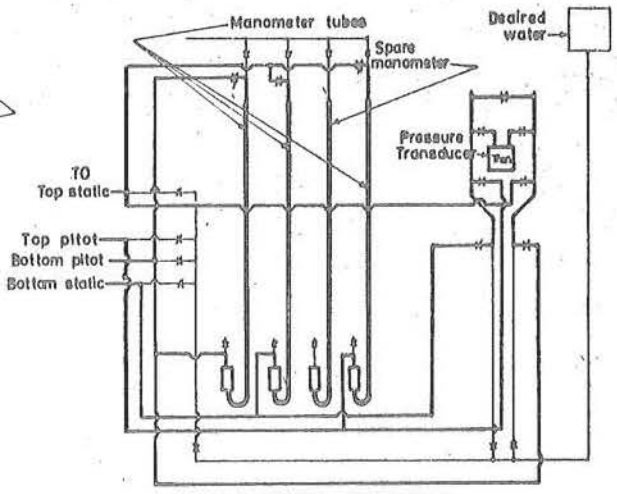

MANOMETER SYSTEM
FIG. 4-6

at a distance of 3 ft. The safe dose rate used in design for persons working on the flume (all of whom were monitored) was 0.1 roentgen per week, making some form of shielding necessary. Shielding required to collimate the beam and protect the detector was, with slight modifications, sufficient when the source was in the normal working position. For a person working on the floor below the flume, the maximum continuous dose rate was less than 0.045 roentgen per week. Therefore, the dose expected to be received by a person working on the laboratory floor would be less than 0.01 roentgen per week, the maximum allowable for unmonitored persons.

The source was always kept inside a container with a close-fitting door and, just prior to taking measurements, the door was swung clear and the whole unit slid forward on to a matching shield. It was only during this operation that the dose rate was high. All parts of this operation were carried out from behind the source where the shielding remained in place, so that back-scatter of gamma radiation and soft x-rays from the beta emission were all that reached the operator. As the time required was very short (less than a minute) and all operators on the flume were monitored, no shielding against back-scatter was provided.

Normally, excluding the preparatory operation described in the preceding paragraph, and except along the line of the

beam, the dose rate was less than 0.1 roentgen per week for all points more than 1 ft away from the shielded source.

Fluid Velocity and Pressure Measurement

Measuring Head

As the conditions in the moving bed were extremely rugged, a very simple, strong and wear-resistent form of velocity meter was required. After an examination of the various possibilities, the only two feasible methods appeared to be the use of a probe measuring the thickness of the boundary layer over an electrode or the use of a pitot-static tube. In the boundary layer thickness method, the usual measurements are of the transfer of heat or electric current across a surface. Measuring the current flowing through an electrode with a very dilute alkaline solution of ferri-cyanide used for the working fluid gave a low response time (in the region of 0.001 seconds) and gave satisfactory test results with the possibility of measuring the total velocity vector, but, because ultimately the flume was operated with a continual discharge of water to a local stream, the method proved to be unsuitable from both the cost and pollution points of view.

Pitot-static tubes were therefore used for fluid velocity measurement. Two tubes made up of ¼ inch stainless steel tubing and with solid stainless steel noses were mounted

1¾ inches apart. Included in Fig. (4-5) is a drawing of these tubes and Fig. (4-12) is a photograph of them, taken after the experimental runs were completed. The tubes consisted of a section parallel to the flow for measuring purposes and perpendicular to this was a leg going up to a mounting. To stiffen the tubes and also reduce the disturbance at the surface of the supercritical flow, a sharp-edged leading section was attached to the perpendicular section of the tubes. Previous experiments had proved the stiffness of the supporting mount to be important. A mount was built to hold the pitot-tubes while allowing rotation about two perpendicular axes and movement along one axis (normally that perpendicular to the flow). The mount could also be shifted from one side of the flume to the other. Fig. (4-5) is a drawing of the mount and Fig. (4-13) is a photograph of it in position with the pitot tubes attached.

Pressure Measurement

The four leads from the two pitot-static tubes were taken along the mount, across the deck and down to a manometer system mounted on a stand about 4 ft above the floor and over 7 ft below the flume deck. Earlier attempts to mount the manometers on the flume deck had failed because any small leak allowed air into the system and, furthermore, the valves used were not reliable at pressures below atmospheric.

For a manometer circuit measuring the head h between two points, an equation can be written relating h to h_m, the measured head

$$h = h_m + R\,C\,\frac{dh_m}{dt} + S\,C^2\,\frac{dh_m}{dt}\left|\frac{dh_m}{dt}\right| + I\,C\,\frac{d^2h_m}{dt^2} \quad . \qquad (4\text{-}23)$$

In (4-23), if the flow is Q, then $C = Q\Big/\frac{dh_m}{dt}$, the hydraulic-resistance is $R\,Q + S\,Q\,|Q|$ and the inertial head is $I\,\frac{dQ}{dt}$. Both R and S are not true constants as, in general, the flow resistance equation will vary with Q. However, if $R < S\,Q$ for $Q \ll$ maximum value of Q, then a close approximation is to assume S constant and R = 0. In the system used in these experiments, the assumption R = 0 is satisfactory. If R, C, S and I are known, then the true fluctuating value of h can be found, provided h_m, dh_m/dt and d^2h_m/dt^2 are all measured as functions of time.

If S is some function of Q, that is symmetrical about Q = 0, then a randomly varying signal h applied to the system, of mean value $\bar{h}$, will result in a fluctuating value of h_m such that $\bar{h}_m = \bar{h}$. The effect of a departure from symmetry, of the function S of Q, (that is, if the magnitude of head loss is dependent on the flow direction) will be to bias the value of h_m. If the value of S is lower for flow from P to Q than for flow from Q to P, then the measured head at P relative to

Q will be greater than the true value.

From (4-23) it can be seen that, for a quick response, C should be kept as small as possible.

Perchlorethylene Manometers

The first manometer system used was based on a set of single column manometers with dyed perchlorethylene (specific gravity 1.623) as the working fluid. Two manometers were used for measuring the velocity heads and one for measuring the head difference between the two static connections. Valves were arranged to allow flushing back with de-aired water through the pitot-static tubes. Each manometer consisted of a 3 m.m. bore glass tube, the pressure connection being to the top of the glass tube and the top of the reservoir. A diagram of the system is shown in Fig. (4-6) and the complete assembly can be seen in position in Fig. (4-9). All valves, manometers and fittings were attached to a single board together with the valves used when measuring the pressure in various parts of the flume. A fourth manometer, identical with the other three, was fitted to provide against failure of one other during a run. A kerosene-water manometer was tried but found far too sluggish in operation.

Pressure Transducer System

Even with the 3 m.m. tubes, the response of the system was quite slow and the large amount of fluid flowing into the

pitot-static tubes when the pressure changed tended to introduce air into the system, making frequent flushing necessary. Consequently, it was decided to build a system with a much smaller value of C and a high sensitivity to low heads. The apparatus considered the most suitable was an electrical pressure transducer as, if successful, this equipment could ultimately be used to obtain the actual fluctuating value of h, using equation (4-23). Because at the time a suitable commerical transducer could not be obtained, one was built up. A bellows was immersed in transformer oil, one pressure connection going directly to the inside of the bellows and the other to a reservoir of oil with a water-oil interface. The oil reservoir was connected to the oil surrounding the bellows and a Phillips displacement transducer P.R.9310 was used to measure the bellows displacement. A drawing of this apparatus is included in Fig. (4-7). The complete system was contained in a well insulated box and the electrical leads from the P.R.9310 taken to a Phillips direct reading bridge PR.9300. The output could be read directly on the bridge meter or taken through a Phillips GM4531 D.C. amplifier to a Kelvin Hughes MK5 single channel pen recorder. This system required less than 0.2 ccs of fluid per foot head difference applied. A section of the output record is shown in Fig. (4-14).

Particle Velocity Measurements

The only method of directly measuring the particle velocities that was attempted was observation, frame by frame, of a movie negative. Particles used in the flume were river gravels and, when the flume was operating, a fine flour was generated by abrasion of the stones. This flow could be settled out in a beaker over a period of hours, but treatment of the large quantities of water flowing in the flume was not practicable. The best that could be done was to continuously discharge two cusecs to waste and replace this with clean water from the laboratory supply. Even then, the visibility was such that a ruler could just be read through three inches of the contaminated water in the flume.

Originally it was intended to photograph the particles through the surface of the flow, using a system of prisms to form a stereoscopic pair in each frame. Because of the opaque nature of the circulating water, this was not possible.

The only photographs that could be taken were through the glass sides of the flume. Various techniques were employed, the three main ones being as follows:-

A Phillips stroboscope was used as a light source while the film was pulled continuously through a Southern instruments oscilliscope camera. The image was formed on 35 mm. film and was of good resolution. However, even with the fastest avail-

able film, the light was insufficient at frame rates above 20 - 30 frames per second; these frame rates were unsatisfactory for useful measurements and this method was not persevered with.

The next device used was a Bolex 16 mm. H16 movie camera operated at 64 frames per second with an exposure time of 1/640 second. Light was supplied by eight 500 watt photofloods and this gave a good clear image, but it was found that the photographs were not suitable for analysis as, at 64 frames per second, the time elapsed between frames was so great that it was not possible to trace a given particle from one frame to the next. This method was therefore abandoned.

Finally, a Magnifax high speed camera was used. The image was not as good as that produced with the Bolex, but the high frame speed made visual analysis possible. To obtain a reasonable image of rapidly moving small particles, a short exposure time was necessary and also, if possible, a depth of field of about 2 inches. As both decrease of the exposure time and increase of the depth of field required increased illumination, it was important to have the maximum possible light. A bank of six 500 watt photofloods was placed just above the surface of the flow, two 500 watt photofloods on one side of the camera and a 1,000 watt Baur "Sungun" on the other. A photograph of this arrangement can be seen in

Fig. (4-15). The film used was 16 mm. Kodak Plus-X negative and the lens was, in normal use, fully opened at f2.0.

After the film had been developed, it was analysed using a motion analysis projector and a sheet of tracing paper placed over a screen, the film being projected frame by frame and selected stones sketched on the paper for a series of frames.

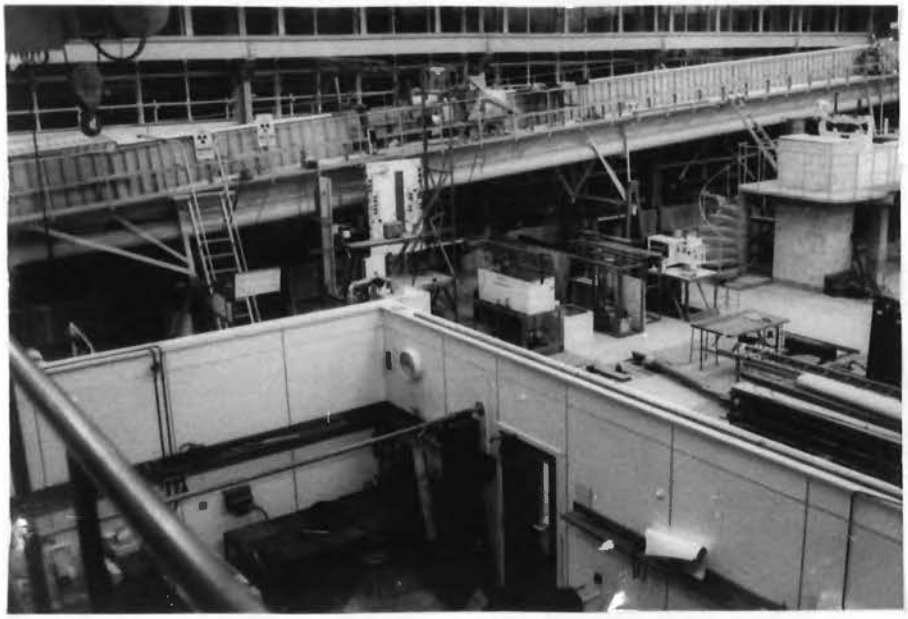

FIG. 4-8
TILTING FLUME

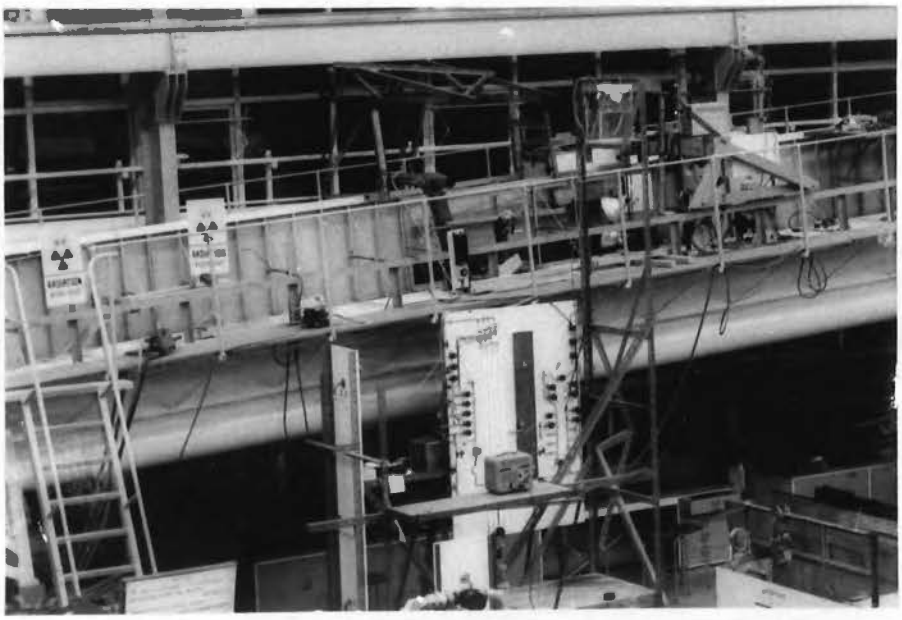

FIG. 4-9
WORKING SECTION AND
MANOMETERS

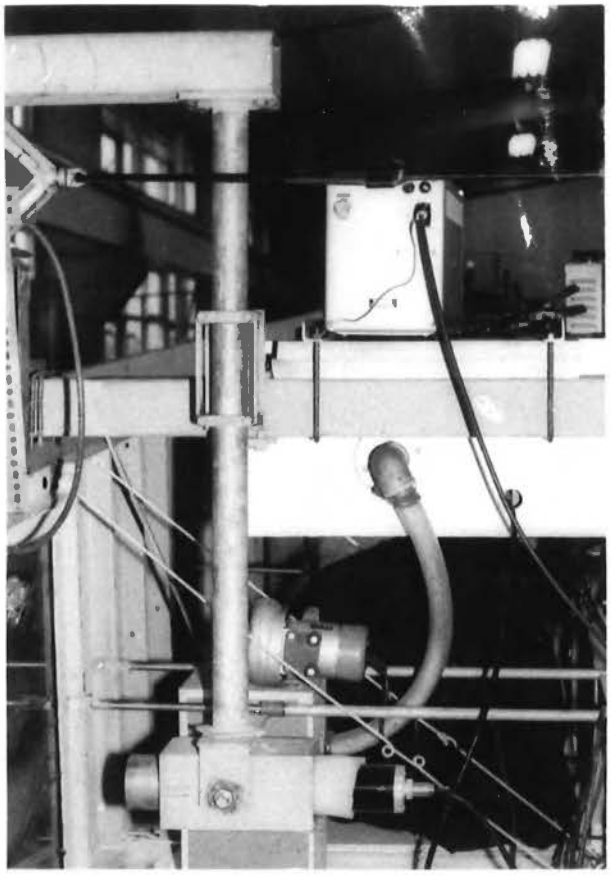

Scintillation Tube

Source and container in position

FIG. 4-10
CONCENTRATION METER

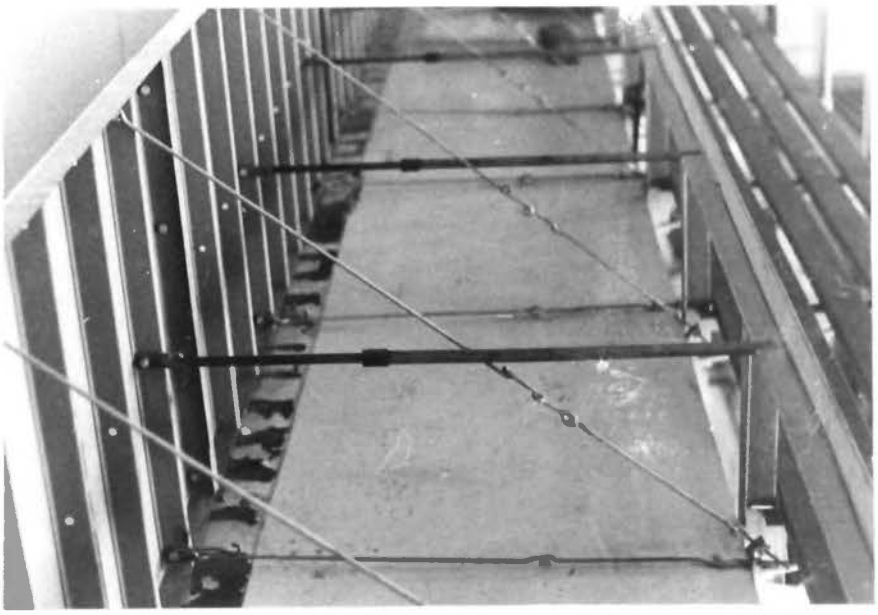

FIG. 4-11
PANELS AND TIE DOWN SYSTEM

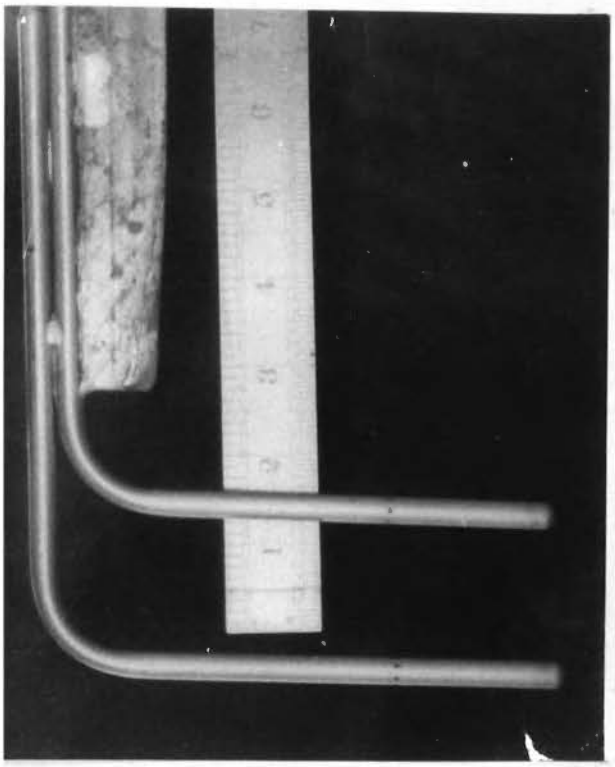

FIG. 4-12
PITOT-STATIC TUBES

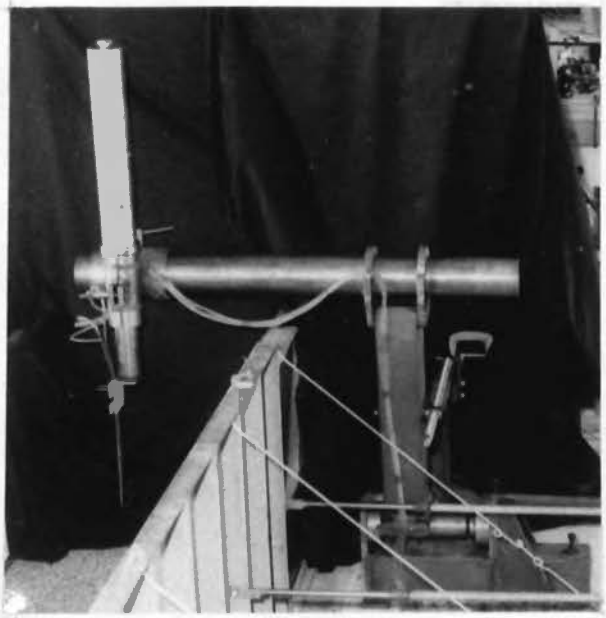

FIG. 4-13
PITOT-STATIC TUBE MOUNT

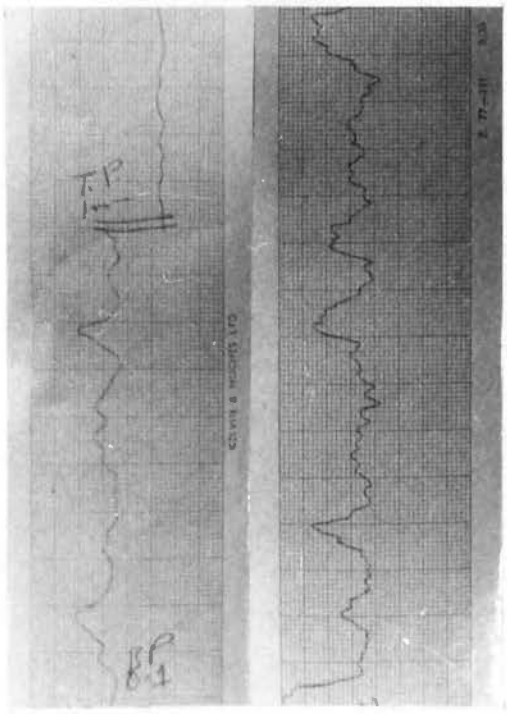

FIG. 4-14
TRANSDUCER OUTPUT

FIG. 4-15
PHOTOGRAPHIC SYSTEM

CHAPTER 5

EXPERIMENTAL PROGRAMME

SYNOPSIS

This chapter starts with a note on the objects of the experimental programme and then describes the measurements taken and the programme carried out to attain these objects. Details of the apparatus used are given in Chapter 4 and the results of the experiments are to be found in Chapter 6.

OBJECTS

In Chapter 2 it is shown that for a wide range of sediment carrying flows the assumption of a high particle Reynolds number is justified. In Chapter 2, a method of calculating the velocity and concentration profile in the bed of a stream is developed in terms of two functions of the concentration, F_1 and F_3, where $F_1 = P/T_t$ and $F_3 = T_t/\rho_s D^2 (\frac{du}{dy})^2$. An implied assumption made in this approach was the existence of a deep moving bed at high values of $T_* = T_t/(\rho_s - \rho_f) g D$.

The first object of the experimental programme was to observe the general behaviour of a moving bed of stones for $T_* > 1.0$ and in particular to examine the thickness of this bed layer. Other objects of the programme were to measure

F_1 and F_3 at high Reynolds numbers for $\rho_s/\rho_f > 1.0$ and to compare the experimental values obtained with those predicted from the equations derived in Chapter 3.

GENERAL FORM OF EXPERIMENTS

Measurements were made of a more or less uniform steady, open channel flow generated with the flume described in the previous chapter. These measurements were of solids concentration, fluid velocity, particle velocity and static pressure distribution as functions of depth, and also of the bed slope and particle grading. Some sets of runs did not include all of these parameters.

Three different particle sizes were used, there being one flow rate for the first size and two flow rates for each of the others, making a total of five sets of results.

Operation of Flume for Measuring Runs

At the beginning of each experimental run, the flume was filled and, using both the main pump and jet pump, gradually brought up to full flow. During this operation, care was necessary as too rapid a start could lead to an overflow. About 5 minutes were required to reach full flow and another 10 minutes were allowed for equilibrium to be attained. Normally, no further measurable change occurred after the

first five minutes operation subsequent to reaching full flow. As many measurements as possible were taken and, when the available water supply ran out, the flume was stopped.

MEASUREMENTS

Concentration Measurement

To take advantage of the lower air temperature and consequent greater reliability of the scalar, all concentration measurements were taken in the evening. The scalar was turned on at least an hour before the start of all the runs made for these measurements. To allow the counter head time to reach an equilibrium temperature, the voltage supply for the scintillation detector was brought up to the full operating value. Immediately prior to the run being started, a measurement of the background was made, then the source container was opened and the source brought into position.

When the 10 minutes allowed for the flow to reach a steady state had elapsed, the beam was lowered to just below the surface of the fixed bed and counting started. The electronic counter on the scalar indicated in lights the binary count up to any preset integral power of 2 equal to or less than 256. Upon reaching the preset limit, a pulse was registered on the mechanical counter and the electronic counter reset to zero. Counting was stopped when a preset

number of pulses was registered on the mechanical counter. This mechanical counter was normally set to stop at 10, the minimum possible. During the count, the time taken for 0.1, 0.3 and 0.6 of the total count (or some other similar set of fractions) was noted and, if any discrepancy appeared in the rates during any interval, the count was restarted. This latter precaution was necessary because the mechanical counter was not always reliable, but occasionally failed to count when pulsed by the electronic counter.

When a satisfactory count had been achieved at a given level, the beam was raised to the next level where a count was required and the process repeated. Although it was normal to measure from the deepest point upwards, this procedure was reversed on occasions, the order of taking the results being that of their listing in Chapter 6. If a complete traverse was not obtained in one run, four or more points from the first run were repeated on the second. The increments used were governed by the rate of change in the count, the more rapid the rate of change the smaller being the increment.

After each run was completed, a further background count was obtained. To calculate from λ_t, λ_b was assumed to vary linearly with respect to time between the values obtained at the beginning and end of the run.

Fluid Velocity and Static Pressure

The pitot-static head described in the previous chapter was used for fluid velocity and static pressure measurement. While the flume was settling down to a steady state before a series of measurements was begun, the pitot-static tubes were lowered to the bed. All parts of the system were flushed with water containing very little dissolved air, the final flushing being always back through the pitot-static tubes into the flume. Just before taking the readings, the tubes were aligned parallel with the bed slope and the walls of the flume.

Two different types of apparatus were used in measuring the pressures, namely, manometer tubes and an electrical pressure transducer. Details of both pieces of apparatus are given in Chapter 4. In using the manometer tube system, the pitot-static tubes were set at the required depth and the time taken for the manometers to reach the new steady mean value was noted. After a further wait for a period of half the time taken to reach the steady state, the readings of all three manometers were recorded. The pitot-static head was then shifted to the next position and the process repeated. A traverse was made from the lowest depth to which the tubes would sink under their weight to a point where air-entrainment or separation affected the top tube. During the traverse, frequent flushing of the pitot-static tubes was carried out.

The same point was measured before and after flushing and, if any significant disagreement occurred, the measurements taken since the previous flushing were repeated.

In using the pressure transducer, the following procedure was adopted. Before each run, flushing of the tubes was carried out and, to enable all the electronic equipment to reach a steady operating temperature, it was left operating for an hour. Just prior to starting the run, the two sides of the pressure cell were inter-connected and the bridge and pen recorder set to zero. The cross-connection was then closed and each differential measurement made separately, normally in the following order: top velocity head, bottom velocity head, static head difference.

The measurement was taken by recording with the pen recorder the trace of the transducer output and noting on this output the scale setting of the bridge, the level of the pitot-tube and any other relevant information. A record at least 30 seconds long was taken for each measurement.

For the earlier runs, the method adopted was to read the three differential heads at each point in turn, shift the pitot-static tubes to the next point and then repeat the procedure. Later in the series, it was found that a procedure less subject to error and less time consuming was to make a traverse of all the top velocity heads, followed by a traverse

of all the bottom velocity heads, and finally a traverse of all the static head differences.

During the measurement runs, the zero point was checked at each change of scale and at intervals of not more than ten readings. This zero check was performed by inter-connecting the two sides of the pressure transducer.

Particle Velocities

The only successful method of measuring the particle velocities was to measure the velocity of individual particles from photographs taken with the Magnifax high speed camera and the lighting system described in Chapter 4. After being positioned on the flume deck with its lens axis perpendicular to the walls of the channel, the camera was focused on a grid placed on the glass side panel. Adjustment of the lens was then made to shift the plane that was in focus a further 1½ inches from the camera. This adjustment meant that the camera was focused on a point inside the flume. After the flume had been operated at the required flow rate for a period of at least 15 minutes, the lights were turned on and the camera was operated for a period of approximately 3 seconds then allowed to stop. This procedure was carried out twice for each of two flow rates and on all occasions the camera speed was set at the minimum possible value. Following these runs, the camera was shifted from a point 32 inches away from the side panels to a point 45 inches away and a similar set of four

sequences of photographs was made.

After the film had been developed, the negative was projected frame by frame on to a sheet of tracing paper. When the first frame was projected, the images of a number of the particles as well as the image of the grid on the side of the glass panel were sketched on the sheet of tracing paper. The next frame was then projected and the new image of the grid position over the previously sketched grid. Then the new images of the same particles as had been sketched for the previous frame were sketched in a different colour. This process was repeated frame by frame until eleven frames had been sketched on the one sheet. At this stage, the sheet of tracing paper was changed and the eleventh frame shown on the former sheet was sketched as the first frame of the new one. This procedure was followed until all the useful frames in a sequence had been sketched. As particles moved out of view to the right of the picture, sketches of new particles appearing on the left were started.

Two sequences of photographs for each of two flows were treated in this way, all photographs having been taken when the camera was 32 inches from the flume side panels. A timing mark made on the film during exposure enabled the film speed in frames per second to be calculated as a function of frame number. Hence, the component of velocity in the flow

direction, as well as the vertical co-ordinate relative to the grid, was obtained for each particle sketched.

The velocity profile for each sequence was obtained by dividing the vertical co-ordinate into small elements and finding the mean height and velocity of all the particles contained within each element. The join of the points defining these mean heights and velocities was then taken as the velocity profile. After correction for shift of the top of the fixed bed, the average of the two sequences was used as the particle velocity profile for each flow rate.

WORK PROGRAMME

Tests on ¾-½" Gravel

After the flume and associated equipment had been tested, the side panels were set up as shown in the plan, Fig. (5-1). A channel 30 inches wide extended from the head tank to the gravel separating screens. Each side of this channel was constructed of one glass panel and a number of light steel panels. A layer of light welded steel mesh was placed along the floor of the channel. About 14 ft upstream from the overflow weir, two further walls branched off the channel and formed a tail tank with a maximum width of 8 ft.

The concentration meter, including the scalar, was mounted on a movable trolley spanning the whole width of the deck.

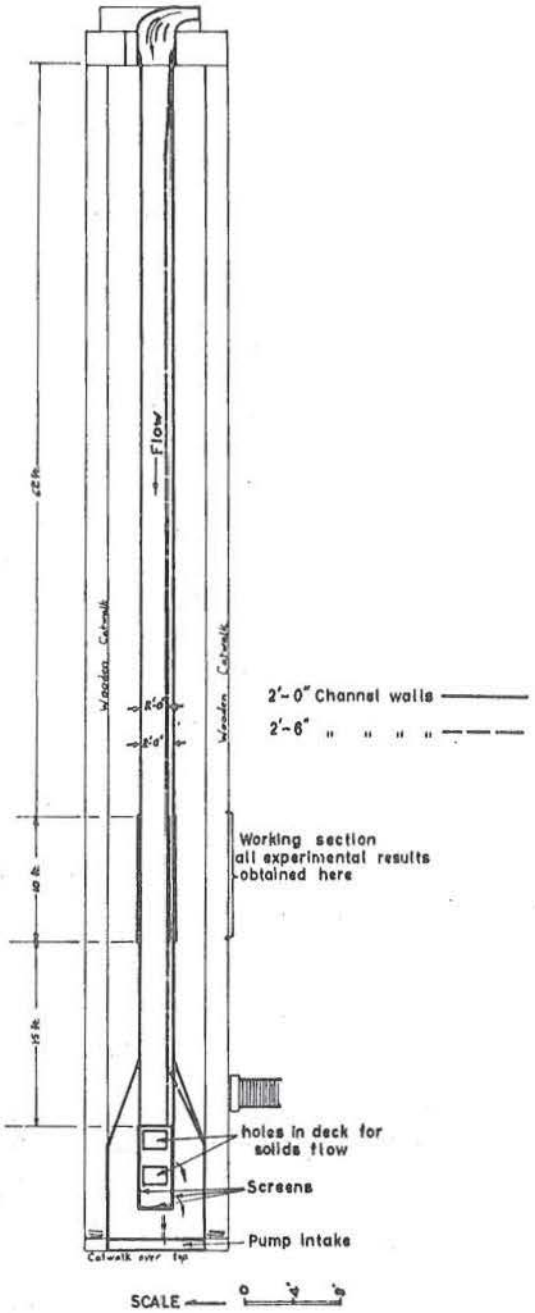

PLAN OF FLUME AS USED FOR THE EXPERIMENTS

FIG 5-1

At the downstream end of the glass panels, the pitot-static tubes were set up.

Initially, 6 cubic yards of ¾ - ½ inch gravel were loaded into the flume and circulated until a steady state was obtained. Further small quantities of gravel were then added until a bank had been formed just downstream of the head tank. It was found that this bank stabilized the flow pattern and made the velocity more uniform across the flume. Because this particle size was large and consequently T_* was small, only the maximum available flow was used in the experimental runs. This flow gave the maximum possible value of T_* and there was no apparent development of waves in the bed material.

Concentration measurements were made using the apparatus previously described and the concentration obtained directly from the values of λ.

Using the perchlorethylene manometers with the technique described earlier in this chapter, the velocity heads and static pressure difference were measured over as much of the channel depth as possible.

A sample of the gravel loaded into the flume was subjected to a sieve analysis and at the end of the runs two further sieve analyses were made. One sample analysed was taken from the whole load of gravel in the channel; the other sample was taken from the top layer of material only.

The surface and bed profiles were measured during the course of the series of runs and the slope over the measuring section was checked three times during this period. Finally, the flume was thoroughly cleared of all solid material.

Tests with 3/8 - 3/16 inch Gravel

Before loading the flume with the next size of particles, the channel width was reduced to 24 inches, with the first panel of the flume tapering from 30 inches at the head tank to 24 inches as shown on the plan, Fig. (5-1). After this adjustment, the flume was loaded with 3/8 - 3/16 inch gravel until a bank had formed about 8 ft downstream from the head tank. Although the channel and consequently the flow just below the head tank were not symmetrical, the flow downstream from the bank was symmetrical about the centre line of the 24 inch channel.

Two different flow rates were examined and, after the detector had been shifted 6 inches closer to the source, the concentration for each was measured in the same manner as described above.

The pressure transducer was used to measure the two velocity heads and the static pressure difference at both flow rates. All three differential heads were measured at each point before shifting the pitot-static head to the next point of the traverse.

Photographs of the flow were taken with the 16 mm. Bolex movie camera operated at 16 frames per second and also at 64 frames per second. Sieve analyses were carried out before and after this series of runs.

At the higher flow rate, some bed instability developed, but this was not observed at the lower flow rate. The bed instability consisted of a series of low waves (at about 5 ft spacing) in the moving bed material, these waves moving slowly downstream.

Tests on ¼ inch Pea Gravel

On completion of the previous series of tests, the 3/8 - 3/16 inch material was replaced by ¼ inch pea gravel. No changes were made to the flume geometry or to the equipment used in the previous series of tests. As the ¼ inch pea gravel was the smallest size of particle to be used and therefore would be that giving the maximum value of $T_* = T_t/(\rho_s-\rho_f)g\ D$, the results were more comprehensive than those taken for the particles of other sizes. In particular, the particle velocity was measured directly from photographs taken with the Magnifax camera. Details of the method employed may be found in an earlier part of this chapter.

No change was made in the method of obtaining the concentration measurements, except for the higher flow rate. In

this case, the instability of the bed had developed into a fairly regular wave pattern moving slowly downstream. The values of λ taken from the concentration meter were corrected to give a profile of λ relative to the top of the fixed bed rather than to a fixed datum. The method used for this correction and its derivation are detailed in an appendix to this chapter.

When measuring the velocity heads and static pressure difference using the pressure transducer, a traverse of all the top velocity heads was made, followed by a traverse of all the bottom velocity heads, and finally a traverse of all the static head differences.

Photographs were taken with the Bolex 16 mm. movie camera. Sieve analyses were carried out before and after the series of runs.

APPENDIX TO CHAPTER 5

CONCENTRATION PROFILE CORRECTION MADE NECESSARY BY BED WAVES

INTRODUCTION

In the full flow case with ¼ inch pea gravel, a regular series of waves formed in the bed and moved slowly downstream. As the wave period was shorter than the time required to obtain a reasonable count on the concentration meter, these waves led to an incorrect profile. The shape of these waves was steady with respect to an observer moving downstream with a velocity c. Therefore, we can consider a fixed point relative to the flume as having a velocity, -c, relative to a stationary wave pattern.

A method of calculating the concentration profile relative to the top of the fixed bed is required. Measurements of λ_m, the long term mean count, have been made at various values of y. These show that y can be divided into three sections, an upper section with a large constant value of λ_m, a central section in which λ_m is varying, and a lower section with a small constant value of λ_m.

CORRECTION PROCEDURE

As the waves were small (about 1½ inches in height) and

the transport rate was high, it was assumed that the surfaces of constant concentration were all parallel with the top of the fixed bed. The profile of the intersection of the top surface of the fixed bed and the side panels was obtained by observing a sequence of photographs. From these photographs, the wave height was measured and divided into seven equal elements of length , labelled 0, 1, 2 . . . 6. The proportion of time that the profile height was between $(i + 1)\delta$ and $i\delta$ was called $\phi(i)$ where the height was measured from the lowest part of the profile.

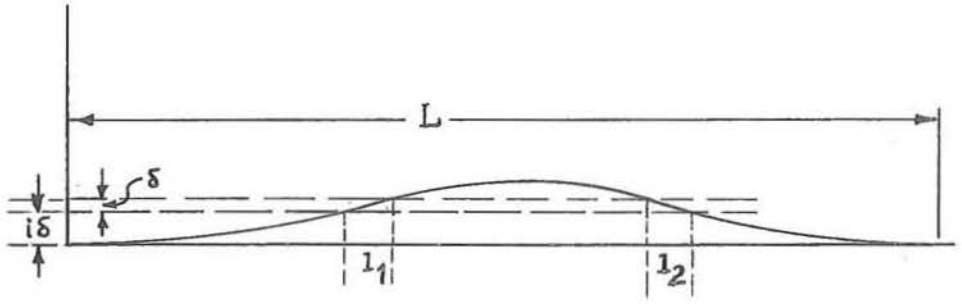

Fig. (5-2)

In Fig. (5-2), a plot of the top of the fixed bed as a function of y is given and here $(i) = \frac{l_1 + l_2}{L}$.

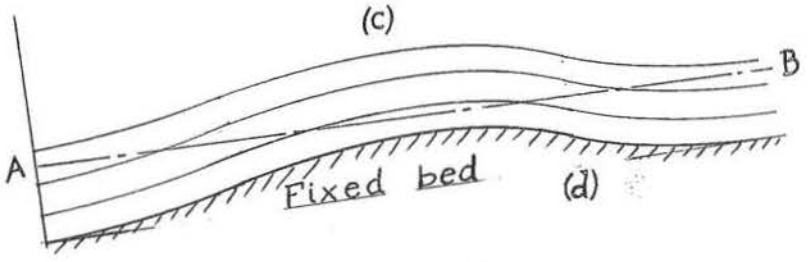

Fig. (5-3)

The assumed system of parallel isoconcentrations all moving downstream together can be replaced by the system shown in Fig. (5-3). Here the detector point is moving along straight lines cutting a set of fixed isoconcentrations. If the datum for the fixed co-ordinate system intersects the lowest point of the top of the fixed bed and the mean count rate along the line A - B at a height of $k\delta$ is called $\lambda_m(k)$, then $\lambda_m(k)$ is related to $\lambda(k)$ as follows,

$$\lambda_m(k) = \lambda(k-6)\ \phi(6) + \lambda(k-5)\ \phi(5) + \ldots + \lambda(k)\ \phi(0), \quad (5-1)$$

where $\lambda(k)$ is the count rate along the isoconcentration at height k above the top of the fixed bed.

An equation in the form of (5-1) can be written for each measured value of $\lambda_m(k)$, giving a total of n equations and (n + 6) unknown $\lambda(k)$. In both regions (c) and (d) in Fig. (5-3), $\lambda(k)$ will be constant and known.

Solution is possible, therefore, by starting from a point in a region (c) where $\lambda(k)$ is known and proceeding step by step down through the region of varying $\lambda(k)$ using the equation

$$\lambda(k-6) = \lambda_m(k) - \sum_{i=0}^{5} \lambda(k-i)\ \phi(i) / \phi(6). \quad (5-2)$$

Region (c) can be considered as either the clear water

region or the fixed bed region, so long as the values of $\phi(i)$ are arranged accordingly.

OBTAINING NUMERICAL SOLUTIONS

The most serious disadvantage of (5-2) is that $\phi(i)/\phi(6)$ is generally of order 1. An error in $\lambda_m(k)$ can therefore propagate and increase. Normally, the negative sign in the equation causes an oscillation in the effect of the errors.

A computer programme was used to solve (5-2). It was found that, if the λ-profile was calculated twice, firstly from the clear water down and secondly from the fixed bed up, the two solutions were reasonably stable over half the thickness of the rapidly varying region. Beyond this area, oscillations in the solution increased rapidly. The results in the areas of large oscillation were discarded as, by including results from the stable part of both calculations of the profile, a complete profile was obtained.

From the λ-profile obtained in the above manner, the concentration profile was found by direct application of equation (4-11)

$$C = \frac{1}{B} \log_{10} \frac{A}{\lambda} \qquad (4\text{-}11)$$

where A and B were measured. This equation is discussed in Chapter 4.

CHAPTER 6

E X P E R I M E N T A L R E S U L T S

SYNOPSIS

This chapter is arranged in four parts, the first listing the results of tests carried out on the measuring equipment, such as the concentration meter and the pressure transducer.

Each of the last three parts contains the complete results of the flume tests carried out on a given size of particle, the order of these parts being that of decreasing particle size.

PART I

Concentration Meter

All concentration measurements were taken using a Phillips scintillation detection type PW4111 connected to a nuclear Chicago counter-scaler model 183B. For all counts the resolution was kept at one microsecond (that is, the counter was set to distinguish between two pulses separated by one microsecond or more) and the counter operated by measuring the time taken for a previously set number of counts.

Values of the count rate as a function of voltage for a constant photon flux are given in Table (6-1) and plotted

in Fig. (6-1). As a measure of the resolution of the system, the apparatus was traversed across a step change in density and the count rate recorded as a function of distance from the step. To reduce the results to a general dimensionless form, they were transformed to the dimensionless variation, d.v., by

$$d.v. = \log\left(\frac{\text{Count Rate}}{\text{minimum ct rate}}\right) \Big/ \log\left(\frac{\text{maximum ct rate}}{\text{minimum ct rate}}\right) .$$

Results of this test are tabulated in Table (6-2) and plotted in Fig. (6-2).

Table (6-1)

Count rate as a function of the voltage supplied to the scintillation detector for a constant photon flux.

Voltage	Count Rate	Voltage	Count Rate
1,100	8.74 c/m	1,500	37,100
1,150	9.55	1,525	38,200
1,200	21.0	1,550	39,000
1,250	102	1,575	40,000
1,275	970	1,600	41,000
1,300	14,800	1,625	41,300
1,325	16,610	1,650	41,600
1,350	21,500	1,675	41,900
1,375	25,300	1,700	41,900
1,400	28,400	1,725	42,000
1,425	30,500	1,750	42,300
1,450	33,200	1,775	42,200
1,475	35,000	1,800	42,400

Table (6-2)

Variation of count rate as a function of the distance, d, of the beam centre-line from a step change in mean density; also the dimensionless variation, d.v., equal to

$$\log\left(\frac{\text{ct rate}}{\text{min. ct rate}}\right) \Big/ \log\left(\frac{\text{max. ct rate}}{\text{min. ct rate}}\right)$$

d	Cts/Min.	d.v.
+.688	148,000	.999
+.437	149,000	1.000
+.187	149,000	1.000
+.063	118,900	.903
-.063	20,200	.142
-.187	13,360	-.036
-.312	14,400	-.004
-.437	14,380	-.004
-.688	14,480	-.000

Pressure Measuring Equipment

The following tables, (6-3) and (6-4), contain results of the calibration tests carried out on the pressure transducer referred to in Chapter 4. Pressure differences were applied to the transducer by two methods, one used for values of differential head greater than 5 inches and the other for differential heads less than 5 inches. The first loading system consisted of two tanks fitted with hook gauges measuring to 0.001 ft, one tank being connected to each side of the transducer. In the second loading system, two large vessels were connected, one to each side of the transducer, and water added in small quantities from a burette to one of the vessels,

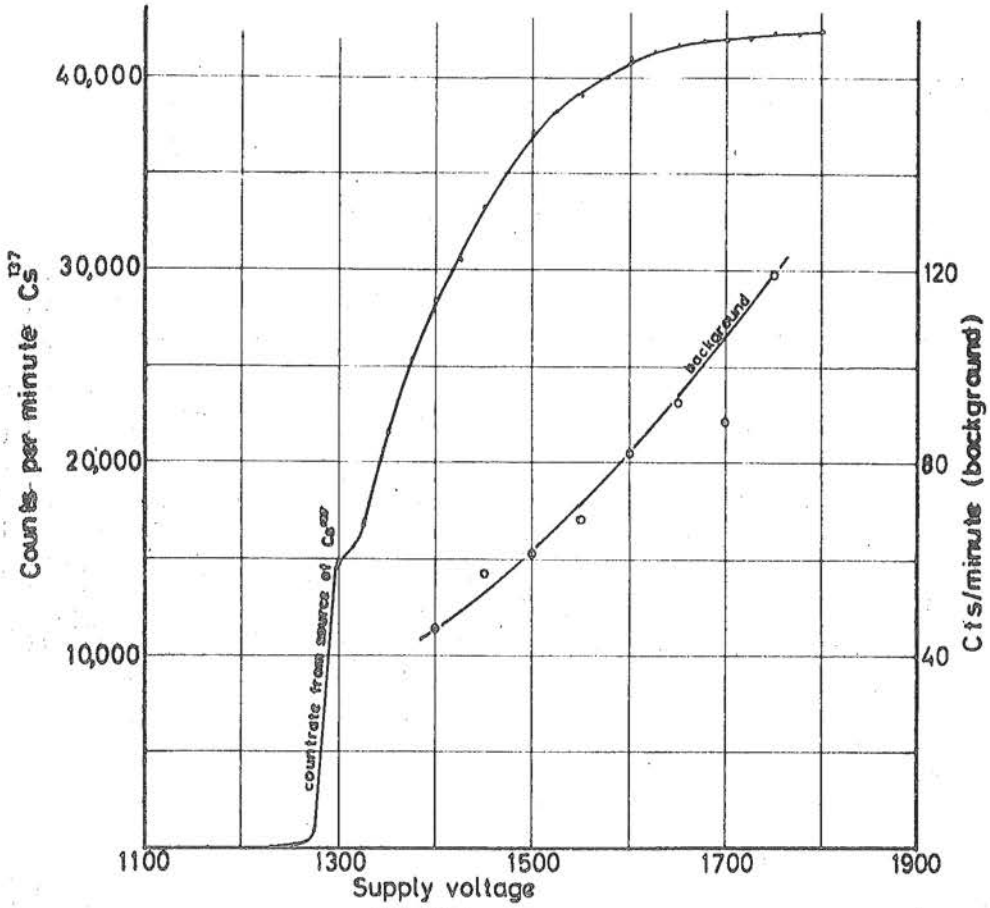

FIG 6-1

Voltage sensitivity of counting equipment used in concentration meter.

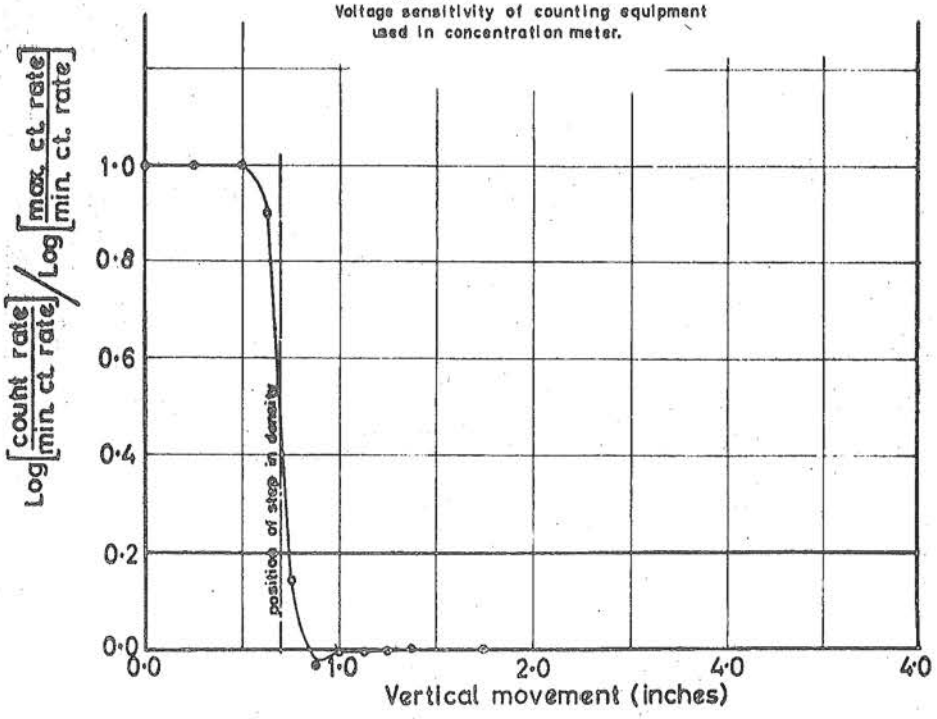

FIG 6-2

Resolution of conentration meter.

the change in head being calculated from the geometry of the system. The pressure transducer was connected to a Phillips PR9300 direct reading bridge. The output was read either on the bridge meter or supplied to a Phillips GM4531 D.C. amplifier connected to a Kelvin Hughes mark 5 pen recorder.

Differential pressures are given in equivalent feet of water at $68^{o}F$. The setting of the step attenuator on the PR9300 is given in the "Range" column. Meter readings (where shown) and the attenuator settings are given in microns.

The results have also been plotted in Figs. (6-3) and (6-4).

Table (6-3)

Pressure transducer calibration carried out using the meter of the PR9300 immediately prior to the flume experiments.

Range	Meter	Pressure	Range	Meter	Pressure
3	.60	.00238	100	6	.0223
3	1.30	.00477	100	14.8	.0492
3	2.05	.00750	100	22.6	.0738
3	2.62	.00954	100	32.2	.1036
3	.08	.0000	100	37	.1190
			100	37	.1190
30	1.9	.0059	100	43.2	.1381
30	3.7	.0119	100	50.2	.1595
30	5.6	.0181	100	55.7	.1750
30	7.3	.0238	100	61.7	.1929
30	9.1	.0298	100	68.5	.2141
30	11.0	.0357	100	76.2	.2380
30	12.9	.0417	100	81.9	.2553
30	14.8	.0479	100	88.1	.2761
30	16.6	.0536	100	97.0	.3015
30	18.3	.0597			

(Table continued overleaf)

Table (6-3) Contd:

Range	Meter	Pressure	Range	Meter	Pressure
300	20.1	.0607	300	239	.715
300	40.0	.1189	300	254	.764
300	62	.1834	300	278	.834
300	80	.2383			
300	105	.313	1,000	270	.834
300	120	.357	1,000	284	.885
300	134	.399	1,000	306	.951
300	160	.476	1,000	325	1.014
300	178	.529	1,000	345	1.070
300	200	.595	1,000	362	1.129
300	218	.651			

Table (6-4)

Pressure transducer calibration using the Kelvin Hughes pen recorder with maximum amplification on the GM4531. The pen displacement is given in millimetres. This run was made at the completion of the flume experiments.

Range	Pen	Pressure	Range	Pen	Pressure
3	0	.000	100	14.1	.377
3	5.0	.006	100	16.5	.442
3	10.0	.013	100	18.6	.518
3	17.2	.024	100	19.4	.552
10	5.5	.024	300	7.3	.552
10	12.1	.051	300	8.4	.619
10	20.1	.079	300	11.5	.839
			300	13.9	1.011
30	7.9	.079	300	16.4	1.236
30	9.0	.086	300	18.2	1.419
30	12.7	.115			
30	16.1	.146	1,000	6.1	1.419
30	17.4	.156	1,000	7.3	1.765
30	18.2	.165	1,000	7.8	1.945
30	19.6	.184			
30	20.3	.218	300	8.2	.542
100	8.1	.218	100	9.2	.206
100	9.2	.243			
100	11.5	.307	3	2.5	0.000
			3	0.0	.000

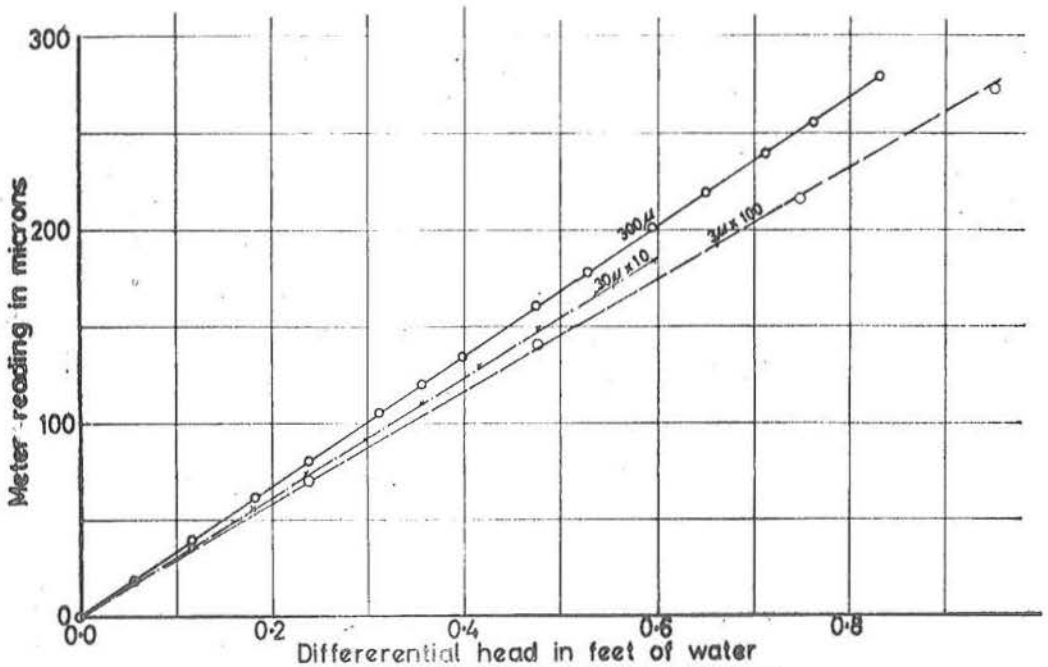

FIG 6-3(a) 3,30,300 μ ranges

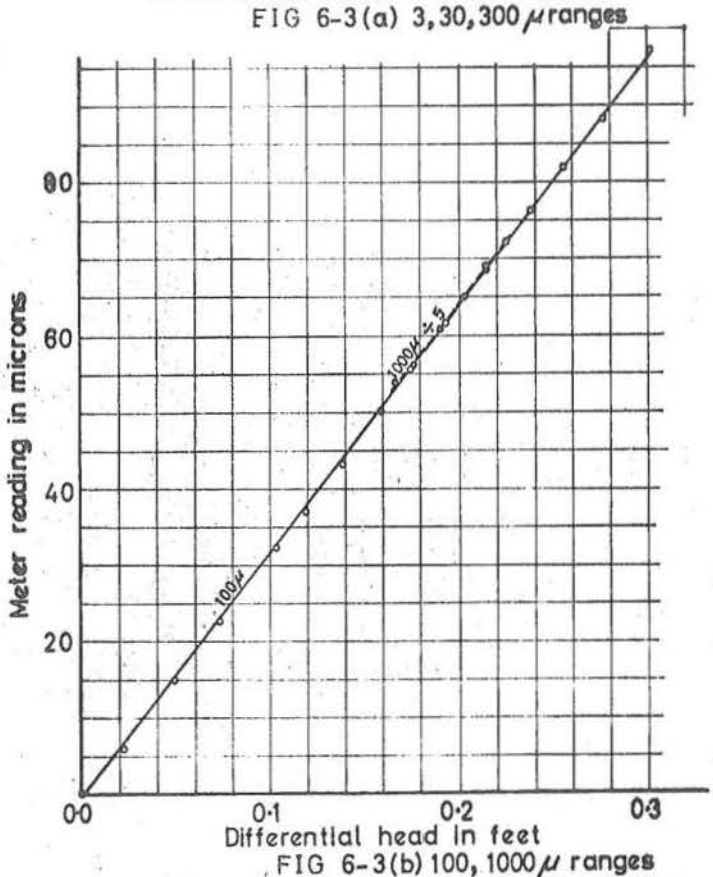

FIG 6-3(b) 100, 1000 μ ranges

Figs 6-3(a) and 6-3(b) are experimentally obtained calibration curves for the pressure transducer connected to the Phillips PR9300 bridge. The output is the bridge meter reading.

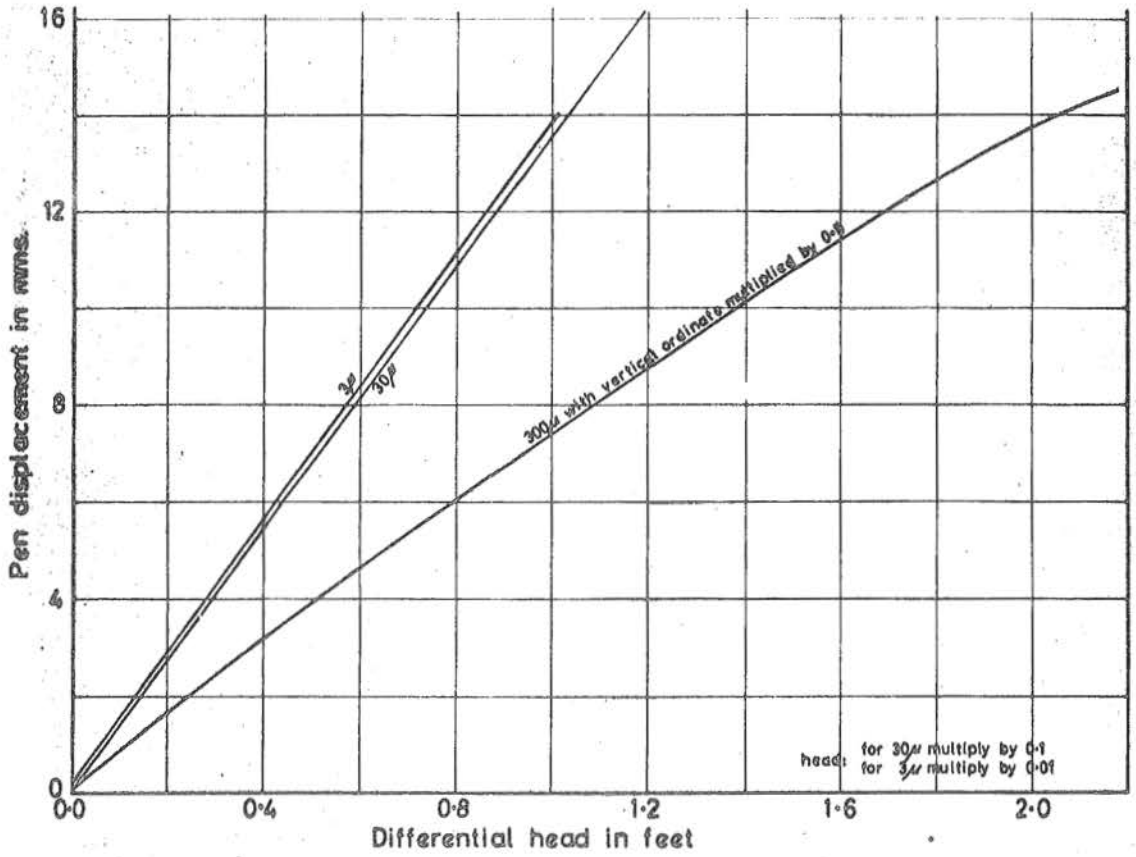

FIG 6-4(a) 3, 30, 300μ ranges

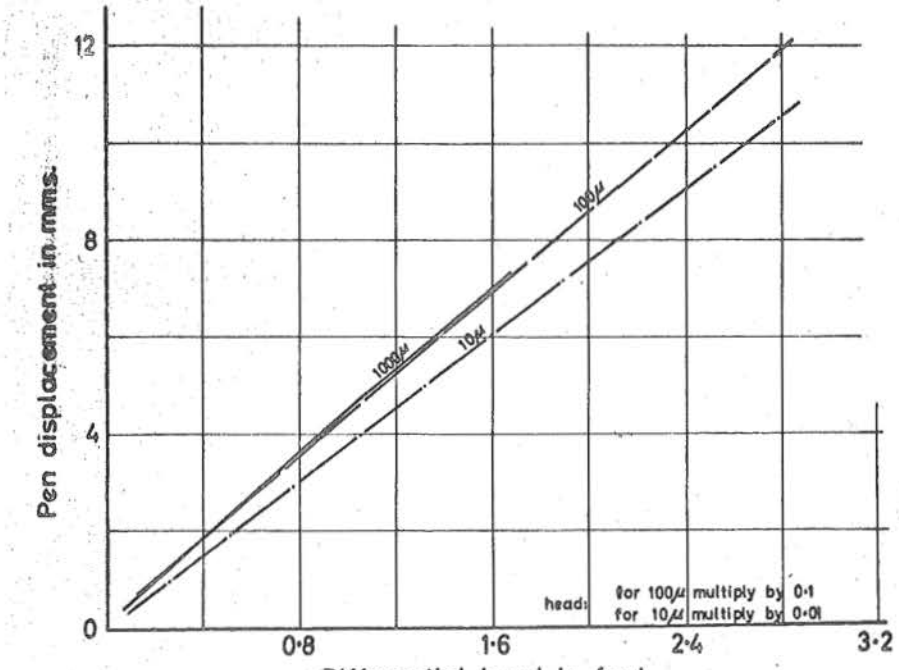

FIG 6-4(b) 10, 100, 1000μ ranges

Fig. 6-4(a) and fig 6-4(b) are experimental calibration curves. The transducer output was fed via the PR 9300 and amplifier to the pen recorder. Output is recorder pen displacement.

PART II

EXPERIMENTAL RESULTS WITH ¾ INCH - ½ INCH GRAVEL

Flow Geometry

Only one flow was used (estimated from the velocity profile to be 5.7 cusecs/ft) and the flume was maintained at a fixed slope of 0.063 and width of 2.5 ft. The water surface profile and bed profile measured during the runs are plotted in Fig. (6-5). After a steady state was reached, the slope over the test section was measured with a surveyor's level and ruler.

Bed slope at test section = 0.048.

Particles

The particles used were mainly a very hard sandstone (known locally as "greywacke") in the form of river washed gravel commercially screened to ¾ inch - ½ inch limits. During experimental runs, the gravel was broken up by the action of the flow, the small fragments of stone tending to lodge in the interstices in the stationary part of the bed. Near the end of the tests, two samples were given a sieve analysis. One consisted of material sampled from the total solid material in the flume. The second consisted of material sampled from the top 2½ inches of the bed only; on analysis,

this second sample was found to be similar to the original material loaded into the flume. Both sieve analyses are plotted in Fig. (6-6) and a photograph showing a sample of the original gravel used can be found in Fig. (6-24).

As in the dimensional studies described in Chapter 2 the predominant parameter contained (D^2), the effective diameter of the particles was taken to be the square root of average value of D^2. Averaging was carried out by weighting each increment of diameter according to the total proportion, by weight contained within that increment. This r.m.s. diameter as calculated for the top 2½ inches of the bed was used in later calculations of F_3.

r.m.s. diameter of ¾ inch - ½ inch
particles from top of bed = 0.0478 ft

Concentration Measurements

All the concentration measurements were carried out with the gamma ray measuring equipment using the Na I scintillation detector. In operation, the counter was used to time a preset count. The count rate obtained was corrected for background and the corrected counts per minute are listed (denoted as λ) in the tables below. The depth was measured relative to an arbitrary datum and this depth listed in the table. From the value of λ the concentration C was obtained

by using equation (4-11). The clear water count A was measured and the parameter B in (4-11) calculated from the attenuation of the beam when passing through a weighed sample of gravel.

Clear water count A = 708 c.p.m.

Detector supply voltage = 1,600 volts

From equation (4-11), putting B = 4.42,

$$\lambda = 708\ 10^{-4.42C}$$

which on rearranging becomes

$$C = (\log_{10} \frac{708}{\lambda})/4.42 \qquad (6-2)$$

During the counting, time checks were made to test for a failure of the mechanical count register. Where this occurred, the count was restarted. Only the final counts and count rates are listed below in Table (6-5).

Background counts where included in the main runs are marked "Bg". The free surface was at -¾ inch with respect to the datum used below.

Table (6-5)

(Dist. below surface).

Concentration meter results for
¾ inch - ½ inch gravel

Depth	Cts	Cts/Min.	λ	C
Bg	1024	114	-	-
8.625 + 0.75	640	108	-6	-
8.375 "	640	118	+4	.51
8.125 "	640	117	3	.54
7.875 "	640	117	3.5	.52
7.75 "	640	123	9	.43
7.625 "	640	120	6	.47
7.5 "	640	125	11	.41
7.375 "	640	133	19	.36
7.25	640	141	27	.32
7.125	640	134	20	.35
7.0	640	151	37	.29
6.875	640	177	63	.24
6.75	640	179	65	.24
6.625	640	202	88	.21
6.5	640	220	106	.19
6.375	640	218	104	.19
6.25	640	230	116	.18
6.125	640	260	146	.15
6.0	640	320	206	.12
		Break Between Runs		
2.875	640	94.9	-1.1	-
3.125	640	105.1	+9.1	.43
3.375	640	100.6	3.6	.52
3.625	640	102.4	5.4	.48
3.875	640	132.5	35.5	.29
4.125	640	134	37	.29
4.25	640	147	49	.262
4.375	640	143	45	.270
4.5	640	177	79	.215
4.625	640	180	82	.212
4.75	640	200	101	.191
4.875	640	214	115	.178
5.0	640	232	133	.164
5.125	640	242	143	.157
5.25	640	296	196	.126
5.375	640	328	228	.111
5.5	640	362	262	.098
5.625	640	352	252	.101
5.75	640	464	363	.0656
5.875	640	451	350	.0693

(Table continued overleaf)

Table (6-5) Contd:

Depth	Cts	Cts/Min.	λ	C
6.0	640	485	384	.0601
6.125	640	478	377	.0618
6.25	640	581	479	.0384
6.375	640	615	513	.0314
6.5	640	615	513	.0314
6.625	640	736	634	.0106
6.75	640	673	570	.0212
6.875	640	692	589	.0181
7.0	640	706	603	.0158
		Break Between Runs		
Bg	768	95.2	-	-
4.0	2,560	713	616	.015
3.5	2,560	747	650	.008
3.0	2,560	770	672	.005
2.5	2,560	771	673	.005
4.0	4,864	715	616	.015
4.5	2,560	671	571	.021
5.0	2,560	560	460	.042
5.5	1,280	375	274	.093
6.0	1,280	274	173	.139
Bg	512	103	-	-

The results listed in Table (6-5) have been plotted as concentration, C, against depth in Fig. (6-7) and, from this, a continuous curve of C in the C - y plane is shown in Fig. (6-10). From this continuous curve, the gradient of C and the integral of C, both with respect to y, have been obtained. Measurement of y is in feet and the integral plotted against y is taken between y and the free surface. Both these curves were obtained graphically and are included in Fig. (6-10).

Velocity Measurements

The fluid velocity only was measured. This was done by

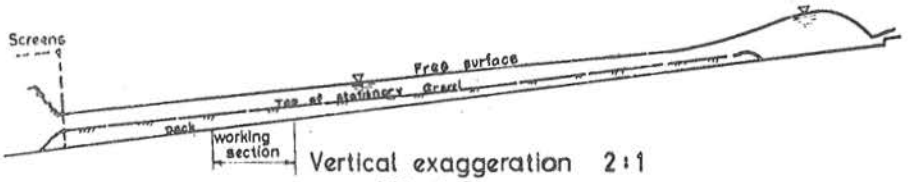

Vertical exaggeration 2:1

FIG 6-5

Longitudinal section with $\frac{3}{4}$"-$\frac{1}{2}$" stone

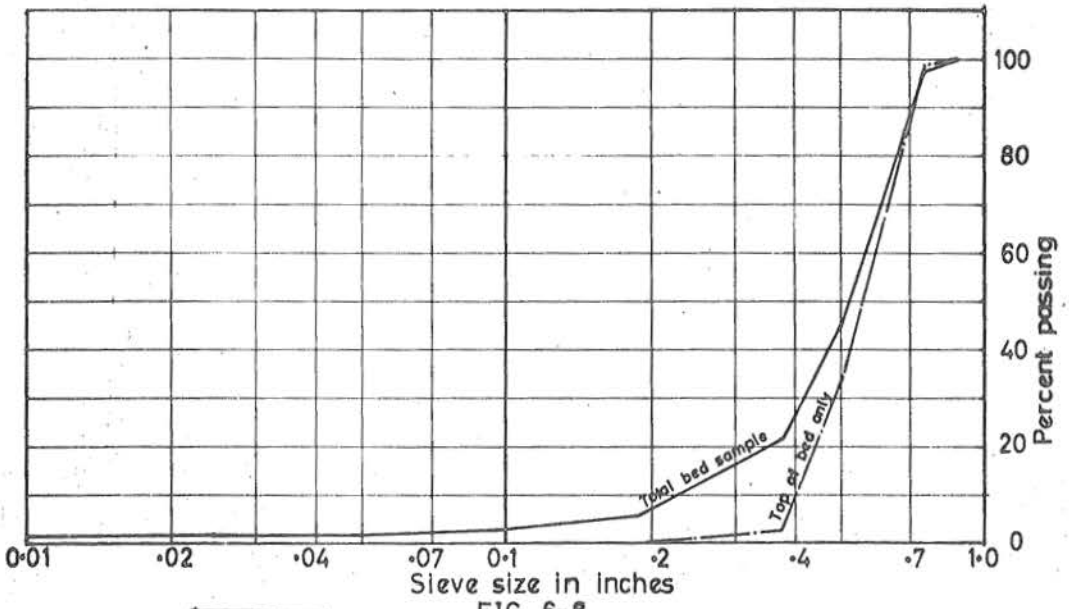

FIG 6-6

Sieve analysis of $\frac{3}{4}$"-$\frac{1}{2}$" stone

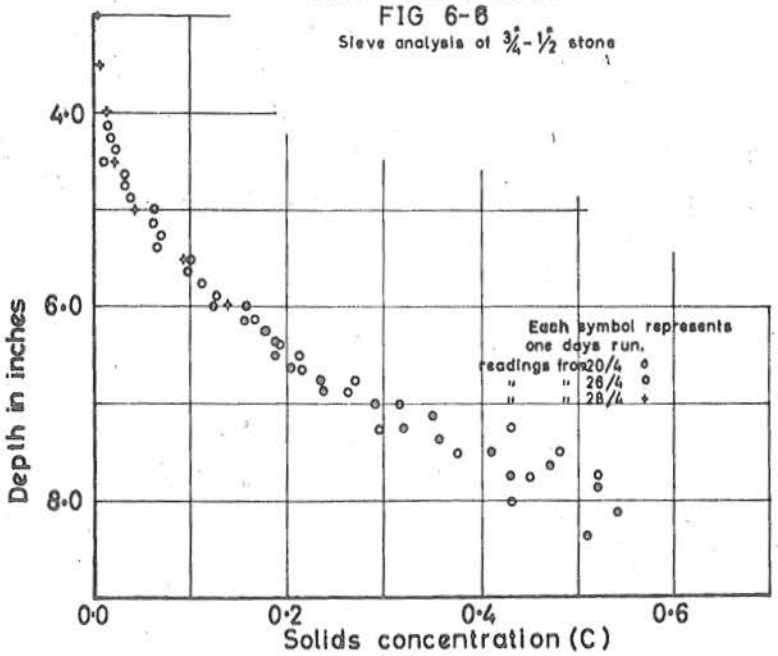

FIG 6-7

Experimental concentration measurements with $\frac{3}{4}$"-$\frac{1}{2}$" stone

using the two stainless steel pitot-static tubes described in Chapter 4. The tubes were mounted rigidly together and spaced 1¾ inches apart in a vertical direction. Differential heads were measured using perchlorethylene manometers as described in Chapter 4 and the measured heads converted to feet of water at ambient temperature. The depth from the free surface to the bottom tube was measured in inches and is recorded with each reading. During early runs, the top pitot tube behaved erratically and all readings from this have been abandoned for the first two runs. This also means that the static head difference reading was abandoned for these two runs.

Flushing of the pitot-static tubes was carried out at intervals of not more than six readings, as well as before each set of runs. In Table (6-6) the depth to the bottom tube, the velocity heads in both tubes and the velocities have been tabulated. From the arrangement of the tubes, it follows that the velocity measured with the top pitot-static tube is that of the fluid at a depth 1¾ inches less than the depth tabulated for that reading. All readings, unless stated otherwise, were made on the flume centreline.

The velocities calculated from the readings taken above have been plotted against depth in inches in Fig. (6-8).

Static Head Difference

The static tubes of the pitot-static heads were connected, each to one side of a manometer similar to that used for velocity head measurement. This difference in static heads was measured at the same time as the velocity heads and converted to feet of water at ambient temperature. Results have been included in Table (6-6) under "Static Diff." and, in Fig. (6-9), plotted against depth in inches.

Table (6-6)

Velocities and pressure reading from the pitot-static head. All heads are given in feet of water and velocities in ft/sec. The depth is given in inches from the free surface to the bottom pitot-static tube.

Depth	Velocity Head		Static Diff.	Velocity	
Inches	Top	Bottom		Top	Bottom
1.0		2.13			11.7
1.56		2.13			11.7
2.0		2.25			12.0
2.5		2.24			11.9
3.0		1.71			10.4
3.5		1.84			10.8
4.0		1.71			10.5
4.5		1.49			9.8
5.0		1.15			8.6
5.5		.93			7.7
6.0		.62			6.3
6.5		.40			5.0
7.0		.200			3.6
7.5		.109			1.6
8.0		.026			1.3
8.12		.011			.8
		Break Between Runs			

(Table Continued Overleaf)

Table (6-6) Contd:

Depth	Velocity Head		Static Diff.	Velocity	
Inches	Top	Bottom		Top	Bottom
1.0		2.04			11.5
1.5		2.21			11.9
2.0		2.11			11.7
2.5		2.00			11.4
3.0		1.84			10.9
3.5		1.74			10.6
4.0		1.59			10.2
4.5		1.40			9.4
5.0		1.31			9.2
5.5		1.02			8.1
6.0		0.63			6.4
6.5		.46			5.4
7.0		.29			4.4
7.5		.08			2.3
		Break Between Runs			
3.625	2.16	1.67	-.006	11.8	10.4
3.875	2.25	1.77	-.019	12.0	10.7
4.125	2.09	1.53	-.020	11.6	9.9
4.375	2.02	1.45	-.021	11.4	9.7
4.625	1.93	1.43	-.024	11.1	9.6
4.875	1.91	1.27	-.021	11.1	9.1
5.125	1.77	1.18	-.032	10.7	8.7
5.375	1.74	.96	-.019	10.6	7.9
5.625	1.65	.84	-.024	10.3	7.4
5.875	1.55	.67	-.016	10.0	6.6
6.125	1.45	.60	-.006	9.7	6.2
6.375	1.34	.407	-.006	9.3	5.1
6.625	1.22	.300	.000	8.9	4.4
6.875	1.18	.209	+.003	8.7	3.67
7.125	1.04	.134	+.008	8.2	2.94
7.375	.892	.080	.018	7.6	2.27
7.625	.738	.040	.027	6.9	1.61
7.875	.566	.016	.021	6.0	1.02
8.125	.471	.008	.037	5.51	.72
8.375	.326	.005	.027	4.59	.6
8.625	.257	.005	.032	4.07	.6
8.875	.172	.005	.019	3.33	.6
9.125	.107	.005	.021	2.63	.6

(End of Table)

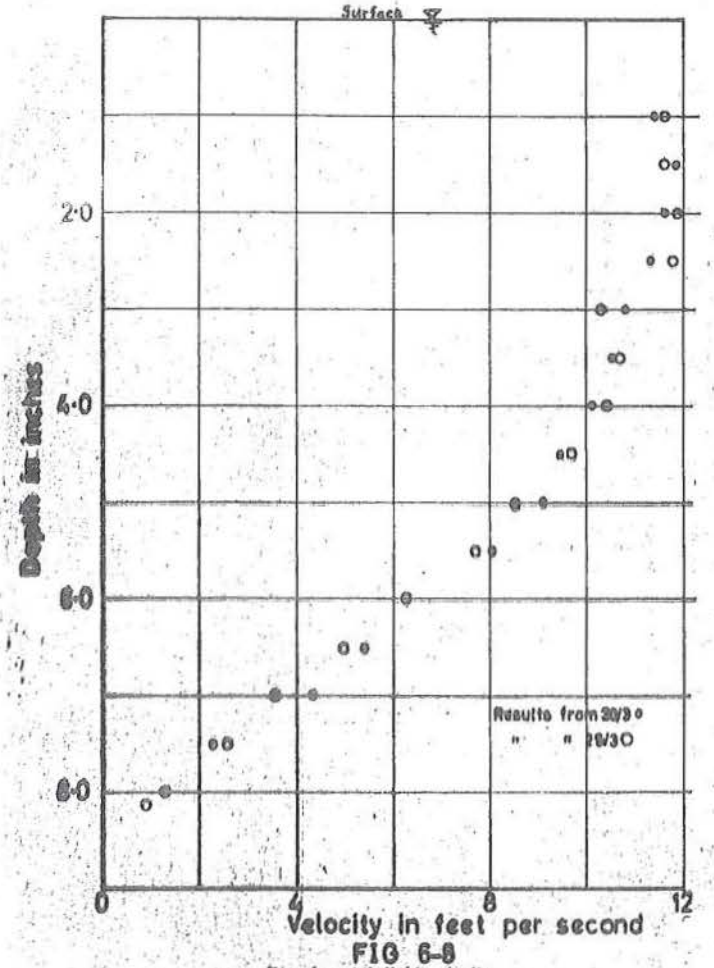

FIG 6-8
Experimental fluid velocity

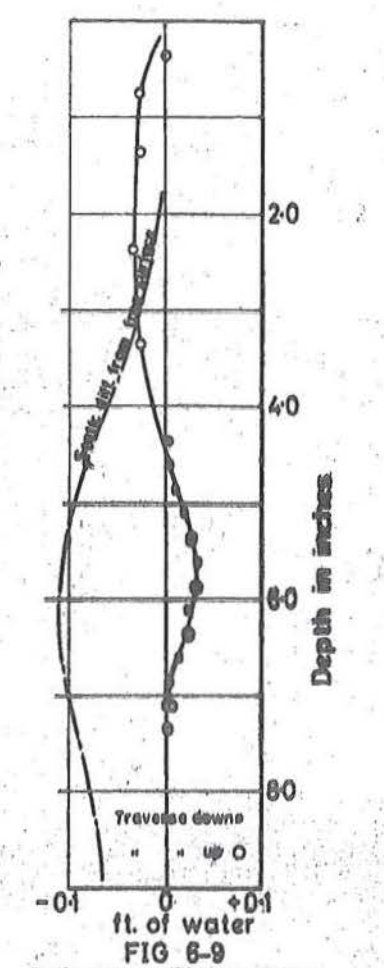

FIG 6-9
Static pressure difference relative to Xy. The experimental points show the piezometric reading between a pt. 1·75" below the given depth and the given depth.

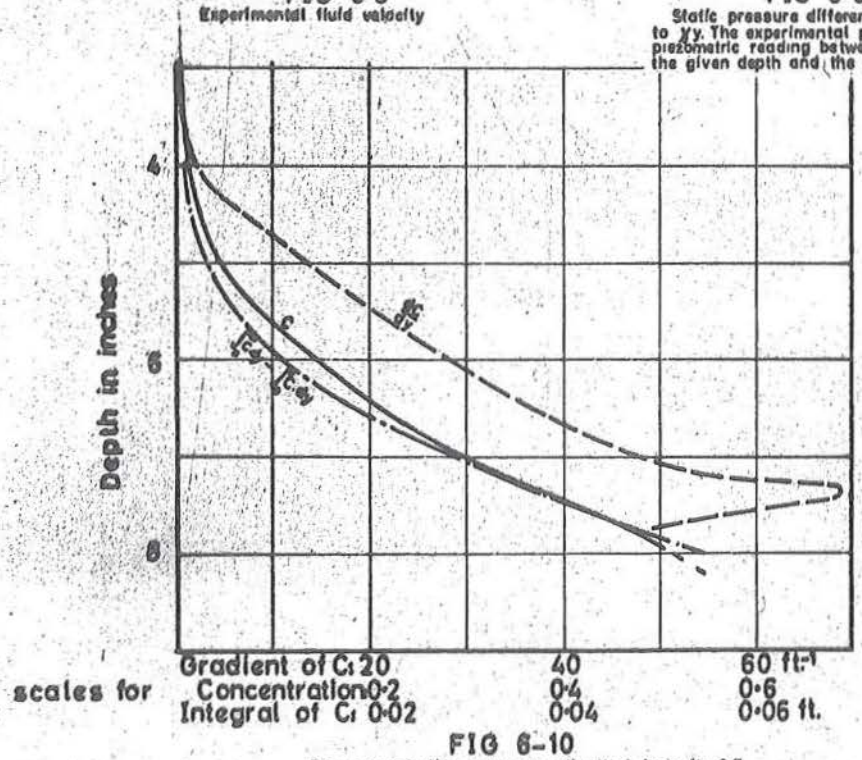

FIG 6-10
The concentration curve is estimated from fig 6-7
The gradient and integral curves are obtained from this estimated curve.

Calculated Parameters

From the concentration profile, the total shear stress and dispersive stress were calculated, assuming no significant suspended load. These calculations were carried out as follows.

All particles were assumed to be supported by inter-particle forces and the total interparticle stress at y is therefore simply the component of the submerged weight of solids above y where y is measured perpendicular to the bed. As $(\rho_s-\rho_f)g\cos\theta = 103$ lbs/ft^3, the stress P is given by

$$P = 103 \int_y^\infty C\, dy \quad . \qquad (6-2)$$

Because the depth from the free surface to the fixed bed was 0.729 ft, it follows from equation (2-30) that, for a slope of 0.048,

$$T_t = 0.048 \left[(0.729-y)62.4 + 103 \int_y^\infty C dy\right] \qquad (6-3)$$

where y is measured from the top of the fixed bed.

$F_1 = P/T_t$ was then obtained.

From the u - y curve, the velocity gradient du/dy was obtained graphically and the previously derived value for r.m.s. diameter of 0.0478 ft used as a measure of D to obtain

F_3 as follows,

$$F_3 = T_t/\rho_s D^2 \left(\frac{du}{dy}\right)^2,$$

and, substituting $\rho_s = 5.14$ and $D = 0.0478$ ft, we obtain

$$F_3 = 86\ T_t/\left(\frac{du}{dy}\right)^2. \qquad (6\text{-}4)$$

The stability parameter $\Pi = \frac{\rho_a}{D^2 \rho_s} \frac{F_3}{(dF_3/dy)^2}$ can then be written

$$\Pi = 166\ (1 + 1.65C)\ F_3/\left(\frac{dF_3}{dy}\right)^2 \qquad (6\text{-}5)$$

and has been evaluated, using numerical differentiation to obtain $\frac{dF_3}{dy}$.

The values of C, F_1, F_3, and Π are tabulated for various values of y in Table (6-7) below.

Table (6-7)

Calculated parameters for ¾ inch - ½ inch gravel.

y	C	F_1	F_3	Π
.000	.465	2.30	1.21	.51
.025	.404	1.77	.68	.70
.050	.325	1.51	.37	1.22
.075	.265	1.23	.22	4.04
.100	.217	.98	.165	22.0
.150	.135	.59	.125	440
.200	.07	.29	.115	25,000
.250	.03	.15	.126	169
.300	.015	.08	.182	7.9

PART III

EXPERIMENTAL RESULTS WITH 3/8 INCH - 3/16 INCH GRAVEL

Flow Geometry

Two different flows were used (of 4.9 and 3.1 cusecs/ft), these being denoted "full flow" and "partial flow" respectively. In both cases, the flume was set to a slope of 0.062 and a width of 2.00 ft. At full flow the bed showed a tendency to develop very flat waves. These waves were about 6 - 7 ft long and moved downstream with a celerity of about 3 inches per second. Measured from trough to crest, the height of the waves varied but was never observed to be greater than 1 inch. For the partial flow, no waviness was detected.

Bed slope at partial flow = .044

Bed slope at full flow = .052

Particles

The particles, rounded stones commercially graded to pass a ⅜ inch sieve and be retained on a 3/16 inch sieve, were of a similar material to the ¾ inch - ½ inch gravel. Sieve analyses of the top 2.5 inches of the bed and of the full depth of material were not significantly different.

Results of the sieve analysis of the top 2.5 inches of the bed are plotted in Fig. (6-11). Only isolated cases of stone fracture occurred, although a fine floury material was produced at a similar rate as with the ¾ inch - ½ inch gravel. From the sieve analysis, the r.m.s. diameter of the particles was estimated, using a similar procedure to that used for the ¾ inch - ½ inch gravel.

r.m.s. diameter of 3/8 inch - 3/16 inch particles = 0.0231 ft

Concentration

All concentration measurements were made using the gamma ray equipment and timing a preset number of counts. The results, after correction for the background, have been listed in the form λ/A. In this case, λ is the measured total count rate less the background and A is the clear water count rate less the background. Measurements of A were made before and after each run. The height of the counting head was measured positively upwards in inches above an arbitrary datum level. The complete list of concentration measurements for each of the two flows is given below, the full flow results in Table (6-8) and the partial flow results in Table (6-9). In both tables, the total counts taken, total count rate and λ/A are listed for various values of height. Normally, four check readings were taken at each point and, if any

fault in the counting was detected, the count was re-started. Concentrations were obtained from λ using equation (4-11), substituting for A and B the experimentally obtained values of 2,960 and 3.81 respectively to obtain

$$C = \log_{10} \left(\frac{2,960}{\lambda}\right) 3.81 . \qquad (6-6)$$

Values of C so obtained, as well as the gradient and integral of C with respect to y, are all plotted against y in Figs. (6-12) and (6-13). The integral plotted against y is evaluated between y and the free surface.

Table (6-8)

Concentration meter results for full flow with 3/8 inch - 3/16 inch gravel.

Height	Cts	Cts/Min.	λ/A
0.0	320	126	.0025
2.50	640	127	.0028
2.625	640	126	.0025
2.75	640	130	.0038
2.875	640	124	.0018
3.00	640	133	.0046
3.125	640	141	.0075
3.25	640	164	.0161
3.375	640	162	.0157
3.50	640	169	.0179
3.625	640	222	.036
3.75	640	249	.046
3.875	640	364	.087
4.00	640	352	.083
4.125	640	429	.111
4.25	640	512	.140
4.375	640	674	.198
4.50	640	736	.220

(Table Continued Overleaf)

Table (6-8) Contd:

Height	Cts	Cts/Min.	λ/A
4.625	1,280	719	.214
4.750	1,280	800	.243
4.875	1,280	851	.261
5.00	1,280	981	.308
5.125	1,280	1,197	.385
5.25	1,280	1,230	.397
5.375	1,280	1,560	.515
5.50	1,280	1,750	.583
5.625	1,280	1,710	.569
5.75	1,280	2,130	.718
5.875	1,280	2,240	.757
Bg	2,560	119	-
	Break Between Runs		
3.25	2,560	214	.031
5.25	2,560	1,320	.443
5.5	2,560	1,620	.552
5.75	2,560	1,970	.681
6.0	2,560	2,150	.748
6.25	2,560	2,390	.836
6.5	2,560	2,640	.930
6.75	2,560	2,660	.936
7.0	2,560	2,560	.900
7.25	2,560	2,660	.936
7.5	2,560	2,820	.995
7.75	2,560	2,720	.959
8.0	2,560	2,780	.981
8.25	2,560	2,750	.970
8.50	6,400	2,760	.974
8.75	6,400	2,840	1.000
Bg	2,560	129	-

(End of Table)

Table (6-9)

Concentration meter results for partial flow with 3/8 inch - 3/16 inch gravel.

Height	Cts	Cts/Min.	λ/A
3.5	1,280	131	.0015
3.75	1,280	141	.0055
4.0	1,280	137	.0039
4.25	1,280	142	.0055
4.5	1,280	169	.0161
4.75	1,280	252	.0487
4.875	1,280	256	.0502
5.0	1,280	346	.086
5.125	1,280	431	.118
5.25	1,280	447	.125
5.375	1,280	520	.154
5.5	1,280	706	.226
5.625	1,280	795	.262
5.75	1,280	941	.319
5.875	2,560	1,180	.413
6.0	2,560	1,305	.461
6.25	2,560	1,520	.546
6.5	2,560	2,130	.785
6.75	6,400	2,430	.903
7.0	6,400	2,510	.935

Velocity Measurements

The velocity was measured with the two pitot-static tubes described in Chapter 4 and used with the ¾ inch - ½ inch gravel. Pressure measurements were taken with the pressure transducer and recorded on the Kelvin Hughes pen recorder. Details of this apparatus can be seen in Chapter 4. Using a perchlorethylene manometer, the pen recorder was calibrated at the beginning of each run, and the zero point was checked after every change in range of the measuring bridge. As only

one channel of measuring equipment was available, the three readings at each point were taken in turn. A system of valves allowed all connections (except those required) to be isolated from the transducer. The recording obtained showed oscillations caused by turbulence and also more systematic oscillations caused by the propagation of waves along the bed. The mean value of pressure was taken in each case. In Table (6-11) the height in inches of the bottom tube above an arbitrary datum, the velocity head and the velocity in ft/sec. are tabulated for full flow. In Table (6-12) the same parameters are tabulated for partial flow. The velocities for full and partial flow have been plotted against height in Figs. (6-14) and (6-15) respectively.

Static Head Difference

To obtain the static head difference, the two static tubes from the pitot-static head were connected one to each side of the pressure transducer. The results were converted to feet of water at ambient temperature and have been included in Tables (6-11) and (6-12) under "Static Diff." They have also been plotted against y in Figs. (6-14) and (6-15).

Table (6-11)

Velocity and static head difference measurements for full flow with 3/8 inch - 3/16 inch gravel. All heads are given in feet of water and velocities in feet per second.

Height	Velocity Head		Static	Velocity	
Inches	Top	Bottom	Diff.	Top	Bottom
1.5	.028	.005	+.0026	1.3	.6
1.75	.064	.011	.0138	2.0	.8
2.0	.044	.012	.0178	1.7	.9
2.25	.228	.012	.0232	3.8	.9
2.5	.262	.012	.037	4.1	.9
2.75	.61	.007	.026	6.3	.6
3.0	.60	.012	.026	6.2	.9
3.25	.680	.016	.018	6.6	1.0
3.5	1.29	.030	.019	9.1	1.4
3.75	1.58	.105	.014	10.1	2.6
4.25	1.63	-	-.005	10.3	-
4.75	2.1	.692	-.013	11.6	6.7
5.25	2.25	1.12	-.034	12.0	8.5
5.75	2.42	1.51	-.034	12.5	9.9
6.25	2.50	1.8	-.040	12.7	10.8
6.75	2.72	1.93	-.038	13.2	11.2
7.25	-	1.96	-	-	11.2
7.75	-	2.26	-.025	-	12.1
8.25	-	2.27	.000	-	12.1

Table (6-12)

Velocity and static head difference measurements for partial flow with 3/8 inch - 3/16 inch gravel. All heads are given in feet of water and velocities in feet per second.

Height	Velocity Head		Static	Velocity	
Inches	Top	Bottom	Diff.	Top	Bottom
2.06	.283	.014	+.042	4.3	1.0
2.25	.350	.063	+.044	4.7	2.0
2.5	.180	.017	.046	3.4	1.0
2.75	.650	.017	.053	6.5	1.0
3.0	.64	.016	.048	6.4	1.0
3.25	.76	.040	.044	7.0	1.6
3.5	.86	.026	.043	7.4	1.3
3.75	.92	.021	.034	7.7	1.2
4.0	1.06	.20	.026	8.3	3.6
4.25	1.07	.19	.019	8.3	3.5
4.75	1.18	.40	.017	8.7	5.1
5.25	1.28	.44	.011	9.1	5.4
5.75	-	-	.012	-	-
6.25	-	-	.008	-	-

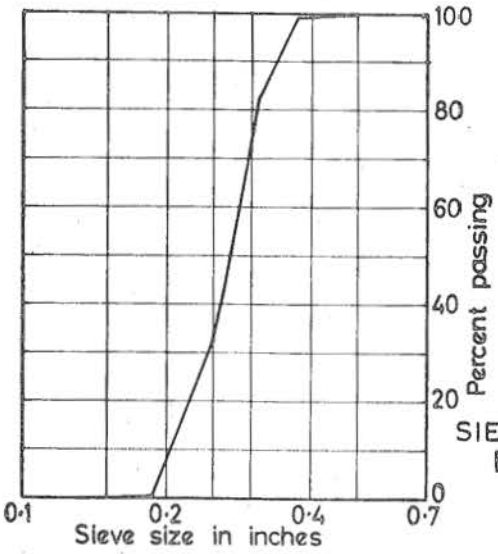

ALL GRAPHS ON THIS PAGE ARE FOR $\frac{3}{8}$ — $\frac{3}{16}$" GRAVEL.

SIEVE ANALYSIS
FIG 6-11

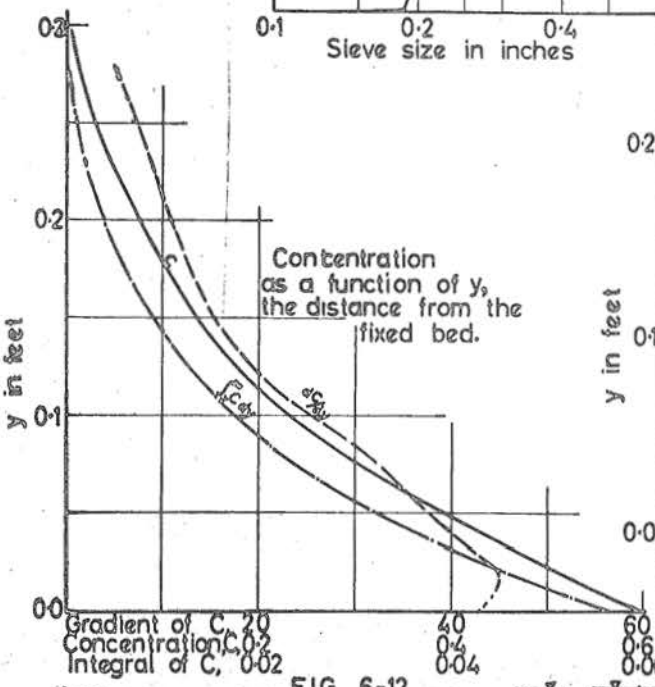

FIG 6-12

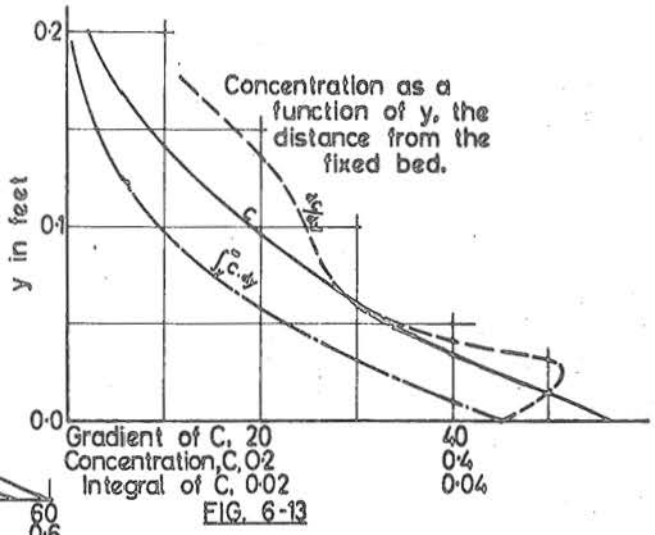

FIG 6-13

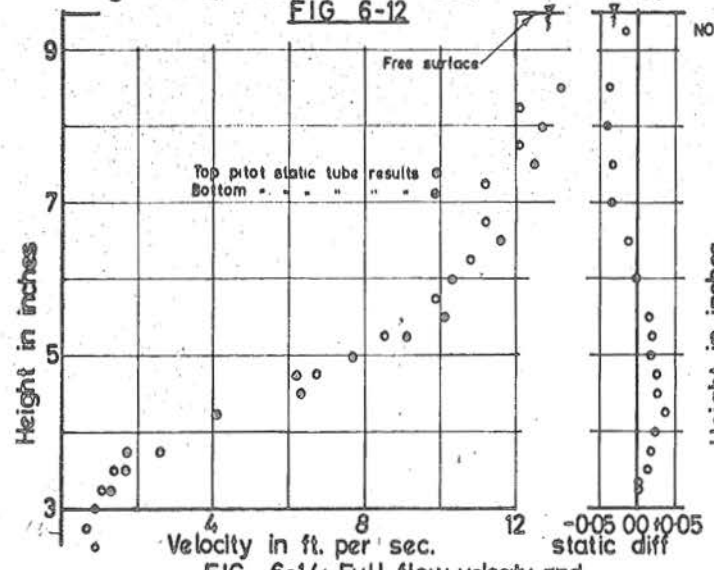

FIG. 6-14: Full flow velocity and static difference profiles.

NOTE FOR FIGS. 14 & 15. The height is measured above an arbitrary datum. Static diff denotes the difference in piezometric head in feet of water between the height shown and and a level 1·75" lower.

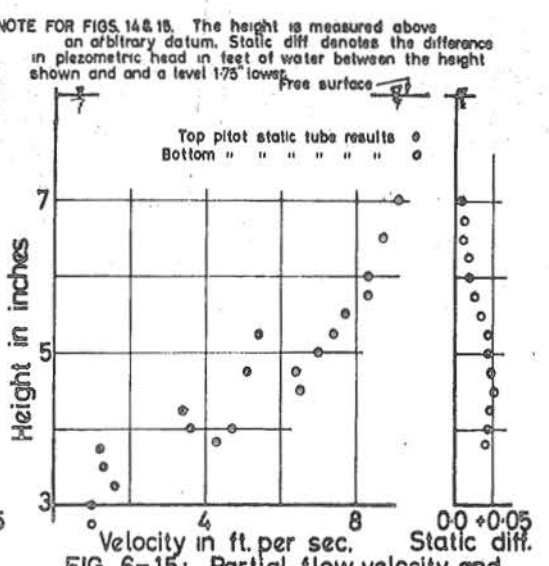

FIG. 6-15: Partial flow velocity and static difference profiles.

Calculated Parameters

From the concentration profile, the shear stress and dispersive stress were calculated assuming no significant suspended load. Equation (6-2) was used to obtain the dispersive stress for both flows. The total shear stress was calculated from equation (2-30) by rearranging in the form

$$T_t = \sin\theta \left[g\rho_f (d - y) + 103 \int_y^\infty C dy \right] \qquad (6\text{-}7)$$

and, substituting the numerical values of d (the depth to the fixed) = 0.572 and $\theta = 0.052$, we obtain for full flow

$$T_t = 0.52 \left[62.4\ (.572 - y) + 103 \int_y^\infty C dy \right] \qquad (6\text{-}8)$$

and for partial flow where d = 0.458 and $\theta = 0.044$

$$T_t = .044 \left[62.4\ (.458 - y) + 103 \int_y^\infty C dy \right]. \qquad (6\text{-}9)$$

Using T_t and P calculated as above, $F_1 = P/T_t$ was determined. From the velocity profile $\frac{du}{dy}$ was obtained graphically and from this and T_t the value of $F_3 = T_t/\rho_s D^2 \left(\frac{du}{dy}\right)^2$ was calculated. These results for C, F_1, F_3 and the stability parameter Π are tabulated for various values of y

in Table (6-13) for full flow and Table (6-14) for partial flow.

Table (6-13)

Calculated parameters for full flow with 3/8 inch - 3/16 inch gravel.

y	C	F_1	F_3	Π
.00	.60	2.70	.641	30
.02	.51	2.33	.512	3.9
.04	.43	1.94	.345	10.8
.06	.36	1.62	.265	26
.08	.29	1.35	.231	40
.10	.23	1.12	.189	122
.12	.186	.91	.185	640
.14	.150	.75	.176	113
.16	.124	.59	.260	6.5
.18	.098	-	.346	4.5

Table (6-14)

Calculated parameters for partial flow with 3/8 inch - 3/16 inch gravel.

y	C	F_1	F_3	Π
.00	.57	3.14	.236	34
.02	.47	2.59	.193	42
.04	.375	2.06	.163	163
.06	.30	1.66	.153	1,700
.08	.24	1.27	.167	-
.10	.19	.95	.161	58
.12	.14	.67	.24	13
.14	.10	.45	.38	-
.16	.07	.27	-	-

PART IV

EXPERIMENTAL RESULTS WITH ¼ INCH PEA GRAVEL

Flow Geometry

Two different flows were used, 6.4 and 2.0 cusecs/ft width, denoted "full flow" and "partial flow" respectively. In both cases, the flume was set to a slope of 0.062 and a width of 2.00 ft. The bed waviness at full flow was more pronounced than was the case with full flow using 3/8 inch - 3/16 inch gravel. At partial flow, however, there was no detectable waviness of the bed. Photographs of full flow at 2 second intervals can be seen in Fig. (6-28). The bed slope was measured during the runs and is shown below.

Bed slope at partial flow = 0.035

Bed slope at full flow = 0.047

Particles

The particles were of hard, river washed stone, predominantly greywacke and commerically screened to pass a ¼ inch sieve. This material is sold locally as "¼ inch pea gravel". Abrasion of the stone appeared to occur at about the same rate as for the larger material previously used. However, stone fracture was not observed and the grading of the stone was found on analysis to be the same throughout the bed. Results

of a sieve analysis are plotted in Fig. (6-16). From this sieve analysis, the r.m.s. diameter of the particles was calculated.

r.m.s. diameter of ¼ inch pea gravel = .0147 ft

Concentration

All concentration measurements for both flows were made using the gamma ray equipment and timing a preset number of counts. The clear-water count rate was measured before each run and, after subtraction of the background count rate, is called A. The total count less the background is termed λ and the values of λ/A are listed in Tables (6-15) and (6-16). Also shown in these tables are the total counts taken, total count rate and the height in inches above an arbitrary datum. Table (6-15) contains the results for full flow and Table (6-16) the results for partial flow. A plot of λ/A against height for full flow can be seen in Fig. (6-17). The concentration profile for the partial flow was obtained by drawing the estimated best fit curve to λ/A as a function of height and converting this to concentration using equation (4-11) substituting for B the measured value 3.81,

$$C = \log_{10} (A/\lambda)/3.81. \qquad (6\text{-}10)$$

The resultant graph of C against y can be seen in Fig. (6-19) as can the gradient and integral of C with respect

to y. The integral plotted against y is taken between y and the free surface.

For the full flow case, a wave was detected in the channel bed. Methods discussed in Chapter 5 were used to allow for this effect when calculating the concentration profile. The shape of the wave was determined from photographs of the type shown in Fig. (6-27). From a series of photographs, a set of fixed bed profiles was obtained. The wave height was divided into seven equal elements and the proportion of time the interface between the fixed and moving beds at the working section spent within each element was determined. Working from the top down, the percentages of time spent within each element were 3.4, 1.4, 5.1, 15.1, 37.7, 20 and 17.3.

Using a computer programme, the correction procedure described in Chapter 5 was carried out. From the final results of λ/A against height relative to the top of the fixed bed, the concentration was obtained using equation (6-10). In Fig. (6-18) the values of C, and the gradient and integral of C with respect to y have been plotted against y, measured in feet from the top of the fixed bed. The integral plotted against y is taken between y and the free surface.

Table (6-15)

Concentration meter results for full flow with ¼ inch pea gravel.

Height	Cts	Cts/Min.	λ/A
1.5	1280	128	.0019
2.0	1280	129	.0022
2.25	1280	137	.0052
2.5	1280	147	.0090
2.75	1280	150	.0102
3.0	1280	172	.0184
3.25	1280	259	.051
3.5	1280	357	.088
3.75	1280	416	.110
4.0	1280	587	.175
4.25	1280	766	.242
4.5	2560	1085	.361
4.75	2560	1270	.431
5.0	2560	1660	.579
5.25	6400	1950	.687
5.5	6400	2270	.808
5.75	6400	2510	.897
Bg	3200	123	-
	Break between runs		
Bg	2560	102	-
1.75	1792	126	.0018
5.5	6400	2380	.807
5.75	6400	2680	.914
6	6400	2720	.929
6.25	6400	2710	.926
6.5	6400	2820	.965
6.75	6400	2830	.968
7	6400	2820	.965
7.25	6400	2830	.968
7.5	6400	2840	.972
7.75	6400	2840	.972
8.0	6400	2870	.982
8.25	6400	2810	.961
8.5	6400	2750	.940
7.5	6400	2880	.986

Table (6-16)

Concentration meter results for partial flow with ¼ inch pea gravel.

Height	Cts	Cts/Min.	λ/A
5.25	6400	2940	.981
5.0	6400	2970	.992
4.75	6400	2990	1.000
4.5	6400	3000	1.000
4.25	6400	2970	.992
4.0	6400	2910	.970
3.75	6400	2660	.882
3.625	6400	2215	.727
3.50	3200	1830	.594
3.375	3200	1430	.454
3.25	2560	859	.255
3.125	2560	515	.135
3.0	1280	300	.0603
2.875	1280	213	.0300
2.75	1280	189	.0216
2.5	1280	152	.0087
Bg	2560	127	-

Velocity Measurements

Fluid

For both flows, the velocity of the fluid was measured as for the 3/8 inch - 3/16 inch gravel, using the pitot-static head and pressure transducer. The same procedure was used and the results showed similar oscillations, but a more systematic oscillation was observed than for the 3/8 inch - 3/16 inch gravel. This more regular oscillation is believed to have been caused by the more consistent wave pattern set up with the ¼ inch particles. In general, the recording at a given point would show a fairly steady reading followed by

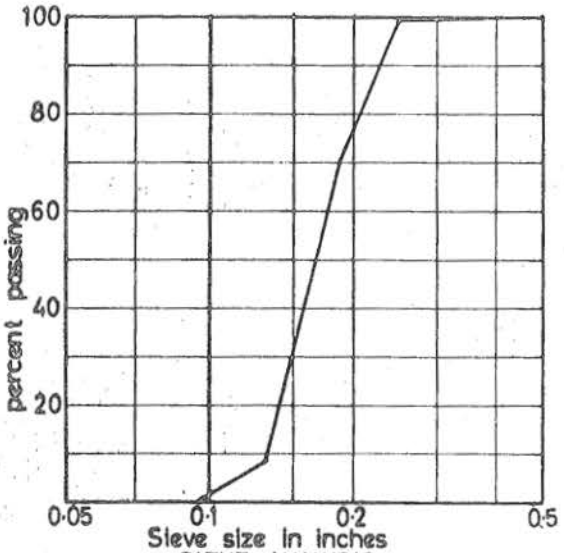

SIEVE ANALYSIS
FIG 6-16

ALL GRAPHS ON THIS PAGE APPLY TO ¼ INCH PEA GRAVEL

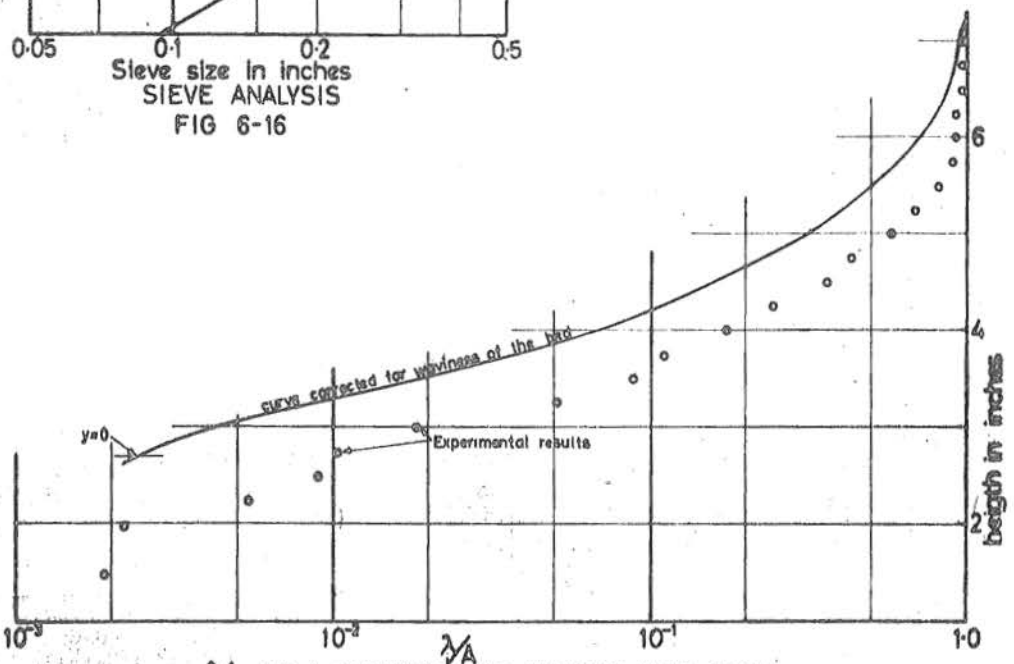

λ/A AS A FUNCTION OF HEIGHT, FULL FLOW
FIG 6-17

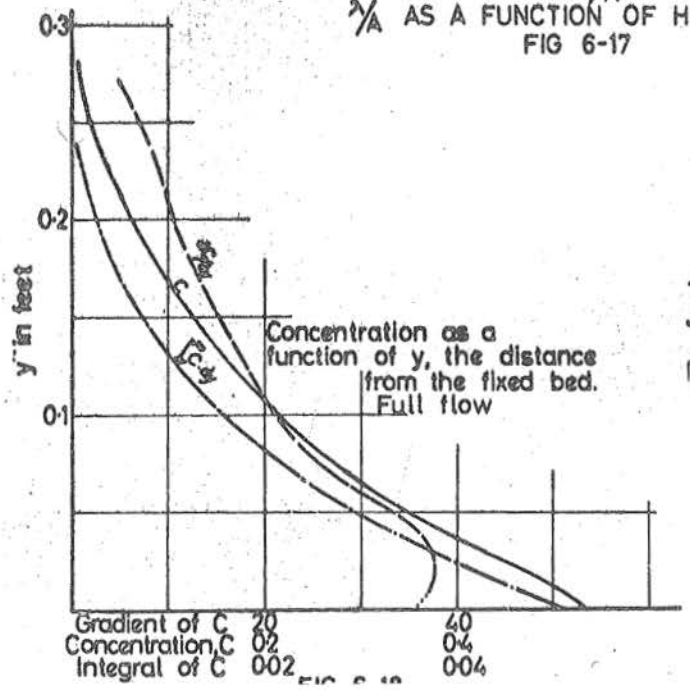

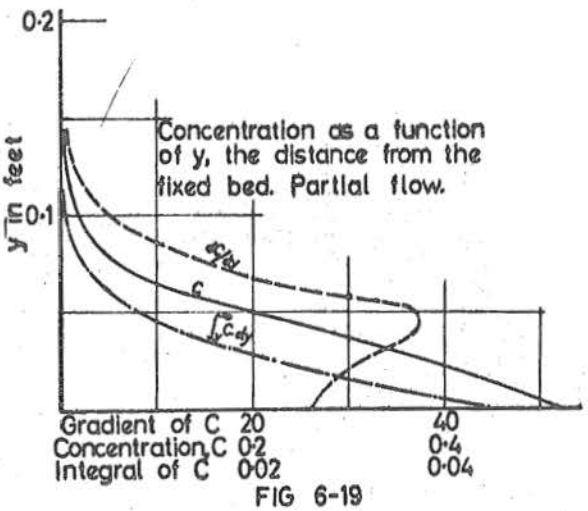

FIG 6-19

a sharp dip and quick recovery. Typical recordings are shown in Fig. (4-14). The velocity heads were measured from the flat section of the recording and the dips were not included. Table (6-17) lists results for full flow and Table (6-18) for partial flow. From the velocity heads obtained, the velocities were calculated and these have been included in the same tables.

Fluid velocities obtained for full and partial flows are plotted against height in Figs. (6-22) and (6-23).

Table (6-17)

Velocity and static head difference measurements for full flow with ¼ inch pea gravel. All heads are given in feet of water and the velocities in feet per second.

Height	Velocity Head		Static	Velocity	
Inches	Top	Bottom	Diff.	Top	Bottom
2.25	.89	.008	+.012	7.6	.72
2.75	1.07	.027	.012	8.3	1.32
3.0	1.20	.048	.021	8.8	1.76
3.25	1.52	.051	.000	9.9	1.81
3.5	1.87	.33	.002	11.0	4.6
3.75	2.19	.458	.001	11.9	5.4
4.0	2.16	.39	-.011	11.8	5.0
4.25	2.35	.60	-.019	12.3	6.2
4.5	2.43	.88	-.025	12.5	7.5
4.75	2.43	1.14	-.032	12.5	8.6
5.0	2.62	1.16	-.032	13.0	8.6
5.25	2.70	1.32	-.038	13.2	9.2
5.5	2.79	1.71	-.042	13.4	10.5
5.75	3.00	1.81	-.038	13.9	10.8
6.0	3.01	2.03	-.036	13.9	11.4
6.25	3.06	2.14	-.034	14.0	11.7
6.5	3.06	2.30	-.026	14.0	12.2

(Table Continued Overleaf)

Table (6-17) Contd:

Height	Velocity Head		Static Diff.	Velocity	
Inches	Top	Bottom		Top	Bottom
6.75	3.28	2.32	-.036	14.5	12.2
1.5	.240	.017	+.029	3.9	1.05
1.0	.049	.025	+.012	1.8	1.27
		Break Between Runs			
6.75	3.42	2.92	-	14.8	13.7
7.0	3.42	2.96	-	14.9	13.9
7.25	-	3.23	-	-	14.4
6.5	3.40	3.20	-.012	14.8	14.3
6.25	3.37	2.92	-.010	14.7	13.7
6.0	3.30	2.88	-.007	14.6	13.6
5.75	3.32	2.68	-.012	14.6	13.1
5.5	3.35	2.47	-.015	14.7	12.6
5.25	3.32	2.40	-.015	14.6	12.4
5.0	3.20	2.21	-.007	14.4	11.9
4.75	3.12	2.08	-.015	14.2	11.6
4.5	2.92	2.08	-.014	13.7	11.6
4.25	2.81	1.37	-.016	13.5	9.3
4.0	2.72	1.61	-.012	13.2	10.2
3.75	2.43	1.16	-.008	12.5	8.6
3.5	2.40	.96	-.008	12.4	7.9
3.25	2.51	.74	-.006	12.7	6.9
3.0	2.35	.66	+.000	12.3	6.5
2.75	2.10	.25	+.000	11.6	4.1
2.5	1.55	.120	+.010	10.0	2.8
2.25	1.31	.080	+.014	9.2	2.3
2.0	1.07	.055	+.018	8.3	1.9
1.75	1.01	.040	+.022	8.1	1.6
1.5	.85	.032	+.022	7.4	1.4
1.25	.67	.027	+.019	6.6	1.3
1.0	.37	.026	+.015	4.9	1.3
0.75	.15	.019	+.010	3.1	1.1
0.5	.042	.014	+.008	1.6	1.0
0.25	.020	.013	+.000	1.1	0.9

(End of Table)

Table (6-18)

Velocity and static head difference measurements for partial flow with ¼ inch pea gravel. All heads are given in feet of water and velocities in feet per second.

Height	Velocity Head		Static Diff.	Velocity	
Inches	Top	Bottom		Top	Bottom
1.0	.006	-	.000	.6	-
1.25	.009	-	.000	.8	-
1.54	.032	.008	+.004	1.4	.7
1.75	.089	.009	+.011	2.4	.8
2.0	.211	.009	+.013	3.7	.8
2.25	.404	.008	+.013	5.1	.7
2.5	.55	.009	+.015	6.0	.8
2.75	.67	.009	+.016	6.6	.8
3.0	.86	.007	+.013	7.5	.7
3.25	.91	.021	+.009	7.7	1.2
3.5	.93	.107	+.001	7.7	2.6
3.75	1.01	.200	-.003	8.1	3.6
4.0	1.11	.42	-.004	8.5	5.2
4.25	1.15	.57	-.004	8.6	5.5
4.5	1.15	.66	-.009	8.6	6.5
4.75	1.16	.79	-.009	8.6	7.1
5.0	1.25	.84	-.005	9.0	7.4

Solids

The particle velocity was measured separately. Such measurement had been unsuccessfully attempted with previous flows, but with ¼ inch pea gravel successful measurements were made for both flows. The method used was to operate at its minimum speed and normal voltage the Magnifax high speed camera described in Chapter 4. The resulting negative was projected directly on to a sheet of tracing paper. The positions of a number of stones were marked and the process

repeated until the paths of such stones had been followed for the full time they were in view. Film speeds were calculated from timing marks along the film and the stone velocities and positions obtained. Each particle recorded was observed an average of ten times. Results obtained for each of the four runs are shown in Figs. (6-20) and (6-21) where the mean velocity and height of each particle measured has been plotted. For each of the four runs (two at each flow), the mean velocity profile was estimated by taking increments of 0.2 inches and calculating the mean height and mean velocity of all points within the given increment. These mean velocity profiles have been plotted in Figs. (6-20) and (6-21). After adjusting the full flow runs so that the height was measured relative to the top of the fixed bed, the mean value of the two full flow curves was taken as the stone velocity profile. A similar process was used with the two partial flow profiles.

Static Head Difference

For ¼ inch pea gravel, the static head difference between the two pitot-static tubes was obtained as described for 3/8 inch - 3/16 inch gravel in Part III of this Chapter. The results in feet of water have been recorded in Table (6-17) for full flow and Table (6-18) for partial flow, under "Static Difference", and have also been plotted against depth in inches from the free surface in Fig. (6-22) for full flow and Fig. (6-23) for partial flow.

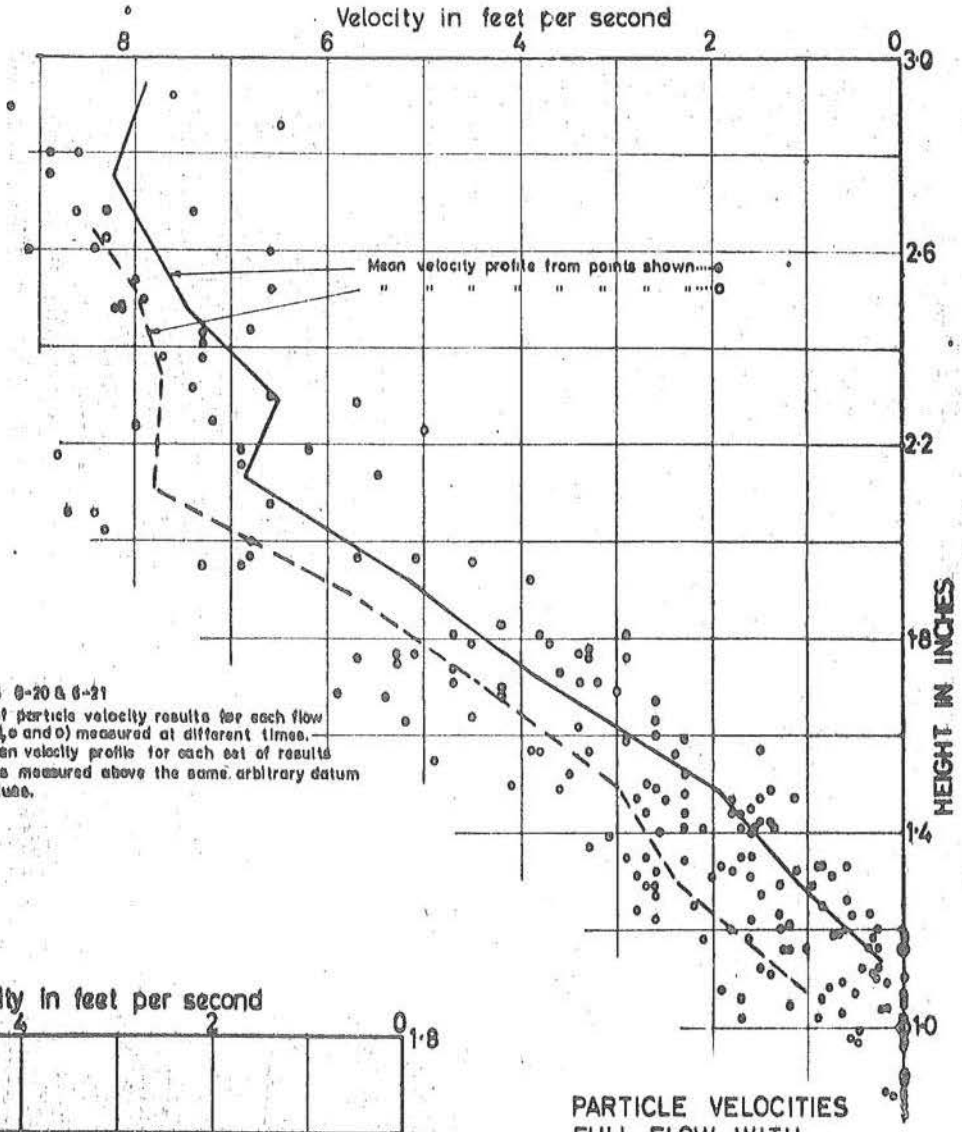

PARTICLE VELOCITIES
FULL FLOW WITH
¼ INCH PEA GRAVEL
FIG 6-20

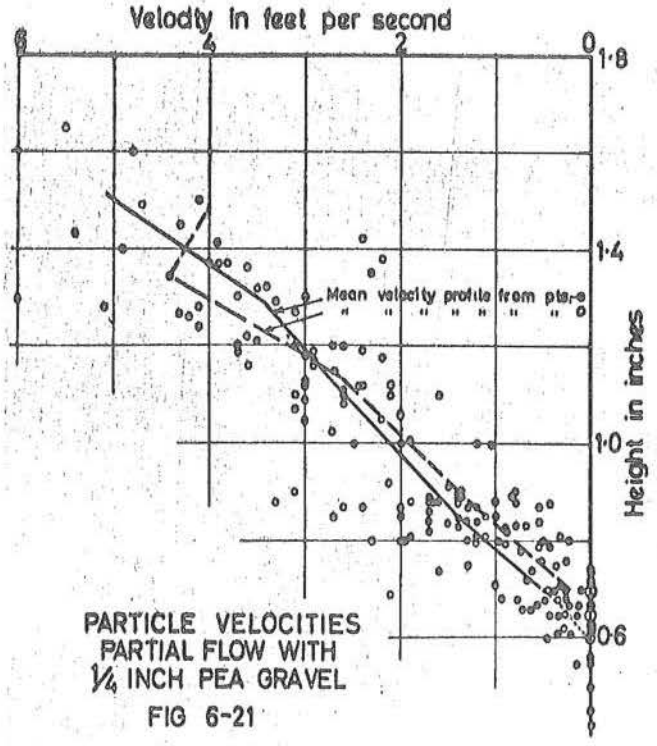

PARTICLE VELOCITIES
PARTIAL FLOW WITH
¼ INCH PEA GRAVEL
FIG 6-21

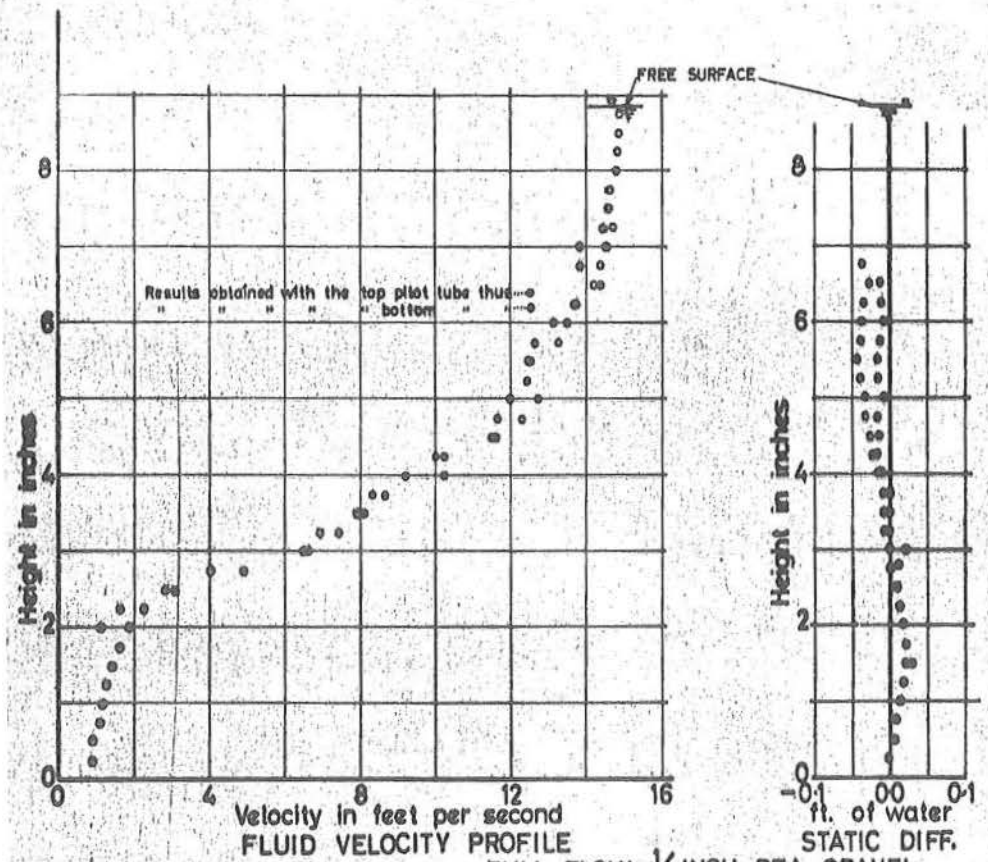

FULL FLOW, ¼ INCH PEA GRAVEL
FIG 6-22

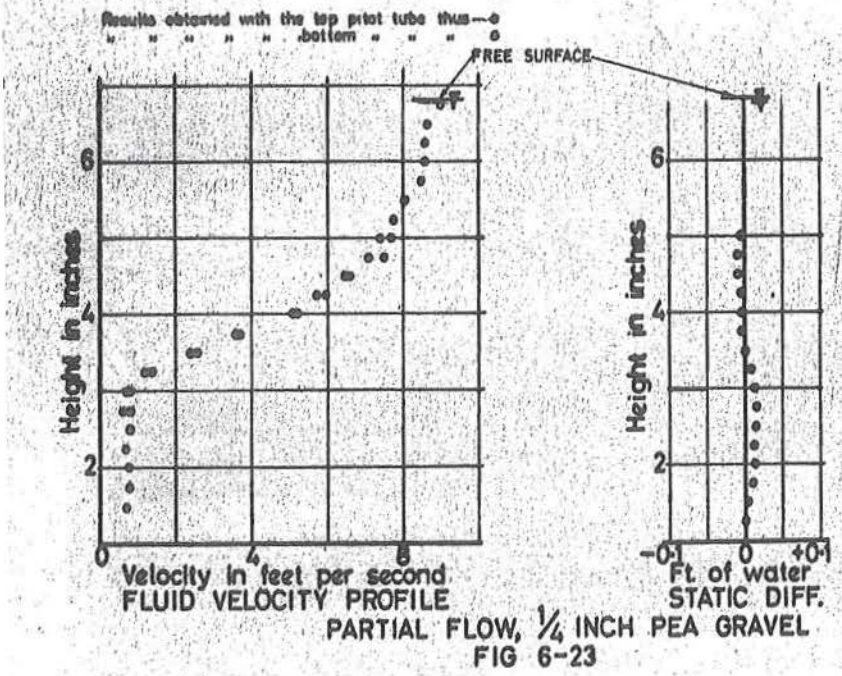

PARTIAL FLOW, ¼ INCH PEA GRAVEL
FIG 6-23

Calculated Parameters

From the concentration profile, the shear stress and dispersive stress were calculated, assuming no significant suspended load. Equation (6-2) was used for both flows to obtain the dispersive stress. The total shear stress was calculated using equation (6-7) and substituting $d = 0.508$ ft, $\theta = 0.047$ and $d = 0.291$ ft, $\theta = 0.035$ for full and partial flows respectively to obtain for full flow

$$T_t = 0.047 \left[62.4\ (.508 - y) + 103 \int_y^\infty C dy\right] \qquad (6\text{-}11)$$

and for partial flow

$$T_t = 0.035 \left[62.4\ (0.291 - y) + 103 \int_y^\infty C dy\right]. \qquad (6\text{-}12)$$

Using T_t and P calculated as above, $F_1 = P/T_t$ was determined and is tabulated in Tables (6-19) and (6-20). The stone velocity profile was then used to obtain $\frac{du}{dy}$ for $0.00 < y < 0.06$ and the fluid velocity profile when $y > 0.06$. From $\frac{du}{dy}$ and T_t the parameter F_3 was calculated. Calculated results for C, F_1, F_3 and Π are tabulated for various values of y in Table (6-19) for full flow and Table (6-20) for partial flow.

Table (6-19)

Calculated parameters for full flow with ¼ inch pea gravel.

y	C	F_1	F_3	Π
0.0	.53	3.14	.378	3430
0.02	.46	2.85	.351	188
0.04	.38	2.50	.291	50
0.06	.28	1.67	.195	20
0.08	.23	1.38	.111	1000
0.10	.19	1.09	1.18	1.0
0.12	.155	.87	-	-
0.14	.12	.66	-	-

Table (6-20)

Calculated parameters for partial flow with ¼ inch pea gravel.

y	C	F_1	F_3	Π
.00	.53	3.25	.163	593
.02	.41	2.12	.132	287
.04	.28	1.15	.115	204
.06	.125	.54	.085	∞
.08	.046	.17	.149	234
.10	.018	-	.212	238
.12	.006	-	.374	-

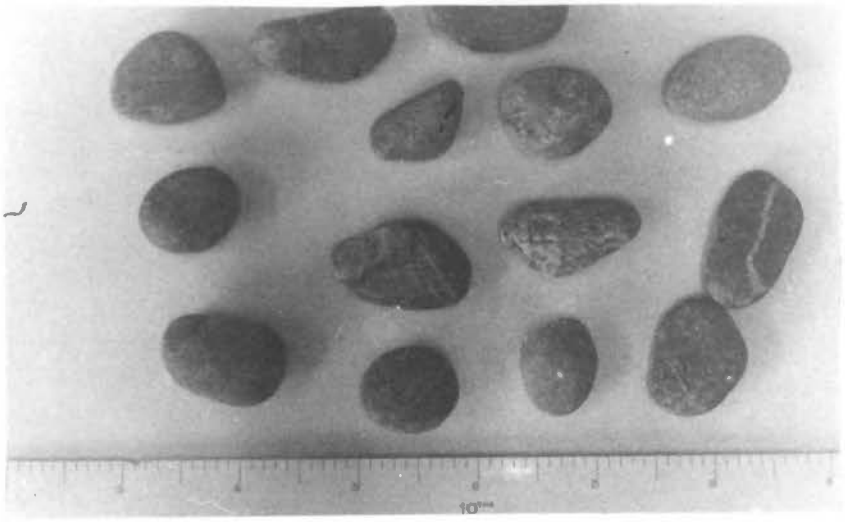

FIG. 6-24
¾" - ½" Gravel

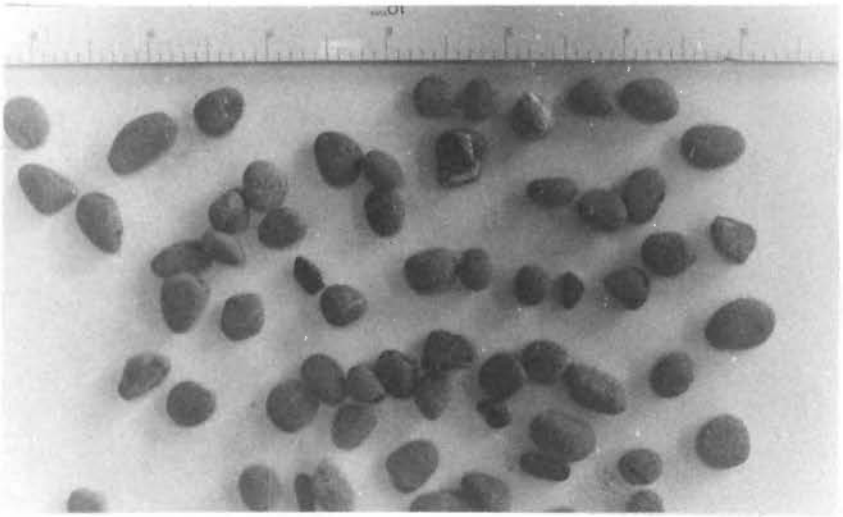

FIG. 6-25
⅜" - 3/16" Gravel

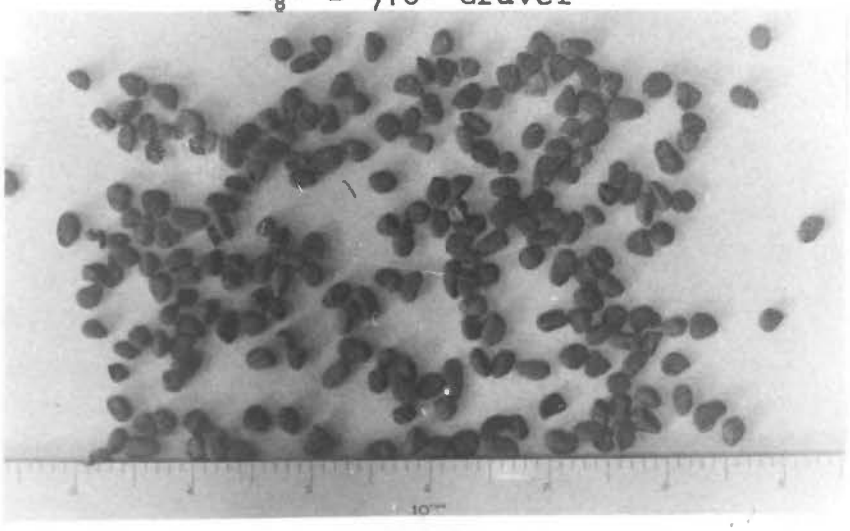

FIG. 6-26
¼" Pea Gravel

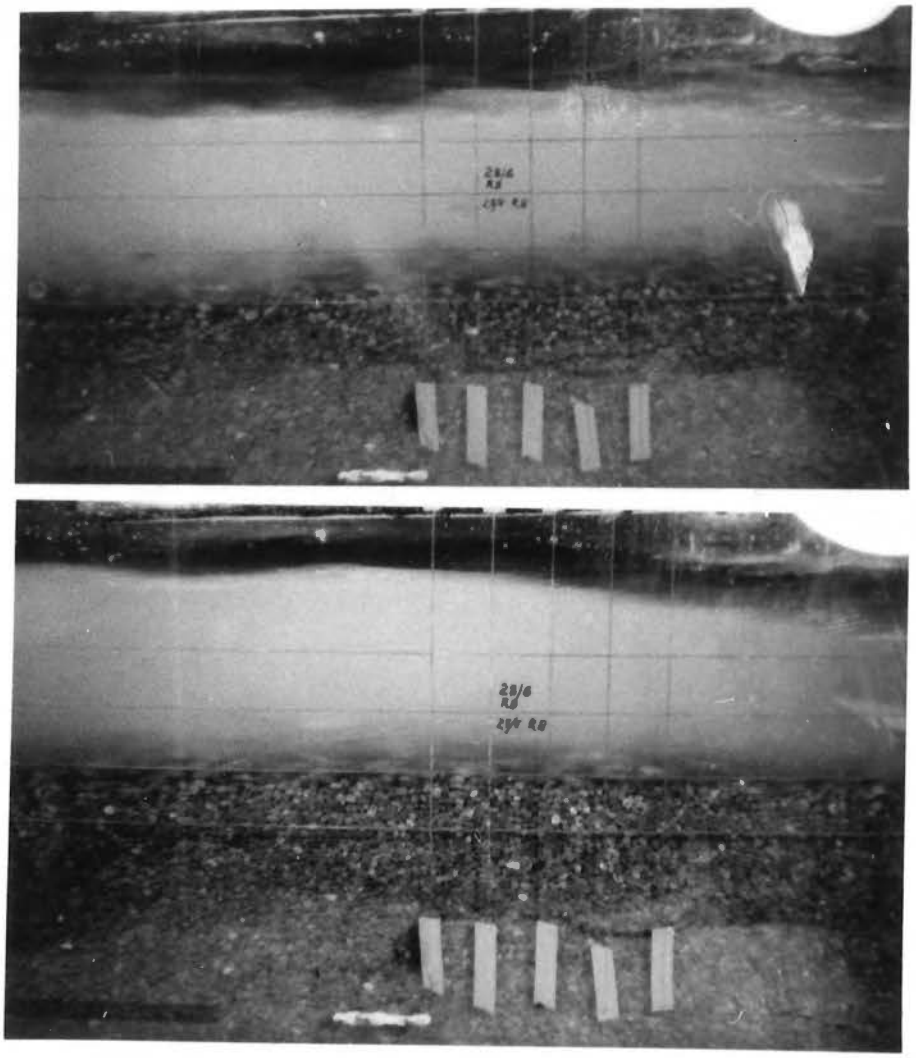

FIG. 6-27

FULL FLOW WITH ¼" PEA GRAVEL

CHAPTER 7

CONCLUSIONS BASED ON THE RESULTS OF THIS THESIS

SYNOPSIS

This chapter sets out the conclusions reached after carrying out the theoretical and experimental programmes described in Chapters 2 to 6. In this thesis, the work can be divided into two distinct sections, the first dealing with the prediction of the behaviour of a fluid-particle system at a point and the second developing methods of using the predictions of behaviour at a point to obtain the complete flow pattern of the bed region in an open channel.

In the first section of this chapter, there is a discussion of the parameters F_1 and F_3 introduced in Chapter 3. These parameters describe the relationship between direct and shear stress on the one hand, and shear stress and rate of strain on the other, both parameters applying particularly to systems in which the gradients of the flow parameters transverse to the flow are small. It is concluded that the theoretical model used in Chapter 3 to calculate F_1 and F_3 is not accurate, and in particular that it predicts values of F_1 less than 0.5 times the measured values at high concentrations. Major reasons for this discrepancy are believed to be the sliding of

particles over each other and the formation of groups or clusters of particles capable of transferring stress over a greater distance than single particles. Theoretical values of F_3 fall within a rather wide band of experimental data and the form of the predicted curve in the F_3 - C plane, where C is the volumetric concentration of particles, is similar to the form of the experimental curves.

In the second section of the chapter, the application of F_1 and F_3 to flow problems is considered. One conclusion reached is that, if F_1 is a known function of C, it is possible to obtain the concentration profile for a given particle size, slope and bed shear stress. The calculation of the velocity profile from F_3 turns out to be less reliable, possibly because of a greater sensitivity to gradients in the flow parameters.

Further possible extensions to the work described in this thesis are discussed in Chapter 9.

DISCUSSION OF F_1 AND F_3

Introduction

In Chapter 3, a model of particle behaviour has been set up and from this model the parameters F_1 and F_3 have been obtained as functions of concentration, C, where

$$F_1 = P/T \qquad (7\text{-}1)$$

$$F_3 = T/\rho_s D^2 \left(\frac{du}{dy}\right)^2 \quad . \qquad (7\text{-}2)$$

This calculation is based on the results obtained using a gas model of rigid, smooth elastic spheres. Miller (9) in previous work found the effective viscosity and pressure of a particle system by direct substitution in the Enskog equations for a gas of rigid, smooth elastic spheres. He noted that, if perfectly rough spheres were postulated in the calculations, the predicted viscosity of the gas was only slightly increased.

In Miller's work, the resulting equations for F_1 and F_3 included the "temperature" of the gas or, alternatively, the random velocity fluctuations of the particles, as an independent variable. Chapter 3 introduces a third equation based on the steady state energy equilibrium of the system. From the three equations, the "temperature" is eliminated to give theoretical predictions of F_1 and F_3 in terms of the particle properties and concentration. In general form, the three preliminary equations are

$$T_s/\frac{du}{dy} = \rho_s D \bar{s} f_1 \qquad (7\text{-}3)$$

$$T_s \left(\frac{du}{dy}\right) = \rho_s \bar{s}^3 f_2/D \qquad (7\text{-}4)$$

$$P = \rho_s \bar{s}^2 f_3 \qquad (7\text{-}5)$$

where $\bar{s}$ is the r.m.s. value of the difference between the instantaneous particle velocities and the mean particle velocities, f_i are functions of concentration, P is the normal inter-particle stress and T_s is the shear stress taken by the particles. The detailed form of equations (7-3), (7-4) and (7-5) is discussed in Chapter 3 and it is shown that F_2 and F_7 follow directly where

$$F_2 = T_s / \rho_s D^2 \left(\frac{du}{dy}\right)^2 = \frac{f_1^{3/2}}{\sqrt{f_2}} \qquad (7\text{-}6)$$

$$F_7 = P/T_s = \frac{f_3}{\sqrt{f_1 f_2}} . \qquad (7\text{-}7)$$

Equations (7-6) and (7-7) are given in full as (3-34) and (3-35) and then developed to allow for the effect of the surrounding fluid. This modification is given by equations (3-74) and (3-75) and was found to be significant only when $C < 0.3$.

Finally, an estimate of the shear stress carried by the fluid T_f was made and, because of the approximate model used, two extreme cases were calculated, giving bands within which F_1 and F_3 were expected to lie. Fortunately, these bands are not excessively wide for high values of C, as can be seen from Figs. (3-9) and (3-10).

Measured Values of F_1 and F_3

The writer knows of three sets of data from which F_1 and F_3 can be found. These are Miller's (9), Bagnold's (6) and that described in this thesis. In the experiments of Miller and Bagnold, C was uniform throughout the flow and consequently the situation should have approached more closely to that used for the theoretical analysis than did the flume experiments. Miller's and Bagnold's experiments were carried out with a density ratio of unity and only the flume experiments described in this thesis used a particle-fluid density ratio other than unity and had a non-uniform distribution of C.

Comparison of Results for F_1

Bagnold's experimental values of F_1 show only a small amount of scatter and are plotted against C in Fig. (3-12). From these results, it would appear that, for high values of Reynolds number, the value of F_1 reaches a maximum of between 3.5 and 4.5 at a concentration, C, of 0.5. Miller's results for F_1 as a function of C cover a much wider range than Bagnold's, with a maximum of 8.8 occurring at C = 0.20. Experimental values obtained by the writer are in reasonable agreement with those obtained by Bagnold and are given in Fig. (7-3). However, there was virtually no agreement between the experimental values of the writer and those of Miller.

Values of F_1 predicted from the theory developed in Chapter 3 are shown in Fig. (7-3) and it can be seen that there is a marked discrepancy between the theoretical values and all three sets of experimental values of F_1. It should be noted in conjunction with these results that the velocity profiles demonstrated that large scale turbulence occurred for $C < 0.20$.

Errors in the experimental work of this thesis are discussed in the following section, after which the theoretical model will be examined.

Experimental Inaccuracies in F_1

Experimentally, F_1 was calculated from the measured slope, fluid and particle densities and the concentration profile. Slope measurements were made over a distance of 8 ft and no difficulty was experienced in obtaining either bed or water surface elevations to an accuracy better than 0.1 inches. As the slope was large, this would give a possible error in the slope measurement of not more than ±5%. Density measurements were readily carried out to better than ±1%. Concentration profile errors are of two types, those caused by the random signal variations and those caused by inaccuracies in calculating the calibration factors for the equipment. As the equipment was effectively checked for calibration during each run, the expected error from this source should be small. Further, the calculation of F_1 used the integral of concentration and the

process of integration would reduce the expected random error to give an expected error in the integrated concentration of not more than ±5%. Direct errors in measurement are therefore unlikely to produce errors in F_1 > ±8% (assuming no correlation of errors).

The normal interparticle stress, P, is developed by the direct effect of one particle on an adjacent one (by bouncing and sliding). It will be equal to the total weight per unit area of solid particles above the plane considered, less the weight per unit area of particles supported by the action of the fluid turbulence on the concentration gradient, that is, less the suspended load. Consequently, the value of P obtained by integration of the concentration above the plane considered will be an upper limit. Although the total suspended load is not known, an upper limit can be obtained by assuming that all solid material above the plane at which C = 0.20 is in suspension. The lower limit of P so obtained will vary from 0 at C = 0.20 to 0.75 times the original calculated value of P at C = 0.50. The correct P will therefore be up to 25% less than the measured value at high concentrations.

A further error in the calculation of $F_1 = P/T$ arises because of an approximation in calculating T from the measured flow parameters. This approximation lies in the assumption that the component, of the total weight of particles above a

plane, acting along the plane is equal to the shear stress on that plane. While this equality will hold for a uniform flow, in some of the experimental flows the bed was distorted by waves or bumps. When this occurs, there will in general be a variation of pressure over the bump in the bed, leading to a profile drag. From observations of the bed, an approximation to the bed wave shape is as follows.

This bed shape is assumed to consist of obstacles 1.5 inches high spaced at 5 ft centres and having a value of $C_D = 0.20$. For a fluid velocity relative to the obstacle of 10 ft per second, and using the data obtained for full flow with ¼ inch pea gravel, a reduction in T of 20% is obtained.

The two errors considered above (reduction in P caused by suspension and reduction in T caused by bed waves) act in opposite ways on F_1, so that the total effect of the two errors will be less than the effect of the larger of the two errors acting by itself. It is, therefore, unlikely that the total error in calculating F_1 from the two effects will exceed ±20% at high values of concentration.

Discussion of Theoretical Model

From the above discussion, it is expected that measured values of F_1 obtained using the flume will be within ±20% of the true value of F_1. Confirmation of the flume results is obtained from Bagnold's work which gives values of F_1 agreeing moderately

well with the flume results as shown in Fig. (7-3). However, for high concentrations, the values of F_1 predicted in Chapter 3 from a theoretical analysis are less than half the values of F_1 obtained using the flume. It is therefore evident that either the analysis or the model (or possibly both) is inaccurate.

In developing the theory predicting F_1, a number of approximations were made when allowing for the effect of the fluid. As, however, the fluid did not have a large effect on F_1 at high concentrations, errors in this part of the theory cannot explain the large discrepancy noted above. The model used to describe the particle-particle interaction must therefore be inaccurate.

Cluster Formation

Two important mechanisms that are expected to affect F_1 will now be discussed. Both of these mechanisms are related to the difference in behaviour on contact between the real and ideal particles. In Chapter 3, the results of the analysis of rigid elastic spheres have been used. An important implication of this model is that all collisions will be instantaneous and, in consequence, all collisions will occur between two particles only. In a real fluid-particle system, there is a loss of energy at collision and also a tendency for particles to rest one on the other to form groups or "clusters" of particles.

Another important property of real particle systems is the ability of the particles to slide or roll over each other. The clusters of particles are therefore capable of distortion under shear flow, behaving in a similar manner to a slowly sheared volume of packed spheres. This sliding or rolling action will become significant when the cluster size is large, a condition occurring at high concentrations, particularly in the close neighbourhood of a solid boundary. For a well graded granular soil, under a slow rate of strain, F_1 is about 2.1 and for uniform spheres is expected to be rather more.

It is apparent from the above discussion that a satisfactory model of high concentration fluid-particle shear flows will take into account the formation of clusters and include sliding and rolling action of the particles.

Energy Dissipation

In the model developed in Chapter 3, energy dissipation is assumed to occur in particle-particle collision as a result of change in the velocities along the line joining the centres of the particles. This assumption is equivalent to assuming perfectly smooth particle surfaces.

One refinement in the analysis that will now be considered is the inclusion of a term allowing for the loss in energy caused by the change in velocities normal to the join of the

particle centres and also the change in rotational kinetic energy.

Consider two colliding particles of radii r and radii of gyration Kr.. Velocities of the particle centres just before collision will be V_{b1} and V_{b2} along the line joining the particle centres and U_{b1} and U_{b2} in the direction perpendicular to this join. The angular velocities will be Z_{b1} and Z_{b2}/r, the positive directions being as shown by the arrows in Fig. (7-1).

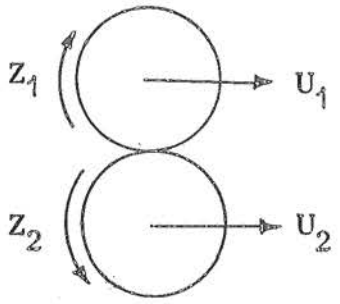

Fig. (7-1)

The velocities, after collision, will be denoted by the suffix "a" (U_{a1}, for example) and it will be assumed that the relative tangential velocities are zero after collision. Three equations for the conservation of linear and angular momentum and one for the zero relative tangential velocities after collision are given below.

$$\left.\begin{aligned} U_{a1} - U_{b1} &= k^2 (Z_{b1} - Z_{a1}) \\ U_{a2} - U_{b2} &= k^2 (Z_{b2} - Z_{a2}) \\ U_{a2} + U_{a1} &= U_{b2} + U_{b1} \\ U_{a1} - Z_{a1} &= U_{a2} - Z_{a2} \,. \end{aligned}\right\} \qquad (7\text{-}9)$$

Equations (7-9) can be simplified by the operators S and Δ where $Sx = x_1 + x_2$ and $\Delta x = x_1 - x_2$ to give

$$\left.\begin{aligned} SU_a &= SU_b \\ SZ_a &= SZ_b \\ SU_a &= SZ_a = (\Delta U_b + k^2 \Delta Z_b)/(1 + k^2) \,. \end{aligned}\right\} \qquad (7\text{-}10)$$

It follows from (7-10) that the energy dissipated, E_t, by the change in U and Z is given by

$$E_t = \tfrac{1}{4} m (\Delta U_b - \Delta Z_b)^2 \frac{k^2}{1 + k^2} \qquad (7\text{-}11)$$

where m is the mass of each sphere.

For a sphere of uniform density, k = 0.5 and from (7-11)

$$E_t = 0.05 m (\Delta^2 Z_b + \Delta^2 U_b - 2\Delta Z_b \Delta U_b) . \qquad (7\text{-}12)$$

The mean value of E_t for a large number of collisions of particles similar to those described above is given by

$$\bar{E}_t = 0.05\ m\ (\overline{\Delta^2 Z_b} + \overline{\Delta^2 U_b} - 2\overline{\Delta Z_b \Delta U_b}). \qquad (7\text{-}13)$$

If ΔZ_b and ΔU_b are uncorrelated random variables of mean value zero, the last term in equation (7-13) will be zero, and, if $\Delta^2 Z_b = \Delta^2 U_b$, an estimate of $\bar{E}_t$ is given by

$$\bar{E}_t = 0.1\ m\ \overline{\Delta^2 U_b}\ . \qquad (7\text{-}14)$$

To use equation (7-14), the value of $\Delta^2 U_b$ must be known. At low concentrations, the particles will be colliding in a random manner and it is expected that the mean values of the two components of velocity $\bar{U}$ and $\bar{V}$ will be equal. It follows from equation (3-19) that the mean difference between the velocity components, $\bar{U}$, is equal to 2 $\bar{s}$ and by substitution in (7-14) it can be shown that the value of K_2 will be increased by a factor of 1.2 where K_2 is defined as the energy lost per collision divided by $m\bar{s}^2$.

Increasing the concentration leads to a restriction in the possible particle paths and in collisions the relative velocity along the line of centres will be greater than the relative velocity normal to the lines of centres. This effect will mean that the absolute change in K_2 will be reduced and,

as the magnitude of K_2 calculated in Chapter 3 is increasing, the proportional change in K_2 will be reduced still further. At very high concentrations, the change in K_2 can be neglected completely.

The viscosity of a system of perfectly rough particles is given by Hirschfelder (10) for a low concentration and is only slightly different from that for perfectly smooth particles.

Upon collision, the tangential velocities of perfectly smooth particles are unaltered, whereas for perfectly rough particles the relative tangential velocity is reversed. As the relative tangential velocity of the real particles is expected to be reduced to zero, a condition intermediate between the smooth and rough models described above, the viscosity will be taken as the mean of the perfectly smooth and perfectly rough values obtained by Hirschfelder.

If the above-described corrections for energy dissipation and viscosity are applied to equations (3-68) and (3-69), we obtain a new value of F_7, 0.64 times the value calculated from equation (3-70) for values of $C < 0.15$. As the corrections are negligible at high concentrations, F_7 will not be altered at high concentrations. The factor F_8 will also be altered in the above model, but, as discussed below, the form of this

alteration is not known. An exact correction to $F_1 = F_7/(1 + F_8)$ cannot therefore be obtained. If F_2 is reduced, then, from equations (3-82) and (3-83), F_8 will be increased and consequently F_1 will be reduced by a greater proportion than F_7.

From Fig. (7-3), it can be seen that a reduction in F_1 will improve the agreement between theory and experiment for $C < 0.25$. Such agreement may be in part fortuitous as, in the region where $C < 0.2$, large scale turbulence is believed to exist.

Comparison of Results for F_3

The experimental results obtained for $T/\rho_s D^2 (du/dy)^2$ (denoted by F_3) by Bagnold, Miller and the writer (Fig. 7-2) show considerable scatter, particularly at high concentrations. Measurement of F_3 is more easily accomplished accurately in an apparatus of the type used by Miller and Bagnold, but there is a large discrepancy between their results as shown in Fig. (7-4). The theory developed in Chapter 3 gives values of F_3 generally greater than most values obtained experimentally, but the general form of the results is similar to that obtained by Bagnold. There is considerable scatter in the results obtained from the flume, particularly at high particle concentrations.

Experimental Inaccuracies in F_3

Experimental values of F_3 were determined by measuring

ρ_s, D, $\frac{du}{dy}$, C and T as functions of y. Measurements of C, T and ρ_s have been considered in a previous section of this chapter. The value of D^2 used in calculating F_3 was the average value of D^2 weighted according to the mass of material within each size range. As the gradings for all types of material were similar, errors in this method of estimation would not affect the relative results for different materials but only modify the experimental results by a constant factor.

The value of the velocity gradient du/dy was obtained by measurement of the gradient of the u - y curve. Measurement of u is discussed in Chapters 4, 5 and 8. It was found that large changes in du/dy occurred within small intervals of y. Near the bed, high concentrations and low fluid velocities accentuated the inaccuracies of measurements made by means of pitot-static tubes. The results were further complicated by the fluctuations in bed level.

Manometer tubes were used during the ¾ inch - ½ inch gravel runs, and difficulty was experienced in obtaining readings for small velocities.

Because photographic methods were used to obtain the velocity profiles during the two ¼ inch pea gravel runs, these two velocity profiles are expected to be the most accurate ones obtained. Errors of about 20% in velocity gradients could

have occurred in obtaining (du/dy) from the photographic set of velocity measurements, Figs. (6-20) and (6-21). This would lead to errors of 45% in the values of F_3.

A correction to T, allowing for the profile drag of the bed formations, has been discussed in a previous section of this chapter and, for the ¼ inch pea gravel, is expected to be a reduction of about 20%. Experimental values of F_3 for ¼ inch pea gravel should therefore be reduced by a factor of 0.8.

Discussion of Theoretical Model of F_3

In a previous section of this chapter, consideration has been given to the possibility of the formation of clusters, as well as to a correction to improve the energy equation at low concentrations. Both these effects will alter the predicted values of F_3.

An increase in K_2 and therefore f_2 will, from equation (7-6), reduce F_2 and therefore F_3. Applying to f_1 and f_2 the correction allowing for a rough particle will give at low concentrations a theoretical value of F_3, 0.7 times the value predicted in Chapter 3, but at high concentrations this correction will be small.

It is not possible to determine the effect of cluster formation on the value of F_3. As an approximation, we can consider the system of clusters as equivalent to a system of

larger particles of diameter D'. If the clusters were rigid, the value of F_3 would be increased by $(D'/D)^2$. However, the clusters are not rigid, but free to distort. Shear stresses set up causing sliding of the particles in the particle clusters will not be proportional to (du/dy) but will be proportional to the direct stress between the particles in the clusters. It follows that F_3 will be a function of du/dy, generally decreasing with increasing du/dy. The distortion of the clusters will reduce f_2 and increase f_1, both these effects tending to reduce F_3 from the rigid cluster value.

Determination of the total effect of cluster formation would require a knowledge of the cluster size as a function of the flow geometry. It is expected that the particle must be in contact for a high proportion of time in order to form large clusters.

A large difference between the experimental curve of F_3 as a function of C obtained by Bagnold and that obtained by Miller is not easily explained, but could be partly caused by the effect of apparatus size on the formation and behaviour of particle clusters, and the effect of the rigid boundaries on the flow.

Summary of Conclusions Relating to F_1 and F_3

Experimental values of F_1 obtained using the flume agreed

closely with those obtained by Bagnold.

A particle model based on the collision of rigid elastic spheres losing energy on collision proportional to the square of the velocity along the line of centres is not accurate. Absolute values of error rather greater than 100% occur and, even more serious, the sign of the gradient dF_1/dC is not predicted correctly.

A modification to the energy equation to give a more accurate representation of the expected particle behaviour is included and caused the theoretical curve to conform moderately well with experimental results from the flume for low particle concentrations. This same correction also improved the agreement between the theoretical F_3 and Miller's and Bagnold's experiments for $C < 0.3$.

Modification of the model to include the finite particle contact times and the consequent formation of groups of particles rolling and sliding over one another is considered generally, and would improve the prediction for F_1; the effect on F_3 has not been calculated.

The model used did not require any arbitrary constants to fit the results to experimental data and therefore was given a rigorous check.

PREDICTION OF CONCENTRATION AND VELOCITY PROFILES

Introduction

It has been shown that, for high Reynolds numbers and a deep bed movement, the velocity and concentration profiles for the bed region of a steady uniform flow can be predicted.

To obtain these profiles, both the concentration, C, and F_1 must be known at some reference level, and it has been shown that these values vary only within a narrow range at the bottom of the moving bed. Consequently, the bottom of the moving bed can be used as a reference level from which the complete profiles can be obtained.

It has been shown in Chapter 2 that, when F_1 is dependent on C alone for a given flow, the solution of the concentration - depth profile reduces to the solution of a first order differential equation.

In this section, the application and limitations of the method are examined with particular reference to the results obtained using the flume.

Boundary Conditions

For all experimental runs carried out with the flume, the concentration, C, at the bottom of the moving bed was within the range $0.53 > C > 0.60$ and the parameter F_1 was within the

range $2.70 < F_1 < 3.25$.

It can be seen from the above that F_1 and C varied over only a narrow range of values at the bottom of the moving bed. Consequently, there will be little difficulty in using as reference points in obtaining the velocity and concentration profiles the values of F_1 and C at this level.

Uniqueness of $F_1(C)$

In all the experimental runs carried out with the flume, the values of $F_1(C)$ all fell within a narrow band for $0.0 < C < 0.2$, while for $C > 0.2$ the experimental results diverged as shown in Fig. (7-3). In the region $C > 0.2$, the value of F_1 increased with increase in $T_* = T/(\rho_s - \rho_f)g\,D$. Bagnold's results could be considered to apply to $T_* \to \infty$ and consequently form an upper limit to F_1.

One cause of the dependence of F_1 on the value of T_* is the dependence of F_1 on the gradient of the stresses, concentration and random velocity fluctuation, this gradient increasing for small values of T_*.

In practice, it should be possible, given a restricted set of conditions, to select a curve of F_1 depending on the value of T_* and hence obtain the required profiles by simple integration of a first order equation. As used in such a method, F_1 is no longer a local parameter but depends on T_*

at the bed.

In the flume experiments, T_* varied over the range $0.48 < T_* < 1.16$ and the maximum variation in F_1 with T_* in this range was 0.8 occurring for $0.38 < C < 0.54$. The general form of $F_1(C)$ for various values of T can be seen in Fig. (7-3).

Uniqueness of F_3

Experimental curves for F_3 as a function of C show a large scatter as seen in Fig. (7-4) and, in particular, that obtained using ¾ inch - ½ inch gravel is very different from any of the others. Inaccuracies in measurement are believed to account for some of the discrepancy, particularly for the ¾ inch - ½ inch gravel. Of the four remaining sets of results obtained using the flume, the two sets relating to the ¼ inch pea gravel are considered the most accurate. These two sets of results show F_3 increasing with increase in T_*, a result consistent with the assumption that Bagnold's curve represents $T_* \rightarrow \infty$.

However, because of the large experimental errors involved (as discussed in a previous section), the experimental results for F_3 are not thought to be conclusive.

Derivation of a Local Equation in Regions of Rapid Change

It has been shown experimentally that the $F_1(C)$ and $F_3(C)$ curves are certainly dependent upon the rate of change of the flow parameters, for $T_* < 1.2$, and probably to a lesser extent for $T_* > 1.2$. Many flow situations of interest lie within the range $0.0 < T_* < 1.2$ and, if a general theory is to be developed, it must include the effect of gradients transverse to the flow in the concentration C, and random fluctuating velocity $\bar{s}$. A brief discussion of some of these effects follows.

Cluster Formation

Cluster formation will be affected by the gradient of concentration and the gradient of direct stress and will alter the equations for F_1 and F_3. As clusters of particles can span a greater depth than single particles, their effect at a given level may be significantly controlled by the system behaviour at a level some distance away.

Variation in Mean Free Path

In the theory developed in Chapter 3, the mean free path of the particles is considered to be independent of direction. If the concentration gradient is large, however, the mean free path will be greatest in the direction of maximum negative

concentration gradient. A large velocity gradient might significantly distort the distribution of the mean free path as a function of direction.

Effect of a Gradient of $\bar{s}$

If $\bar{s}$ is a function of y, there will, in general, be two effects on the flow system. One is the dispersion of energy between different levels and the other is the effect on the viscosity of the system.

Considering the latter effect first, Hirschfelder et. al (10, p.495) give a set of two equations for the stress/rate of strain relation in a dilute gas, assumed to consist of rigid elastic spheres, including in these equations the effect of an energy gradient. If the pressure is p, then, for a parallel uniform flow in the x direction, the xy shear stress is given from these equations as

$$T_{xy} = -\mu\left[\frac{\partial V_x}{\partial y} - \frac{2\lambda}{5p}\left(\frac{\partial}{\partial x}\left\{\frac{\partial Te}{\partial y} + \frac{1}{nk}\frac{\partial T}{\partial y}\right\}\right)\right]. \qquad (7\text{-}15)$$

In (7-15), λ is the conductivity and μ the viscosity for a simple dilute gas. It can be seen that, for a uniform flow system, T_{xy} is given by $-\mu\frac{\partial V_x}{\partial y}$ to the accuracy of (7-15). A further deduction from Hirschfelder's equations is that $T_{yy} > T_{xx}$.

In deriving the energy equation (7-4), the energy dissipated per unit volume in any region was equated to $T \frac{du}{dy}$. If the energy flux q is significant, equation (7-4) should be replaced by

$$T \left(\frac{du}{dy}\right) = \rho_s \bar{s}^3 f_2/D + \frac{dq}{dy} . \qquad (7\text{-}16)$$

From Hirschfelder et. al (10), it can be shown that

$$\lambda = 4C \left(\frac{1}{Y} + 1.2 + 0.755Y\right) 5.47 \frac{k}{m} \qquad (7\text{-}17)$$

or, using a new function of C, f_4,

$$\lambda = 5.47 f_4 \frac{k}{m} .$$

Equation (7-17) applies to a gas of rough elastic spheres where the dilute gas viscosity, μ, is given from (3-8) by

$$\mu = \frac{5}{32\sqrt{2}} \frac{m\bar{s}}{D^2} . \qquad (7\text{-}18)$$

Noting that $q = -\lambda \frac{dTe}{dy}$, it follows from (3-7) and (7-17) that

$$q = -5.47 f_4 \frac{\pi}{8} \mu \frac{d}{dy} (\bar{s}^2) . \qquad (7\text{-}19)$$

Substituting from (7-18) gives

$$q = -0.1582 f_4 \frac{m}{D^2} \frac{d}{dy} (\bar{s}^3) . \qquad (7\text{-}20)$$

Substituting for m in terms of ρ_s and D, then substituting (7-20) in (7-16) gives us the modified energy equation

$$T \frac{du}{dy} = \frac{\rho_s}{D} \left[\bar{s}^3 f_2 + D^2 \left(f_5 \frac{d^2}{dy^2} (\bar{s}^3) + \frac{d\bar{s}^3}{dy} \frac{df_s}{dy} \right) \right], \qquad (7\text{-}21)$$

where $f_5 = 0.0829\ f_4$.

One region where the energy flux is important is the region close to the bed. If, as predicted in the theory developed in Chapter 3, a large negative concentration gradient exists just above the bed, equation (3-16) implies a large positive gradient of $\bar{s}$ and therefore of $\bar{s}^3$.

Consider the region close to the bed with concentration and $\bar{s}^2$ profiles as shown in Fig. (7-2).

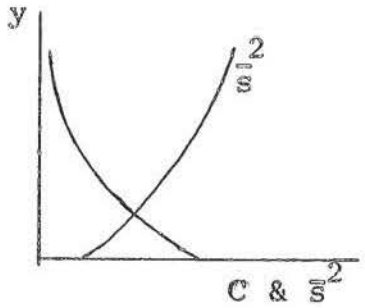

Fig. (7-2)

There will be a flow of energy from the regions above the bed downwards to the region close to the bed and $\bar{s}$ and therefore F_2 and F_7 at the bed will be greater than a simple analysis would indicate.

Summary of Conclusions on Finding the Concentration and Velocity Profiles

Methods developed in Chapter 2 enable the concentration profile to be found using F_1 curves that are functions of $T_* = T/(\rho_s - \rho_f)g\,D$ at the top of the fixed bed.

Experimental results for F_1 as a function of C and T obtained using an open channel flow and in the range $0.45 < T < 1.16$ showed little scatter.

More general methods of obtaining F_1 and F_3 require the solution of the local equations where the gradient of concentration and energy is significant.

Because of the difficult measurements required, particularly with the type of apparatus employed (a flume), the experimental results obtained for F_3 show much more scatter than those obtained for F_1.

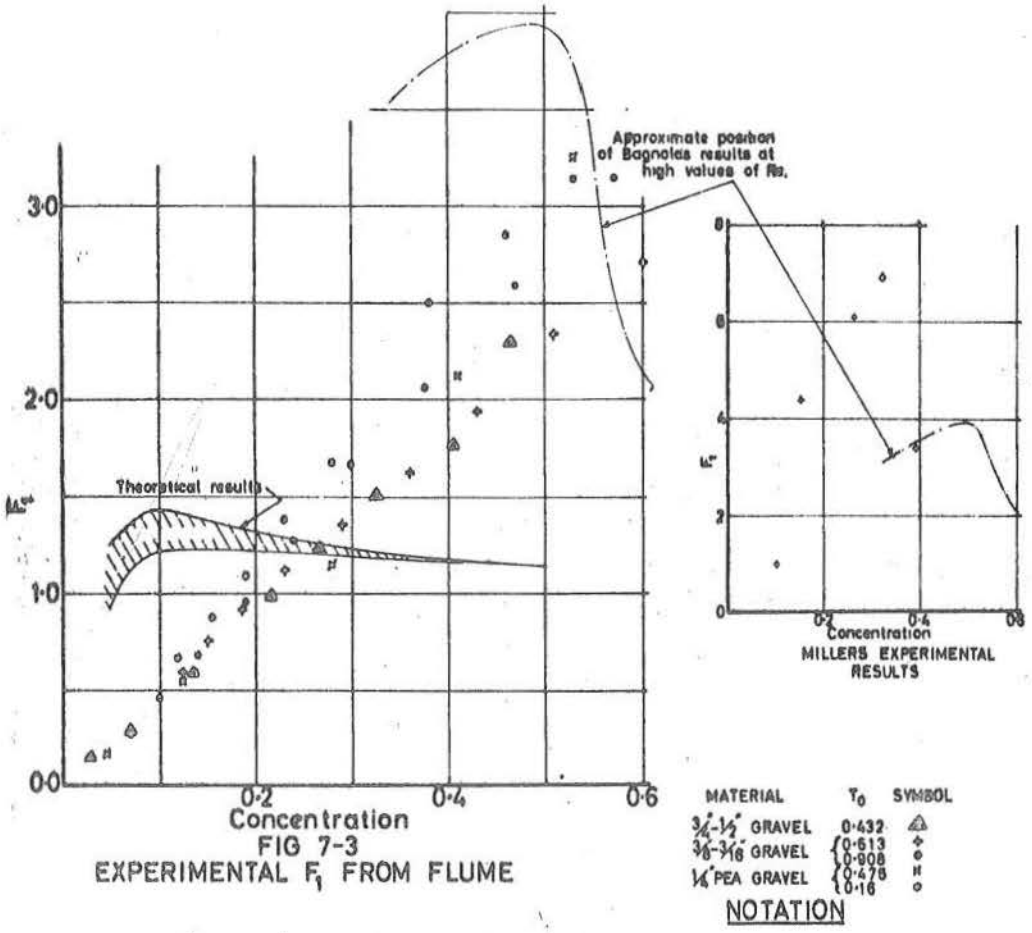

FIG 7-3
EXPERIMENTAL F_1 FROM FLUME

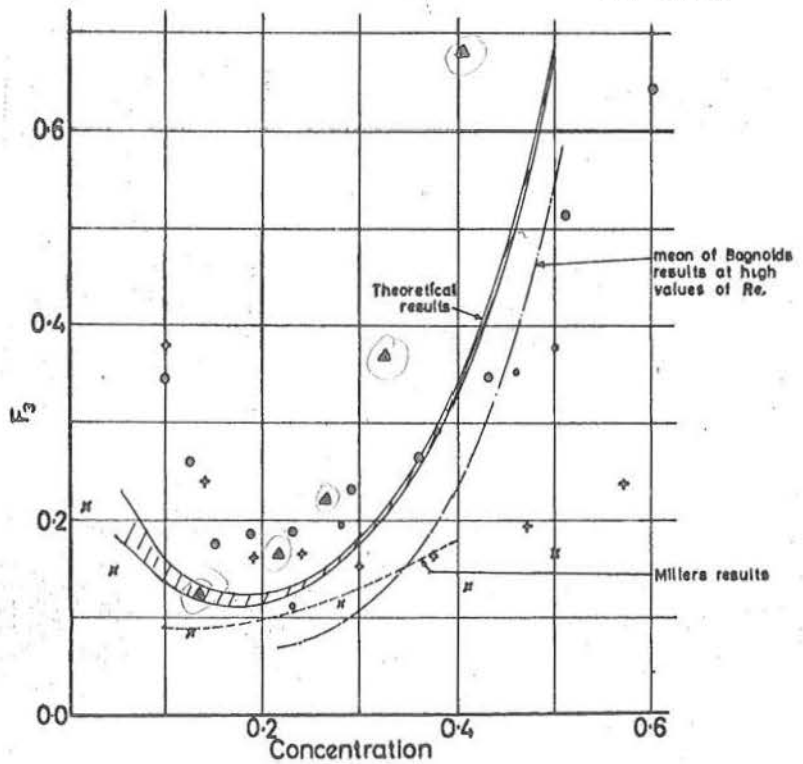

FIG 7-4
EXPERIMENTAL F_3 FROM FLUME

CHAPTER 8

CONCLUSIONS ON THE BEHAVIOUR OF, AND POSSIBLE MODIFICATIONS TO, THE APPARATUS

SYNOPSIS

After carrying out the experimental programme described in Chapter 5, the following conclusions were reached. These conclusions apply to changes that are expected to improve the results of future work, or make such work easier to carry out. Modifications that would be advantageous for other types of work are also noted. The first item discussed is the flume, which, after initial modifications, performed satisfactorily. Next, the concentration meter is covered in some detail as this item of apparatus is believed capable of further development, but, even in its present state, proved a very useful tool. Fluid velocity and pressure measurement are then discussed and it is concluded that, in general, the methods employed were not satisfactory; in particular, the methods used to analyse the results need to be improved. Finally, the stone velocity measuring technique is mentioned and here the method used was very tedious although moderately accurate.

FLUME

Wear

Initially, fluid and gravel were passing through the axial flow pump and, after 20 hours, the wear on the pump was found to be excessive. After modification of the pumping arrangements and the introduction of a jet pump system to pump the particles, no further pump trouble was experienced. The 3/16 inch thick pipes and bends were examined after 20 hours running and no measurable wear had occurred. After about 60 hours running, all the paint was stripped off the floor of the head tank and noticeable wear was apparent on some temporary vanes in the tank. Polyurethane paint was used to protect the mild steel deck and side panels. This paint failed wherever the particles were moving along the surface, and, further, the plate glass was given a sand-blasted effect at the level of the moving bed. However, the roughening of the glass did not seriously affect the photography. It was concluded that, as this was the most arduous duty likely to be required of it, the flume was, with the exception of the paintwork, satisfactory from the wear point of view.

Vibration

Initially the flume vibrated about the hinge support at a low frequency in a horizontal plane. The amplitude of this

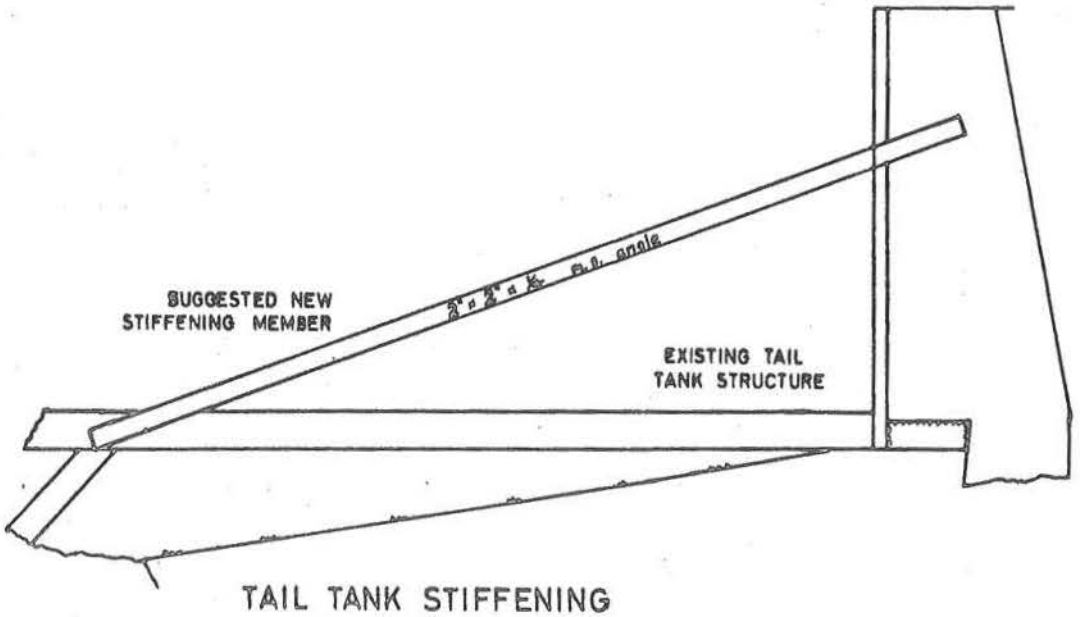

TAIL TANK STIFFENING
Scale: 1" = 2'

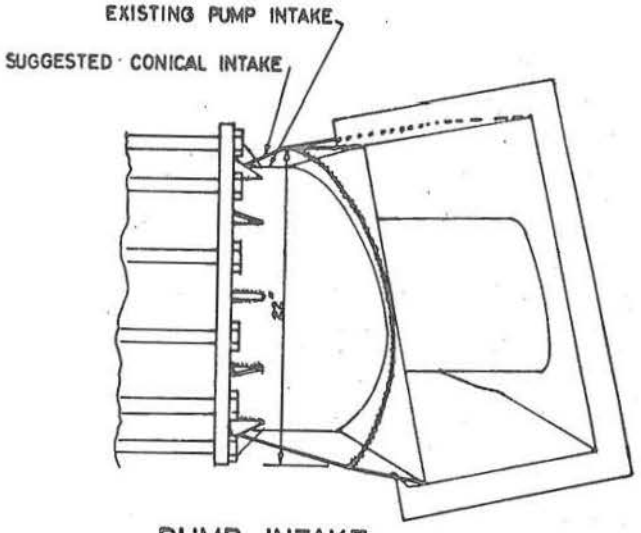

PUMP INTAKE
Scale: 3¼" = 1'

FIG 8-1
MODIFICATIONS TO APPARATUS

vibration was about 1 inch at the head tank. This fault was remedied by clamping the flume to the support furthest from the hinge or to the laboratory structural frame close to the head tank. The vibration of the end of the flume made sealing the last panel a problem and stiffening as shown in Fig. (8-1) would be beneficial.

Hydraulic Design

In the initial design, the pump intake was designed to prevent gravel deposits from forming. As no coarse material is now passed through the pump, the inlet would be better enlarged as shown in Fig. (8-1). From measurements made while the flume was in use, it is calculated that this modification would increase the maximum flow by about 25 per cent. Minor changes were made at the pipe bends during the experiments and no significant improvement could be expected here. The flow conditions at the head tank were very vigorous and the flow was normally allowed to pass more or less unrestricted into the flume channel. A bank was formed about 10 ft from the head tank and the flow rose over this, slowing down to a velocity of about 3 - 4 ft per second before accelerating down to the final flume velocity of about 13 ft per second. This bank was very effective in making the flow uniform across the channel and was also very stable in height and position.

Operation and Controls

The flow controls were satisfactory for the particular experiments carried out. The motor and pump were connected by a sprocket and chain drive and initially various speed ratios were used. However, for most of the experimental runs, the ratio was unaltered and the flow controlled by adjusting the motor speed.

A stable flow range greater than 2 to 1 was obtainable, this range being limited by instability caused by boiling at the tips of the electrodes connected to the motor rotor (see Chapter 4) at low speeds. The speed range could, if necessary, be increased by using a modified system of electrode plates and cooling the top surface of the electrolyte.

The loss of water wasted to the river limited the length of each continuous run at full flow to 2.5 hours, as the total available storage of clean water was then exhausted.

Initially the flume was tested with the full width of channel while horizontal. It was then lifted to its maximum slope and altered only once more in the course of the experiment. Lifting was carried out with the assistance of the laboratory crane and a lifting beam. The four lifting rods were turned by hand. The maximum rate of hand operation of the lifting screws was found to give about 0.01 per hour change in slope. If frequent slope changes were required, a motor

drive on the lifting rods would be a big asset. The geometry is such that a 2:1 speed ratio between the two sets of screws will lift the deck as a unit.

Acoustics

In the design of the flume, no consideration was given to controlling noise. It was found that for full flow of ¾ inch - ½ inch gravel, the noise level in regions close to the flume exceeded 100 decibels. Because the laboratory and adjacent workshop were used throughout the day, this noise level restricted flume operation to the evenings or week-ends. Persons working on the flume wore ear-muffs and oral communication was almost impossible.

As the size of particles was reduced, the sound level was reduced considerably, but, with ¼ inch pea gravel, was still too high for conversation. The two main sources of noise were at the jet pump and pipe immediately downstream and at the head-tank.

CONCENTRATION METER

In its final form, the apparatus worked well, the resolution was good in the vertical direction, see Fig. (6-2), and the sensitivity was similar to that predicted. The apparatus was not sensitive enough to measure the variation of concentration with time at a given level.

Some improvement in the sensitivity at high concentrations would be desirable, particularly if this could be achieved without increasing the background count.

The sensitivity could be improved by the following changes. Firstly, a pulse-height analyser could be used, that is, a counting system, sensitive to a selected narrow energy band. Such a system would reduce the background count while leaving the main count practically unaltered.

Secondly, any reduction in width improves the count of the main beam with only a slight increase in background count. An increase in counts by a factor of 10 at 0.6 concentration can be obtained for every reduction in width by 5 inches.

Finally, the use of a different source could be of advantage. Any increase in size of source would also mean increased shielding and possibly a different system of moving the source into a working position. The source could be changed by using a greater number of curies or a different isotope. The merits of a given isotope can be examined using the previous equations developed in Chapter 4, but in general a higher energy beam is better suited to high concentrations and widths.

It is believed that an increase in sensitivity by a factor of at least 30 could be obtained using a larger source and a pulse-height analyser before the weight and bulk of shielding became a serious problem.

The detector used contained a cylindrical crystal of 1 inch diameter. As the window facing the source was a slit only 3/32 inch wide, the total area used to measure source photons was 0.09 square inches whereas the total crystal of area 0.785 square inches was detecting background. Using a suitably shaped crystal would therefore have reduced the background count by a factor of 0.115.

Counter

The counter used was fitted with a binary electronic register combined with a mechanical register. The mechanical register was not reliable at temperatures above 75°F, and frequent recounting was required. After discussion with the counter owners, who also had two similar models in use, it was found that the fault was common to all three counters. For work in an open laboratory where temperature control is difficult, a unit able to work at temperatures above 70°F. should be used. The counting head is also temperature sensitive but in a predictable manner.

Other Uses

The counting apparatus could be used in the suspended load region or to measure air entrainment. For such work, where the change in mass between the source and detector is small, a different technique would be required. The clean water count

as a function of height would be required as this varies slightly with irregularities in the side panels. For instance, an increase in width of 1/16 inch in a 24 inch channel is equivalent to 0.15% increase in concentration. If the 30-fold increase in sensitivity noted above were obtained, the apparatus could be used to measure the variation of concentration with time.

FLUID VELOCITY AND STATIC PRESSURE MEASUREMENTS

In reading the pitot-static tubes, no correction was made for the hydrodynamic effect of the solid particles on the readings. Before placing much reliance on the results, it would be desirable in any future work to examine this effect.

The stainless steel pitot tubes withstood the abrasion of the gravel very well and in this respect proved satisfactory. The leads connecting the pitot-static tubes to the manometers were about 16 ft long and, while longer than desired, were found more satisfactory than shorter leads with connections and valves operating below atmospheric pressure. Measurements were further complicated by the unsteady nature of the bed for most flows. The measuring system would be very much improved if the pressure transducers were placed close to the points of measurement, preferably on the pitot-static tube mount, just clear of the surface of the flow.

Interpretation

Output curves derived from the single transducer were used to find the mean velocity only, with some allowance being made for systematic peaks as gravel waves moved past the pitot-static head. The results obtained were not as accurate as desired and a general upgrading of the equipment would be an advantage for future work. If such upgrading were carried out, it would be possible to measure the velocity variation with depth over various sections of the wave along the bed. Also, the mean velocity in the deeper part of the bed would be determined more accurately. Measurement of the deviation in static pressure from ($\rho_f g$ x depth) requires a much more refined analysis of the information than was possible with the equipment used.

For a suspended concentration of 1%, there would be a head difference over 1.75 inches of 0.0025 ft, and, with a velocity head in the system of 2.0 ft, this small difference in head would be very difficult to detect reliably. With continuous measurement of the velocity heads and static pressure heads, followed by corrections to the latter for the effect of velocity head, there would be some possibility of measuring the suspended load. Frequent calibration of the pitot static tubes would also be necessary. Only with a continuous output of all these measurements simultaneously would there be much hope of a

successful analysis of the deviation of static pressure from the clear water hydrostatic value.

Another method not used in these experiments was that using fixed pressure tappings along the side. Accurate work with this system would require a measurement of the velocity field at the sides to enable appropriate corrections to be applied.

STONE VELOCITY MEASUREMENTS

The most important practical consideration when taking photographs under the conditions in the flume is the use of the maximum available light. Ideally, this should be supplied as a rapid series of flashes, but the only available light source of sufficient intensity for these experiments was a continuous source.

Experience showed that a film frequency such that the particles moved not more than half a diameter per frame was suitable. Increase above this frequency led to difficulties in particle identification and also to blurring of the image. Only those particles close to the side of the flume could be observed easily.

With a small scale apparatus, measurement of the particles further into the bed would be possible using transparent particles of the same refractive index as the fluid and including

a small percentage of opaque particles.

A limitation of the photographic method used was the time required to analyse the photographs. This process was not readily amenable to mechanization. One possible improvement that could be made in analysis if more light was available is as follows. The film speed could be increased to give about 100 frames for a complete traverse of the field of view by a particle. A small horizontal slit could then be viewed at a given height and a moving grid superimposed on this. By adjusting the speed of the grid to coincide with the speed of the particles, a mean velocity of the particles could be obtained.

The Baur "sun-gun" was found to be much superior to the photo-floods for this type of work and sufficient light to speed up the film and improve the image could be obtained with a bank of quartz iodine bulbs similar to those used in the sun-gun.

Briefly, the methods used for stone velocity measurement were satisfactory but tedious and time-consuming and, if much work of this nature were undertaken, it would be advisable to develop improved apparatus.

CHAPTER 9

SUMMARY OF AND POSSIBLE EXTENSIONS TO THE WORK

SYNOPSIS

This chapter discusses the results and conclusions of the work detailed in Chapters 1 to 8, particularly from the point of view of extending and improving the results obtained. Theoretical extensions are discussed first, followed by experimental developments. It is concluded that the most desirable programme would proceed with further developments to the local equations describing the behaviour of a fluid particle system at a point, before attempting to extend the methods to solve particular problems.

A brief summary of the thesis results relevant to future extensions of the work constitutes the beginning of this chapter. This summary is followed by a discussion of future developments of the local equations and the manner in which these equations may be applied to particular problems.

SUMMARY OF RESULTS

Fluid particle systems have, in the past, been analysed by considering the fluid to behave in the same manner as it would if the bed were fixed, and the important forces on the

particles to be essentially those acting on fixed particles. Movement is assumed to take place by particles jumping or rolling forward over the essentially fixed bed, the initiation of all these movements taking place at a single surface above which there is a fluid system and below which there is a fixed bed of particles. Such an approach is denoted in this thesis a "single surface" approach. The resultant particle movement has been examined previously, as in Einstein"s or Kalinske"s work. In this thesis, however, the single surface approach is not used and instead the behaviour of a more or less uniform system of particles in a fluid is considered.

In the single surface approach, where a stream of fluid is assumed to act on a nearly stationary bed of particles, the fluid behaviour is generally considered independent of the particle behaviour, and the approach does not include any method of obtaining the velocity or concentration distribution in the direction normal to the bed in the bed region. As it is shown in this thesis that a layer of particles many diameters thick can exist where the concentration will be greater than 0.2 ($C > 0.2$) and that this thick bed influences the total fluid and solid flow rates for a given total depth, this single surface approach will not always be satisfactory.

Another reason for obtaining the concentration profile near the bed arises from the form of solution of the suspended

load equation. This solution relates the concentration at any depth to the concentration at some reference depth, this latter concentration necessarily being obtained by some other means.

At the opposite extreme to the single surface approach is the approach used in this thesis, where a model is set up for local stresses in a fluid particle system, such a model being based on only gradual variations in concentrations, etc., with distance along a line normal to the planes of constant concentration. It has been shown in the thesis that, if these local equations are known, sufficient boundary conditions can normally be found to enable the complete concentration and velocity profiles to be found for the bed region.

It is shown in Chapter 2 that, if the parameter $F_1 = P/T_t$ is a function of C alone, the equation for C as a function of y reduces to the solution of a first-order differential equation.

Experimental results obtained from the flume show that F_1 is dependent on $T_* = T_t/g\ D\ (\rho_s - \rho_f)$ and therefore on the transverse gradient of either C or T_t for values of $T_* < 1.2$, particularly when $C > 0.3$.

In Chapter 3, a model of particle behaviour in a uniform system ($\frac{dC}{dy} = 0$) has been used to calculate $F_1(C)$ and $F_3(C)$. The parameter $F_1(C)$ in particular does not behave as calculated for $C > 0.3$. It appears that for $C > 0.3$ the mechanism of

momentum transfer used in the theory, that of instantaneous collisions, is inadequate; a model more closely representing the actual physical situation must be used.

DEVELOPMENT OF A MORE REFINED MODEL

In the existing model, the viscosity, dispersive pressure and mean free path calculations are based on results obtained by considering collisions between elastic smooth spheres. The only mechanism of momentum transfer considered in this model is the two-body collision. An improvement in the model would include a more realistic force function between the molecules, such function allowing three or more body collisions to be considered. In reality, the velocity of separation of particles will, in general, be much smaller than the velocity of approach. Close to the bed, a large number of particles may be in contact at any given time, allowing a rolling or sliding action to occur.

From the results obtained, it appears that inclusion of these multi-body effects is required if an accurate determination of $F_1(C)$ is to be obtained.

For $T_* < 1.2$, which would be a common condition in many real problems, the solution is dependent upon the gradient of concentration and, in consequence, the model should allow for

such a variation. One effect of $dC/dy \neq 0$ is to make the mean free path vary with direction, that is, the mean free path of a particle will be greater if the particle goes upwards than if it moves downwards.

Unfortunately, the extensions outlined above will seriously complicate any analytical solution and, at present, considerable approximation will be necessary in finding a mathematical solution.

IMPROVEMENTS IN THE MODEL ANALYSIS

In the existing model, the smooth elastic sphere results were used with approximate corrections for the inelastic nature of the spheres. A better analysis would start with the inelastic collisions and continue to obtain the final solution from that basis. However, as the model still requires modification, as described in the previous section, an increase in mathematical accuracy would be warranted only if it could be applied to an improved model of particle behaviour.

It is doubtful whether a much more accurate mathematical approach than has been used in this thesis would be possible when analysing a more difficult model including the effect of dC/dy, inelastic collisions and multi-body effects.

EXPERIMENTAL DEVELOPMENTS

Numerical

It has been noted that a complete analytical solution of the real problem appears unattainable at present. One method that has been used in the study of gas molecules is that of computer simulation, using a numerical model. In one example, Rahman (19, p.573) in 1964 studied a three dimensional model containing just over 890 particles with a force potential between the particles depending on two constants and the centre to centre distance between the particles.

It is believed that, using more modern computers, a larger number of particles could be studied, particularly if the particles were affected only by their immediate neighbours. Such a method could be used to directly examine F_1 and F_3 for various conditions and also to check the approximations required in any analytical solution.

In the writer's opinion, the development of a numerical model should be one of the next steps taken in examining the local equations.

Two immediate advantages of numerical experiments rather than physical ones are, firstly, that the difficult measurement of particle velocities is avoided and, secondly, that flow parameters and boundary conditions can more easily be altered.

Physical

Physical experiments can be divided into two categories, firstly, those examining in detail the behaviour of two particles or some small component of the system, and, secondly, those in which a complete fluid particle system is operated (as in the flume).

If a detailed numerical simulation experiment or a more exact analytical process is to be carried out, the behaviour of two particles approaching each other must be understood. The relation between the inter-particle force and the separation, translational and angular velocities of two particles must be known.

Another subject that could be examined, particularly as the analysis is extended to low concentrations, is the unsteady fluid-particle behaviour with various types of particles.

On a large scale, the experiments carried out in the flume are limited to $T_* < 1.0$ if uniform flows at large values of ρ_s/ρ_f are required at high Reynolds numbers. In experiments on the capacity of steel pipelines carrying solids, Condolios and Chapus (20) noted that the bed remained essentially plane for a wide range of flows. It is suggested that higher values of T_* can be obtained for large Re and ρ_s/ρ_f by using a closed conduit, with suitable equipment for measuring the shear stress on the walls and top of the conduit.

Such large scale experiments will be necessary if the effects of the fluid turbulence are significant, as in this case the bed behaviour may depend on the overall geometry of the system. In the flume experiments, F_1 was a single valued function of C for all sizes of particle in the low concentration region, showing that in these experiments the flow depth to particle diameter ratio did not affect the concentration profile at low concentrations.

APPLICATION OF THE LOCAL EQUATIONS

The equations for F_1 and F_3 are only useful in the end result if they can be applied to the solution of the concentration and velocity profiles. It is considered that the important requirements at present are to obtain these functions more accurately and for a more general case than has been studied in this thesis. Only then should application of these equations be further developed as the methods of application, essentially the solution of differential equations, will depend on the form of F_1 and F_3. It has been shown that for a particular form, namely, dependence on C only, a simple method of solution for the concentration and velocity profiles is available.

Extension of the local equations to non-uniform situations will be required if the open channel flow case is to be solved.

This extension is required to enable the bed oscillations to be examined. Variation in a system can be considered to be slow if the system at any point can be analysed as a steady uniform system. On the other hand, a fast variation will be one in which the system is distorted significantly from the steady state in order to apply a restoring process causing the system to change. The bed waves on the flume were believed to be variations of the fast type, as might also be flow around piles in a river. An example of slow variation in the above context would be the normal changes in direction and overall cross-section in a river.

SUMMARY

It is suggested that the solution of particle-fluid problems may in some situations be best handled by the use of local equations of the type defining F_1 and F_3. Such an approach has the advantage of generalising the problem to include a wide range of specific problems under one system of solution. Further work is required to develop such local equations before the method can be used to handle actual problems reliably and accurately.

REFERENCES

1. T. Blench. "Regime Behaviour of Canals and Rivers," (London: Butterworths Scientific Publications, 1957).

2. A. Shields. "Anwendung der Aehnlichkeitsmechanik und der Turbulenzforschung auf die Geschiebebewegung" (Application of Similarity Principles and Turbulence Research to Bed-Load Movement), Mitteilungen der Preuss. Versuchsanst fur Wasserbau and Schiffbau, Berlin, No. 26 (1936). Available also in a translation by W. P. Ott and J. C. van Uchelen, S. C. S. Co-operative Laboratory, California Institute of Technology, Pasadena, Calif.

3. A. J. Raudkivi. "Study of Sediment Ripple Formation," Proc. Am. Soc. Civil Engrs., Vol. 89, No. HY6 (Nov., 1963), p. 15.

4. H. A. Einstein. "The Bed-Load Function for Sediment Transportation in Open Channel Flows," U.S. Dept. of Agriculture Technical Bulletin No. 1026 (September 1950).

5. A. A. Kalinske. "Movement of Sediment as Bed Load in Rivers" Trans. Am. Geophys. Union, Vol. 28, No. 4 (1947), p. 615.

6. R. A. Bagnold. "A Gravity-Free Dispersion of Large Solid Spheres in a Newtonian Fluid under Shear," Proc. Roy. Soc. (London), A, Vol. 225 (August 1954), p. 49.

7. R. A. Bagnold. "The Flow of Cohesionless Grains in Fluids," Phil. Trans. Roy. Soc. (London), A, Vol. 249 (1957) p. 235.

8. R. A. Bagnold. "An Approach to the Sediment Transport Problem from General Physics," U.S. Department of the Interior, Geological Survey Professional Paper 422-I.

9. J. B. Miller. "The Flow of Turbulent Suspensions," Ph.D. Thesis, University of Auckland, Auckland, N.Z., 1964.

10. J. O. Hirschfelder, C. F. Curtiss and R. B. Bird. "Molecular Theory of Gases and Liquids," (New York: John Wiley & Sons, Inc., 1954).

11. T. C. Fry. "Probability and its Engineering Uses," 2nd ed. (Princeton: D. Van Nostrand Company, Inc., 1965) p. 180.

12. J. Alder and T. E. Wainwright. "Studies in Molecular Dynamics. II. Behaviour of a Small Number of Elastic Spheres," J. Chem. Phys., Vol. 33 No. 5 (Nov. 1960), p. 1439.

13. A. A. Townsend. "The Structure of Turbulent Shear Flow," (Cambridge: Cambridge University Press, 1956).

14. J. Happel and H. Brenner. "Low Reynolds Number Hydrodynamics," (New Jersey: Prentice-Hall, Inc., 1965).

15. V. A. Vanoni. "Transportation of Suspended Sediment by Water," Trans. Am. Soc. Civil Engrs., Vol. 111 (1946), p. 67.

16. Mikio Hino. "Turbulent Flow with Suspended Particles," Proc. Am. Soc. Civil Engrs., Vol. 89, No. HY4 (July 1963), p. 161.

17. J. Kohl, R. D. Zentner, H. R. Luckens. "Radioisotope Applications Engineering," (Princeton: D. Van Nostrand Company, Inc., 1961).

18. B. T. Price, C. C. Horton and K. T. Spinney. "Radiation Shielding," (London: Pergamon Press, 1957).

19. A. Rahman. "Triplet Correlations in Liquids," Phys. Rev. Letters, Vol. 12, No. 21 (1964), p. 575.

20. E. Condolios and E. E. Chapus. "Designing Solids Handling Pipelines," Chem. Eng. Vol. 70 (July 8, 1963), p. 131.